Use of Ionic Liquids and Support Materials for High Performance Enzymatic Conversion of CO_2 into Formic Acid and Formaldehyde

Zhang, Zhibo

Publication date:
2019

Document Version
Publisher's PDF, also known as Version of record

DTU Chemical Engineering
Department of Chemical and Biochemical Engineering

Use of Ionic Liquids and Support Materials for High Performance Enzymatic Conversion of CO_2 into Formic Acid and Formaldehyde

Zhibo Zhang

Use of Ionic Liquids and Support Materials for High Performance Enzymatic Conversion of CO_2 into Formic Acid and Formaldehyde

PhD Thesis

Zhibo Zhang

February 2019

DTU Chemical Engineering
Department of Chemical and Biochemical Engineering

Use of Ionic Liquids and Support Materials for High Performance Enzymatic Conversion of CO_2 into Formic Acid and Formaldehyde

This PhD thesis was prepared by
Zhibo Zhang

Supervised by
Associate Professor Manuel Pinelo (main supervisor)
Associate Professor Nicolas von Solms (co-supervisor)
Professor Suojiang Zhang (co-supervisor)
Professor Bao-Hua Xu (co-supervisor)
Professor Jianquan Luo (co-supervisor)

February 2019

Process and Systems Engineering Center
Department of Chemical and Biochemical Engineering
Technical University of Denmark

Preface

This thesis presents the work conducted during my PhD project from Dec 2015 to Feb 2019 at the Department of Chemical and Biochemical Engineering, Technical University of Denmark (DTU), and the Institute of Process and Engineering (IPE), Chinese Academy of Sciences (CAS).

This work was carefully supervised by Associate Professor Manuel Pinelo, and co-supervised by Professor Suojiang Zhang, Professor Bao-Hua Xu, Professor Jianquan Luo, and Associate Professor Nicolas von Solms.

The project was supported by the Danish Council for Strategic Research and the Danish Council for Technology and Innovation and co-founded by IPE, CAS.

From the bottom of my heart, I really appreciate that my supervisor Manuel Pinelo gave me the opportunity to study in his group for three years. His patient supervision, scientific guidance, cheerful attitude, and warm encouragement accompanied me throughout my entire PhD. I spent a pleasurable and unforgettable time with Manuel in our group. This is not to forget the part played by, Professor Suojiang Zhang, Professor Bao-Hua Xu and Professor Jianquan Luo in ensuring the successful completion of my PhD project.

Thanks to my collaborators Xianglei Meng (PhD student in KT), Jiahuan Tong (PhD student in KT), Ting Song (PhD student in KT), Yingjun Cai (PhD student in KT), and Wenjing Zhang (Researcher in DTU). With their fruitful discussions and help, we created a lot of innovative work during my PhD.

Thanks also to my colleagues Anna Burniol Figols, Sigyn Björk Sigurdardóttir, Konstantinos Asimakopoulos, Antonio Grimalt Alemany, and Antonios Melas, who helped me in various ways, either directly or indirectly, in contributing to fruitful discussions on the analytical work and sharing ideas and information.

Special thanks to my colleague and officemate, Enrico Mancini, who encourage and helped me during the challenges of improving my English-speaking skills, and we also have a lot of fun out of the study. I will miss the time we spent together in Denmark.

Finally, I would like to express my deep gratitude to my dear mother Yun Sun, my beloved wife Mei Luo, my beautiful and kind sisters Jing Zhang and Zhiying Zhang, and my cute daughter Senqin Zhang, who have all loved and supported me and given me the strength to finish the PhD.

Abstract

Enzymatic conversion of CO_2 to fuels and valuable chemicals is a promising way to reduce increasing CO_2 emissions. The research in this thesis was mainly divided into three sequential parts: First, the single enzymatic reactions, CO_2 → formic acid, was studied in detail. Later on, two additional multi-enzymatic reactions were added to the latter (CO_2 → formic acid → formaldehyde → methanol). Lastly, a cofactor (NADH) regeneration system was added to the main sequential reaction, so external cofactor addition would not be required.

There are several limitations that render the inefficiently enzymatic conversion of CO_2 nowadays. One of them is the low solubility of CO_2 in water or buffer. To address this limitation, ionic liquids (ILs), with a higher solubility than water, were explored as alternative co-solvents for increasing CO_2 capture. In studying on this reaction, we found that degradation of NADH, which occurs during the enzymatic reaction, causes overestimation of the CO_2 conversion results when using the conventional analytical method (quantification of NADH reduction – so-called method **N**). Therefore we proposed and established a new detection method (so-called method **C**), further investigated the degradation mechanism of NADH in order to select different kinds of ILs that are suitable for our enzymatic system. As a result, by stabilizing NADH with ILs and optimizing the variables, the yield of formic acid in $BmimBF_4$ was increased two-fold compared to the yield of formic acid in phosphate buffer.

To further increase conversion of CO_2, two more sequential reactions were added to the main one, so the product from one reaction was consumed in the subsequent one and the equilibrium could be switched towards higher conversion. To that purpose, formaldehyde hydrogenase (FaldDH), and alcohol dehydrogenase (ADH), which catalyzed the conversion of formic acid to formaldehyde and methanol, respectively, were added. It was indeed observed that particularly the addition of ADH (with very high activity) contributed significantly to the overall conversion of CO_2. To conduct such a sequential reaction though, several ionic liquids compatible with enzymes were evaluated, a high concentration of CO_2 could be kept in the system. After evaluating the activity of the three enzymes in different ILs, IL [CH][Glu] presented by far the best performance. By using such IL system, CO_2 concentration was detected to be 15 times higher compared with the amount in water. Subsequently, in order to make the platform for the multi-enzymatic reaction even more efficient, a membrane reactor design enabling enzyme immobilization, which should increase enzyme stability, was developed. For that purpose, the so-called “fouling induced immobilization method” was used, which enable to maintain the activity of the immobilization enzymes at approximately that of the free enzymes, due to mild and fast immobilization procedure.

Additionally, a high enzyme loading could also be attained, and the contact time for the substrate-enzyme complex could be controlled by changing pressure. Finally, the yield of product (methanol) in [CH][Glu] was increased three-fold compared to the yield in conventional buffer.

When talking about the economic viability of enzymatically converting CO_2 at large scale, the cost of the cofactor (NADH) is the biggest bottlenecks because three molar equivalents of NADH are consumed to transform one molar equivalent of CO_2 to methanol. NADH regeneration through a photocatalytic method was envisaged as a promising way to decrease the cost because limitless solar energy is available for utilizaiton. Inspired by the natural light-harvesting pigments, the porphyrins, porphyrin-based ionic liquid photosensitizers were synthesized and evaluated for NADH regeneration. After evaluating several photosensitizers, ZnTPyPBr showed the best performance in NADH regenerations. After the regeneration system was developed, a photocatalytic membrane was developed, so the multi-enzymatic reaction could be coupled with *in-situ* NADH regeneration. The selected photosensitizer, enzymes, and electron mediator were immobilized in the surface of the membrane and the multi-enzymatic reaction was performed in the photocatalytic membrane under visible light. The artificial photocatalytic system was successfully developed and investigated. Cost of NADH could be therefore significantly decreased and the overall system showed promise as a preliminary platform for efficient and inexpensive CO_2 conversion.

Dask Sammenfatning

Enzymkatalyseret konvertering af CO_2 til brændstoffer og brugbare kemikalier er en lovende måde at reducere de stigende CO_2-emissioner. Forskningen der ligger bag denne afhandling kan deles i tre sekventielle dele: Først blev den enzymkatalyserede konvertering af CO_2 → myresyre, ved brug af formatdehydrogenase (FateDH), grundigt undersøgt. Derefter var to enzymer tilføjet det førstnævnte for yderligere konvertering af myresyre til metanol (CO_2 → myresyre → formaldehyd → metanol). Den tredje del omhandler implementering af et cofaktor (NADH) regenereringssystem for at undgå behovet for støkiometrisk forbrug af cofaktor i de multi-enzymkatalyserede reaktioner.

Der er flere begrænsninger, der gør, at en effektiv enzymkonvertering af CO_2 ikke endnu er opnået. Den ene af disse begrænsninger er den lave opløselighed af CO_2 i vand eller buffer. Ved brug af ioniske væsker som alternative co-opløsningsmidler kan CO_2 optaget forøges. Vores undersøgelse viste, at nedbrydning af NADH under enzymreaktionerne, forårsager overvurdering af omdannelsen af CO_2 ved anvendelse af den konventionelle analytiske metode (kvantificering af reduktionen af NADH - såkaldt metode N). Derfor har vi foreslået og etableret en ny detekteringsmetode (såkaldt metode C). Vi har undersøgt mekanismen for nedbrydning af NADH for at udpege forskellige typer ioniske væsker, der er egnede til det aktuelle enzym system. Ved stabilisering af NADH med ioniske væsker og yderligere optimering af systemets variabler, blev udbyttet af myresyre i BmimBF4 fordoblet i forhold til udbyttet af myresyre i phosphatbuffer.

For forøget konvertering af CO_2, blev tre enzymer brugt til omdannelsen af CO_2 til metanol i tre sekventielle reaktioner, hvor produktet fra den ene reaktion blev til substrat i den efterfølgende reaktion (CO_2 → myresyre → formaldehyd → metanol). Ligevægten blev derved omstillet til højere omdannelse. Udover FateDH, blev formaldehydhydrogenase (FaldDH) brugt til at katalysere konvertering af myresyre til formaldehyd, og alkoholdehydrogenase (ADH) til at katalysere konvertering af formaldehyd til metanol. Vi fandt ud af, at især ADH (med høj aktivitet) var vigtig for den forøgede konvertering af CO_2. Flere forskellige ioniske væsker blev evalueret som potentielle co-opløsningsmidler med hensyn til høj enzym aktivitet ligesom højt CO_2 optag. På baggrund af vores evaluering, viste den ioniske væske [CH] [Glu] sig at være den bedst egnede til vores system. CO_2-målinger viste at CO_2 koncentrationen var 15 gange højere i denne ioniske væske sammenlignet med koncentrationen i vand. For at effektivisere platformen for de multi-enzymkatalyserede reaktioner, blev der udviklet et membranreaktor-design, hvor enzymimmobilisering kan bruges for forøget enzymstabilitet. Her blev den såkaldte "fouling-inducerede immobiliseringsmetode" anvendt. Ved brug af denne milde og hurtige metode kunne

der opnås høj enzym aktivitet, således at aktiviteten af de immobiliserede enzymer lignede aktiviteten af frie enzymer. Derudover tillader immobiliseringsmetoden høj densitet af enzym, samt styrbar kontakttid mellem substrat og enzym ved at ændre trykket. Endelig blev udbyttet af produkt (metanol) i [CH] [Glu] forøget tre gange sammenlignet med udbyttet i konventionel buffer.

I forbindelse med den økonomiske levedygtighed af enzymkonvertering af CO_2 i stor skala, er omkostningerne ved cofaktoren (NADH) den største flaskehals, eftersom tre molær ækvivalent af NADH bruges til at omdanne én molær ækvivalent CO_2 til metanol. En fotokatalytisk metode for regenerering af NADH blev afprøvet med formålet at reducere disse omkostninger ved at bruge solenergi. Inspireret af de naturlige lyshøstende pigmenter, porfyriner, blev der syntetiseret flydende porfyrinbaserede ioniske fotosensibilisatorer og evalueret for NADH regenerering. Vores evaluering af flere forskellige fotosensibilisatorer viste at ZnTPyPBr ydede den højeste NADH regenerering. For at koble regenereringssystemet med de multi-enzymkatalyserede reaktioner, blev der udviklet en fotokatalytisk membran, hvor den valgte fotosensibilisator, de tre enzymer samt elektron mediator blev immobiliseret i membranens overflade. Enzymreaktionerne foregik i den fotokatalytiske membran under synligt lys. Udviklingen af det kunstige fotokatalytiske system blev en succes og omkostningerne ved NADH kunne betydeligt reduceres. Det overordnede system kan bruges som en foreløbig platform for effektiv og billig CO_2 konvertering.

Table of Contents

Preface I

Abstract II

Dask Sammenfatning IV

List of Abbreviations VIII

List of Publications IX

Chapter 1 – Introduction 1

1.1 Background of Carbon Dioxide (CO_2) 1

1.2 Enzymatic conversion of CO_2 4

1.3 Ionic liquids 6

1.4 Biocatalysts in Ionic liquids 7

1.5 Cofactor NADH regeneration 9

1.5.1 NADH regeneration with the enzymatic method. 9

1.5.2 NADH regeneration with photochemical methods. 10

1.6 Membrane bioreactor 12

1.6.1. Membrane reactor configurations 13

1.6.2. Fouling model 13

Chapter 2 - Purpose, Hypotheses, and Objectives 15

2.1 Purpose and hypothesis 15

2.1.1 Conversion of CO_2 to formic acid (Paper 1) 15

2.1.2 Conversion of CO_2 to methanol. (Paper 2) 15

2.1.3 Conversion of CO_2 to methanol coupled with photocatalytic NADH regeneration. 17

2.2 Research objectives 19

Chapter 3 – Ionic Liquids as Bifunctional Cosolvent Enhanced CO_2 Conversion Catalysed by NADH-dependent Formate Dehydrogenase 22

3.1 Hypotheses 22

3.2 Experimental considerations 22

3.3 Highlights 23

3.4 Significance of the study 24

3.5 Paper 25

Chapter 4 - Efficient Ionic Liquid–based Platform for Multi-Enzymatic Conversion of Carbon Dioxide to Methanol 38

4.1 Hypotheses 38

4.2 Experimental considerations 38

4.3 Highlights 39

4.4 Significance of the study 41

4.5 Paper 42

Chapter 5 - Integration of a Biomimetic Artificial Photocatalysis Membrane for the Production of Methanol from CO_2 53

5.1 Hypotheses 53

5.2 Experimental considerations 53

5.3 Highlights 54

5.4 Significance of the study 55

5.5 Paper 56

Chapter 6 – Conclusions and Future Perspectives 73

References 75

Appendix 77

List of Abbreviations

Ionic liquids: ILs

Ionic liquid: IL

PDA: Polydopamine

PEI: Polyethylenimine

[CH][Glu]: choline glutamate

[CH][Gly]: choline glycine

[CH][Pro]: choline proline

[CH][His]: choline histidine

DBULat: 1,8-Diazabicyclo[5.4.0]undec-7-ene lactate

$BmimBF_4$: 1-butyl-3-methylimidazolium tetrafluoroborate

BmimDCA: 1-butyl-3-methylimidazolium dicyanamide

BmimDMP: 1-butyl-3-methylimidazolium dimethylphosphate

$EmimBF_4$: 1-ethyl-3-methylimidazolium tetrafluoroborate

EmimOAc: 1-ethyl-3-methylimidazolium acetate

NADH: Reduced nicotinamide adenine dinucleotide

NAD^+: Nicotinamide adenine dinucleotide

FDH: Formate dehydrogenase

FaldDH: Formaldehyde dehydrogenas

ADH: Alcohol dehydrogenase

GDH: Glucose dehydrogenase

TEOA: Triethanolamine

HTPyP: 5,10,15,20-Tetra(4-pyridyl)-21H,23H-porphine

HTPyPBr: 5,10,15,20-Tetra(4-pyridyl)-21H,23H-porphine tetrabromide

ZnTPyP: Znic 5,10,15,20-Tetra(4-pyridyl)-21H,23H-porphine

ZnTPyPBr: Znic 5,10,15,20-Tetra(4-pyridyl)-21H,23H-porphine tetrabromide

List of Publications

The thesis was based on the publications as listed as below:

1. **Ionic Liquids as Biofunctional Cosolvents Enhanced CO_2 Conversion Catalyzed by NADH-Dependent Formate Dehydrogenase**

   Zhibo Zhang, Bao-Hua Xu, Jianquan Luo, Nicolas von Solms, Hongyan He, Yaqin Zhang, Manuel Pinelo, and Suojiang Zhang

   Published: accepted in Catalysts (3.465); Catalysts 2018, 8, 304.

2. **Efficient Ionic Liquid-based platform for Multi-Enzymatic Conversion of Carbon Dioxide to Methanol**

   Zhibo Zhang, Jan Muschiol, Yuhong Huang, Sigyn Björk Sigurdardóttir, Nicolas von Solms, Anders Egede Daugaard, Jiang Wei, Jianquan Luo, Bao-Hua Xu, Suojiang Zhang, and Manuel Pinelo

   Published: accepted in Green Chemistry (8.586); Green Chemistry, 2018, 20, 4339-4348.

3. **A Biomimetic Photocatalytic Membrane for Enzymatic Production of Methanol from CO_2**

   Zhibo Zhang, Jiahuan Tong, Xianglei Meng, Yingjun Cai, Wenjing Zhang, Mingbo Ji, Nicolas von Solms, Jianquan Luo, Bao-Hua Xu, Suojiang Zhang and Manuel Pinelo

   Submitted to: Green Chemistry

Chapter 1 – Introduction

1.1 Background of Carbon Dioxide (CO_2)

Carbon dioxide (CO_2) is an essential compound for life – animals exhale it and plants adsorb and convert it. In plant metabolism, CO_2 is converted to carbon hydrate through photosynthesis, and this process and reaction is an important reaction for sustaining ecological balance on the earth[1]. CO_2 is also known as a greenhouse gas (GHG) – a gas that absorbs and emits thermal radiation to create the 'greenhouse effect'. Along with other greenhouse gases, such as nitrous oxide and methane, CO_2 is an important and abundant resource for sustaining a habitable temperature for the earth. If there were absolutely no GHGs, our planet would simply be too cold. It has been estimated that without these gases, the average surface temperature of the Earth would be about -18 degrees Celsius[2].

Since the Industrial Revolution, however, energy-driven consumption of fossil fuels for human activity has led to a rapid increase in CO_2 emissions. Tens of gigatons of CO_2 has been released into the atmosphere every year from the combustion of fossil fuel, as presented in **Figure 1.1.1**[3]**.** Before the industrial era, the atmospheric CO_2 concentration was stable at around 280 ppm. But with the combustion of carbon-based fossil fuels such as coal or oil, this concentration has increased until the current value of 393 ppm[4]. Consequently, the global carbon cycle has been disrupted and this has led to global warming. Climate change leads to extreme weather events, including floods, sea-level rise, iceberg melting, and acidification, and has a range of potential ecological, physical and health impacts.

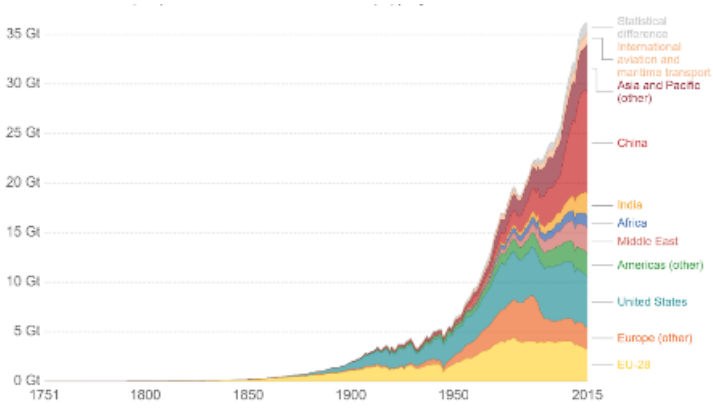

Figure 1.1.1 Global CO_2 emission from 1751 to 2015 by world region (1Gt = 10^9 tons)[3].

Approximately half of the human-based CO_2 emissions are absorbed by the oceans and vegetation, while the remainder enters the atmosphere[4]. To attempt to control CO_2 emissions to the

atmosphere, there will need to be regulations of such emissions in the future. Mitigation of the harmful effects of CO_2 is then also a necessity. How to decrease CO_2 emissions has therefore attracted the attention of researchers.

One approach to decreasing atmospheric CO_2 is Carbon Capture and Storage (CCS). CCS is a combination of technologies to stabilize the CO_2 concentration in the atmosphere while maintaining carbon as the main energy source. As presented in **Figure 1.1.2**, CCS methodologies consist of three major steps. The first is the capture of CO_2 from large point sources, such as power plants and cement manufacturing facilities. In the second step, this gas mixture is liquefied and transported by pipeline or ship to the storage site. In the third and last step, CO_2 is injected into the storage site. The CO_2 storage options comprise geological storage, ocean storage, and mineralization[5].

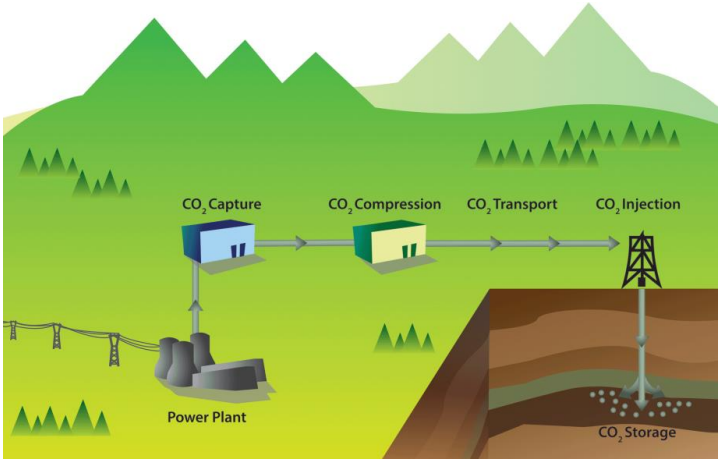

Figure 1.1.2. Schematic view of possible Carbon Capture and Storage system[5].

However, the CCS concept is connected to high costs. The costs for a plant with CO_2 capture are higher than one without due to increased investment costs, reduced plant efficiency, and increased maintenance costs, as well as the costs for CO_2 capture, transport, and storage. In addition, the environmental aspects also have to be considered and the risk of any leakage to the surface.

Apart from CCS, Carbon Capture and Utilization (CCU) offers favorable possibilities for addressing the CO_2 problem[6]. The aim of CCU is to convert CO_2 to useful chemicals and fuels (e.g. methanol) for use as renewable energy and simultaneously to alleviate the problem of CO_2 emission. The products obtained could supplement or replace chemical feedstocks in the chemical, pharmaceutical and polymer industries[7].

Currently, there are three methods of decreasing CO_2 emissions: the first is by developing new energy sources to replace fossil fuel and biomass energy; the second is by capturing CO_2 and storing it in the underground; the third is by the conversion of CO_2 to fuel and recycling it. However, the first two solutions are pretty challenging topics and cannot be achieved in the short run. In contrast, CO_2 conversion to valuable chemicals is a promising approach to alleviate the CO_2 problem and utilize the CO_2. Therefore extensive efforts have been made to bring about catalytic hydrogenation of CO_2 via electrochemical, photochemical and enzymatic conversions[8-10]. Due to the inherent thermodynamic stability and low reactivity of CO_2, production of methanol by enzymatic conversion has a significant advantage over conventional techniques. This is due to the high selectivity, high efficiency, mild experimental conditions, and environmental friendliness of enzymatic catalysis[9].

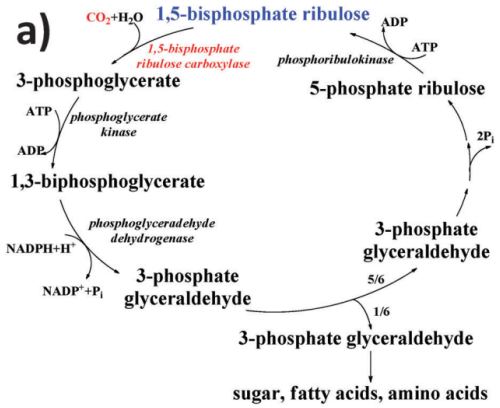

Figure 1.1.3 General illustration of the Calvin cycle or CO_2 metabolic process in cells[11].

In nature, the fixation conversion of CO_2 into organic material is a prerequisite for life and sets the starting point for biological evolution. The Calvin cycle is one of the most important biosynthetic cycles on earth. This metabolic pathway is used by the majority of photosynthetic organisms (such as plants, algae, cyanobacteria, and most aerobic or facultative aerobic Eubacteria) to incorporate CO_2 into the cell carbon cycle (**Fig. 1. 1. 3**)[11]. Thus, this cycle is by far the dominant method for CO_2 conversion in nature. Inspired by this, in vitro conversion of CO_2 catalyzed by an enzyme extracted or screened from cells may provide a high efficiency way to accomplish CO_2 capture, sequestration, and utilization[12].

1.2 Enzymatic conversion of CO_2

A feasible way to achieve CO_2 capture, sequestration, and utilization in vitro seems to be by directly adopting the single enzyme (oxidoreductases, synthases or lyases) that is in charge of accomplishing the CO_2 fixation/reaction in cells to catalyze the conversion of CO_2[13]. Therefore oxidoreductases (i.e. FateDH, CO_2 reductase, CODH, remodeled nitrogenase, etc.) and lyases (i.e., CA) were discovered in and extracted from a specific organism. And several kinds of fuels, chemicals, and materials, including formate, CO, methane, and bicarbonate, etc., have been successfully synthesized. This section will describe the state-of-the-art reaction routes for the catalytic conversion of CO_2 by a single enzyme. In addition, enlightened by the existing form and physicochemical environment of enzymes in cells, some advanced approaches and materials, utilized for constructing enzymatic systems with enhanced catalytic activity and stability, will also be investigated[14, 15].

Theoretically, an oxidoreductase is a type of enzyme that catalyzes the transfer of electrons from one molecule (the reductant or electron donor) to another (the oxidant or electron acceptor). During the redox reaction, NADPH/$NADP^+$ or NADH/NAD^+ is employed as an essential cofactor. The aim of converting CO_2 by an oxidoreductase is to reduce the oxidation state of the carbon element and acquire carbon-based energy resources. The first product obtained from conversion of CO_2 catalyzed by oxidoreductases should be formate[16, 17]. Formate is also an important chemical because it can be utilized for methanol production, hydrogen production, direct formic acid fuel cells, etc. CO_2 could be fixed and converted into formate in vivo when catalyzed by FDH (a typical oxidoreductase) with NADH as a cofactor. The mechanism for the reduction of CO_2 to formate by NADH-dependent FDH can be proposed to be simply the direct transfer of hydride from the C4 atom of the pyridine ring in NADH to the C atom of CO_2 (**Figure 1.2.1**). CO_2 and NADH are positioned in close proximity to facilitate the hydride transfer. After the generation of formate, NAD^+ with a bipolar conformation remains[16].

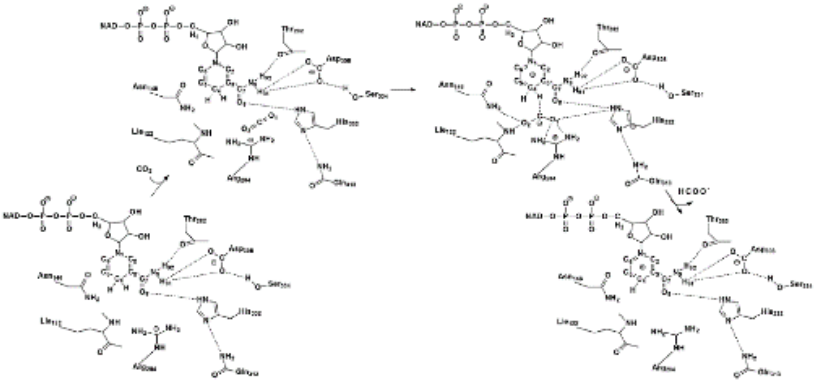

Figure 1.2.1 The mechanism of reduction of CO_2 to formate by NADH-dependent FateDH[16].

Intrigued by this route, several research groups, such as Baeg at al., Amao et al., Müller et al., Hirst et al. and Jiang et al., have utilized NADH-dependent FDH to convert CO_2 and have systematically investigated the catalytic performance[18-21]. Furthermore, to achieve high stability of enzymes, Jiang and co-workers encapsulated FDH into sol-gel carriers, including silica gels, alginate-silica gels, and so on[22].

In addition, converting CO_2 into methanol by a multi-enzyme system has been recognized as one of the most promising possible routes due to the following two attributes: (1) recycling of the ‘‘greenhouse’’ gas, and (2) the efficient production of sustainable or renewable fuel alternatives. In comparison to the fuels (CO, methane, etc.) produced from the single-enzyme route, the liquid methanol produced from the multi-enzyme reaction has a much higher energy capacity and is easier to transport. Yoneyama and co-workers were the first to report the successful electrochemical reduction of CO_2 to methanol with FDH and alcohol dehydrogenase (ADH) as the catalysts and pyrroloquinolinequinone (PQQ) as a cofactor[23]. This approach offered an easy route for the generation of methanol directly from CO_2 under mild conditions. As described in Yoneyama’s report, the type of cofactors greatly influenced the reduction behavior of CO_2, and selecting the appropriate cofactor can improve the rate of this multi-enzyme reaction[23]. Therefore they demonstrated that dehydrogenases can effectively catalyze the reduction of CO_2 in the presence of a suitable cofactor. Dave and co-workers reported an approach involving the consecutive reduction of CO_2 to methanol with three dehydrogenases as the catalysts and NADH as a cofactor[13]. The overall reaction process is shown in **Figure 1.2.2**[24].

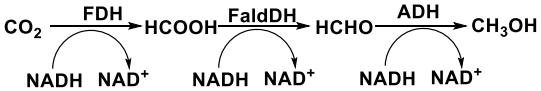

Figure 1.2.2. Reaction route of CO_2 to methanol catalyzed by three dehydrogenases (FateDH – formate dehydrogenase; FaldDH – formaldehyde dehydrogenase; ADH – alcohol dehydrogenase)[24].

Sequential reduction of CO_2 to formic acid, formaldehyde, and methanol can be achieved by using formate dehydrogenase (FDH), formaldehyde dehydrogenase (FaldDH), and alcohol dehydrogenase (ADH), respectively. In all three steps, NADH acted as a cofactor for each dehydrogenase-catalyzed reduction step. However, the yield of methanol achieved in this type of system is very low. The thermodynamic feasibility of this multi-enzyme reduction of CO_2 to methanol was investigated by Luo and co-workers[25]. They point out that the reaction rate of the first reaction in the sequence (CO_2 → formic acid), catalyzed by FDH, is much slower than its reverse reaction (formic acid → CO_2). Indeed, Rusching et al. reported that formic acid oxidation was 30 times faster than CO_2 reduction catalyzed by FDH[26]. Thus the CO_2 → formic acid step is likely to be a bottleneck in the reduction of CO_2 to methanol. In this regard, we envisioned that a higher yield of product, either formaldehyde or methanol, could be reached by increasing the concentration of substrate (CO_2) in the solution, which may drive the transformation of CO_2 to formic acid forward.

1.3 Ionic liquids

Ionic liquids (ILs) are low melting salts composed of cations and anions, which become liquid below a threshold temperature, normally 100ºC. ILs have been considered as green solvents which, due to their negligible vapor pressure, do not pollute the air. This property makes use of ILs attractive and offers the possibility of recycling ILs. Furthermore, ILs have high thermal stability, a wide liquid range, and good ability to dissolve a large number of substances, that are widely used in catalysis, synthesis, separation process. Additionally, the properties of ILs, such as water miscibility, polarity, and pH, can be changed according to our needs by combining different cations and anions or grafting a specific group onto the structure of IL[27].

Therefore ILs have been widely applied in sorption of CO_2, which is classified as physical and chemical sorption. Brennecke et al. have conducted pioneering work on the solubility measurements of CO_2 in 1-butyl-3-methylimidazolium hexafluorophosphate ([Bmim][PF_6]) at 298.2 K and pressure up to 40 MPa[28]. Since their work, a great deal of effort has been made to investigate the solvation of CO_2 in conventional ILs based on a physical mechanism (i.e., no

chemical reaction occurs), with the main focus being on understanding and improving CO_2 solubility. The research results indicate that the anion of ILs plays a key role in CO_2 solubility in ILs. Fluorination of the cations and anions increases CO_2 solubility, but cation fluorination has little effect while for the anion it is crucial. Cations with long alkyl chains or ether linkages improve CO_2 solubility[29]. However, the large-scale application of conventional ILs for CO_2 capture from flue gas is mainly hindered by their low capability due to the low physical adsorption interaction between ILs and CO_2. Therefore to overcome this limitation, functional ILs based on chemical reaction with CO_2 were designed by several researchers. For example, Davis et al. reported the first example of CO_2 chemisorption by a ‘‘task-specific’’ IL (TSIL) an amino group imidazolium cation the functionalized IL was able to capture 0.5 moles of CO_2 per mole of IL, which is higher than conventional IL (~ 0.15 mole) under ambient pressure[30]. Since this breakthrough in CO_2 absorption, there have been many derivative publications, including the strategies that use other functionalized ILs such as amino-based ILs, amino acid-based ILs, azolate-based ILs, phenolate-based ILs, and pyridine-containing ILs.

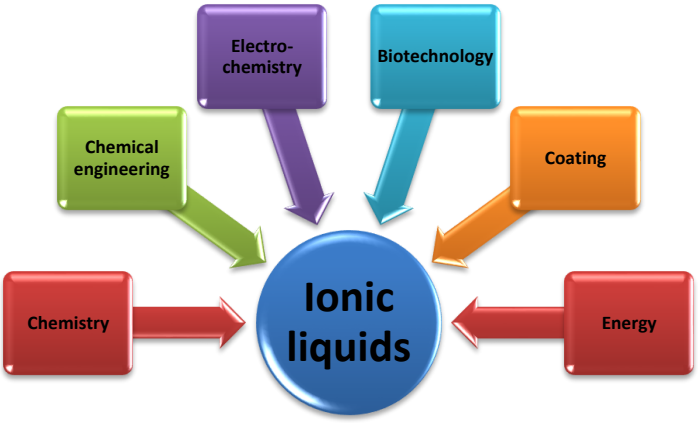

Figure 1.3.1 Applications of ILs are in various fields.

1.4 Biocatalysts in Ionic liquids.

Three biocatalysts, formate dehydrogenase, formaldehyde dehydrogenase, and alcohol dehydrogenase, were used for converting CO_2 to methanol. The detailed introduction of these enzymes is in follows.

Formate dehydrogenase (FDH): FDH is classified as EC 1.2.1.2 by the classification system of

the Enzyme Commission and is a homodimeric enzyme. It is active over a wide pH range (pH 5.5 – 11.0). The dimeric FDH used in this work is from the microorganism *Candida boidinii* and has 364 amino acids residues, corresponding to a molecular mass of 74 kDa for the two subunits. Its thermal inactivation temperature is 55ºC, with an isoelectric point (pI) of 5.4. The FDH monomer is arranged in two domains, called the "NAD binding domain" and the "catalytic domain". The "NAD binding domain" with the residues N119 to S313 displays a Rossmann fold structure. The "catalytic domain" is formed by the remaining residues and has a flavodoxin-like topology, with the conserved residues N119, V123, T256, D282, H311, S313, and G314. FDH is the lead enzyme in the biocatalytic system under study. FDH catalyzes the reversible reduction of CO_2 to formate, and in nature it also catalyzes the reverse reaction, oxidizing formate to CO_2. FDH is also a catalyst for coenzyme regeneration and plays a key role in some organisms. In methylotrophic microorganisms, FDH catalyzes the terminal step of catabolism of C1 compounds and has an important role in energy supply.

Formaldehyde dehydrogenase (FaldDH): FaldDH is classified as EC 1.2.1.46 by the classification system of the Enzyme Commission and is generally a homodimeric enzyme with a molecular mass of 150 kDa. Each subunit has 398 amino acid residues and two zinc ions. FaldDH is thermal stable up to 40 ºC, has a PI of 5.3, and is active from pH 5 to 10. Like in FDH, the FaldDH "NAD binding domain" from contains a Rossmann fold structure composed of a smaller domain of 167 residues - from residues L171 to Q337 - as shown in Figure 1.18 (b). The "catalytic domain" is the larger domain 231 residues S1 to I170 and residues T338 to A398. Two zinc ions per subunit are bound to the ligands within the "catalytic domain". The catalytic zinc is bound to a water molecule and three protein ligands from the catalytic domain C46, H67, and D169.

Alcohol dehydrogenase (ADH): ADH is classified as EC 1.1.1.1 by the classification system of the Enzyme Commission. The homotetrameric ADH has a pI between 5.4 and 5.8, an optimum pH between 8.6 and 9.0 and a molecular mass of 141 to 151 kDa. Each subunit is made up of 347 amino acid residues and 2 Zn atoms. The total molecular weight is 150kDa. The catalytic zinc is bound in the "catalytic domain" to C46, H67, and C174, and the structural zinc is bound to cysteines C 97, C100, C103 and C101.

In the PhD study, ILs were proposed as a reaction medium for capturing CO_2 and providing FDH with high substrate concentration. The requirement for selecting ILs was that ILs should not only have a major ability to capture CO_2 but also should provide an enzyme friendly environment. Nowadays, there are concerns about the toxicity of ILs, especially the imidazolium-based ionic

liquids. To overcome this concern, some other approaches are under development, such as the synthesis of ILs using biomolecules (amino acids, betaines, choline, etc.). Several proteins have been successfully dissolved in choline dihydrogen phosphate [CH][DHP] without denaturation[31]. 70% of the initial redox activity of Cytochrome C remained more than one year after dissolving in a mixture of [CH][DHP] and water. Amino acid-based ILs have been also reported as benign media in biomedical applications[32]. Biocompatible ILs could thus be promising substitutes for traditional buffers for conducting selected enzymatic reactions.

1.5 Cofactor NADH regeneration

In the cascade multi-enzymatic reaction to convert CO_2 to methanol, cofactor (NADH) acts as a sacrificial reagent for providing the reaction with hydrogen and electron. Considering its high cost, NADH regeneration was urgently required. Normally, NADH regeneration is accomplished by chemical, photochemical, electrochemical and enzymatic methods[8, 33, 34]. In these cases, chemical and electrochemical strategies often lack high selectivity and are frequently incompatible with the other components of enzymatic reactions. However, enzymatic NADH regeneration has only applied practically at industrial scale with almost 100% selectivity. In addition, sunlight is the most abundant renewable energy resource available on earth. NADH regeneration using a photochemical method with extremely low cost is a promising approach to achieve reduction of NAD^+. Therefore NADH regeneration with enzymatic and photochemical methods was mainly investigated in this research.

1.5.1 NADH regeneration with the enzymatic method.

Cofactor regeneration using enzymes has been considered a favourable system and has been the only one applied practically at industrial scale (**Figure 1.5.1**). One of the earliest examples demonstrating enzymatic NAD(P)H preparation from $NAD(P)^+$ was published in 1957 when alcohol dehydrogenase (ADH) was used by Rafter and Colowick[35]. Enzymatic approaches for regeneration offer excellent compatibility with the target bioconversions, given their comparable reaction conditions, i.e. low-temperature operation in an aqueous medium at a near neutral pH (5–9). Moreover, enzymatic regeneration is usually associated with high specific activity, exclusive selectivity toward the active NAD(P)H, and low energy consumption.

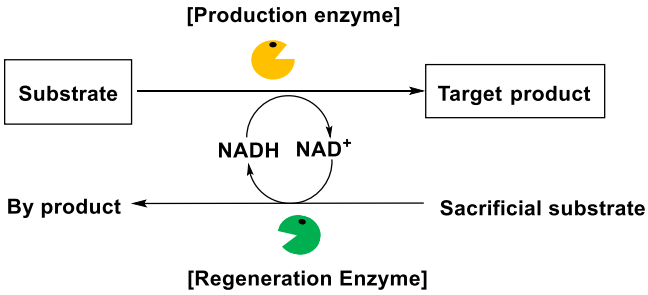

Figure 1.5.1. Schematic representation of NADH enzymatic regeneration.

As presented in Figure 1.5.1, additional regeneration enzyme and sacrificial substrate were coupled with the main enzymatic reaction. The most widely used enzymes for cofactor regeneration in commercial processes are glucose dehydrogenase (GDH) and formate dehydrogenase (FDH), whereas phosphite (PDH), alcohol (ADH), glucose 6-phosphate dehydrogenases, and hydrogenases have been tested at laboratory scale[36]. Among these enzymes, GDH (e.g. from Bacillus species) shows the highest activity (up to 550 U mg^{-1}; 1U = 1 mmol min^{-1}) and stability. Consequently, GDH has become the most widely used. FDH does have a unique feature in generating carbon dioxide (CO_2) as a gaseous byproduct (albeit release to the environment should be minimized) for simplified product separation, but its use is hampered by its low activity (~10 U mg^{-1}).

Although it is the only method industrially employed, cofactor regeneration using enzymes is far from perfect. First, significant quantities of water-soluble byproducts are generated. Additionally, base or acid is needed to maintain the optimal pH for retaining the enzymatic action. Other disadvantages are linked to high cost, enzyme instability, and complexity of product purification. As a result, research and development for cofactor regeneration are being driven systems that show high stability, sustainability, and enhanced downstream product separation and purification.

1.5.2 NADH regeneration with photochemical methods.

Comparing with conventional cofactor regeneration methods, such as the use of a secondary enzyme, have the drawbacks of biocatalyst instability, low specific activity, and limited application, nature hints at an alternative way to regenerate cofactor through the photosynthetic process, where transfer of photo-excited electron regenerates reducing power in the form of NAD(P)H for a further Calvin cycle. Photocatalytic NADH regeneration is attracting researchers who are borrowing the concept of natural photosynthesis that utilizes light-harvesting systems to

generate electrons and transfer electrons. There are three key components of biocatalytic artificial photosynthesis, namely electron donors, photosensitizers, and electron mediators for photo-induced electron transfer and cofactor regeneration (**Figure 1.5.2.**). The electron transfer cascade is initialized by photosensitization. Next, the excited electrons in the photosensitizer are transferred to the electron mediator, while electron donors compensate for electron depletion in the photosensitizers. Finally, the reduced mediators reduce the cofactors to drive the biocatalytic reaction with redox enzymes.

Efficient species of electron donors (mainly TEOA) and electron mediators (M, mainly $[Cp^*Rh(bpy)H_2O]^{2+}$) are involved in photocatalytic regeneration of NAD(P)H. This method strongly relies, however, on the high performance of photocatalysts. Most of these photosensitizers are small molecules (i.e. chlorophyll, proflavine, porphyrin), which show high efficiency in regenerating NADH. The author, Park and Lee et al., investigated six kinds of porphyrin derivatives with different metals at the center of the porphyrin molecule. The results showed that the metal zinc in the center of the porphyrin molecule could accelerate the rate of NADH regeneration[37]. During photocatalytic regeneration of NADH, the porphyrin absorbs photonic energy to create high-energy electrons, which are then transferred to M (the mediator $[Cp^*Rh(bpy)H_2O]^{2+}$). The activated M further transfers hydride (H^-) to NAD^+ in a single step, achieving the regeneration of NADH. Meanwhile, a sacrificial electron donor of TEOA reduces the oxidized porphyrin to avoid its degradation. The resulting yield of NADH achieved was 23%, which can also be applied in the enzymatic synthesis of glutamic acid[38].

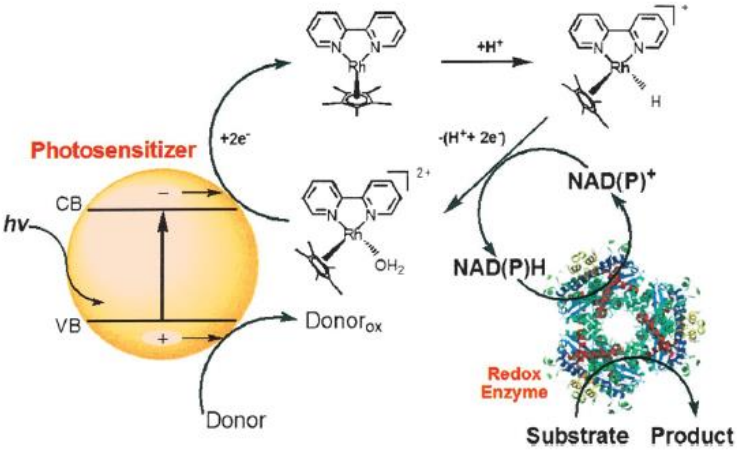

Figure 1.5.2. Photo-induced electron transfer in biocatalytic artificial photosynthesis through a cascade comprised of an electron donor, photosensitizer, Rh-based electron mediator (M), nicotinamide cofactor, and the redox enzyme[38].

1.6 Membrane bioreactor

A separation system platform is additionally required for the in-situ removal of products (methanol and NAD^+) and recycling of enzymes. Recently, inspired by membrane fouling mechanisms, we proposed a facile approach for constructing a membrane bioreactor (MBR) by immobilizing enzymes in membranes using "reverse filtration" of the enzyme solution[25]. In this system, the MBR is a combination of a separation process and a biocatalytic reaction, where the enzymes are confined on the reaction side and continuously reused[39, 40]. The separation usually involves the selective removal of products from the reaction, which reduces both the inhibition by the product and the formation of by-products or further degradation products[38, 39]. Thus, MBR not only provides higher reactor stability and productivity but also improved product purity and quality as well as waste minimization. The main problems facing the development of MBR technology on an industrial level are scale-up difficulties, the lifetime of the enzyme, the availability of pure enzyme at an acceptable cost, the necessity for biocatalysts to operate at low substrate concentrations, and microbial contamination. Special attention therefore needs to be paid to further studies on the design of bioprocesses particularly for large-scale production, and on the control of the reaction kinetic mechanisms and immobilization procedures.

To maintain the stability of such a complicated metabolic process, the cells also create appropriate physicochemical microenvironments to suppress the denaturation of enzymes. Membrane bioreactor technologies, as the name suggests, are those technologies that couple biological treatment with membrane separation. The application of enzymes in industrial processes is growing and the world market for industrial enzymes is estimated to reach USD 6.2 billion by 2020. High selectivity, low by-product formation and the ability to work at mild pH, temperature and pressure are some of the most important properties of enzymatic processes compared to chemical reactions. However, enzymes are costly and therefore it is necessary to develop technologies that enable reuse of the biocatalysts[39]. Retaining the enzymes in or via a membrane is one strategy that could enhance biocatalytic productivity and thus the economic potential of industrial enzymatic processes. Since membranes can be operated at moderate temperatures and pressures, finding compatible operating conditions for the reaction and separation should be possible. Moreover, the use of membranes for continuous product removal may even enhance the productivity of processes that suffer from product inhibition or are restricted by chemical reaction equilibria.

1.6.1. Membrane reactor configurations

A reactor equipped with a membrane capable of retaining enzymes while (partially) removing products is called a membrane bioreactor. Integrating biocatalytic conversion and separation in a membrane bioreactor allows process intensification and a reduction in equipment requirements. In general, there are two main configurations of the membrane bioreactor. One is that the membrane only serves as a selective barrier. In the other, the membrane serves as both barrier and support.

In the first bioreactor configuration, the free enzyme is recovered due to size exclusion or charge repulsion. For example, free sialidase was retained by 10 kDa membrane as reported by Zeuner et al. The sialidase was stable and a 9-fold increase in biocatalytic productivity was obtained compared to free sialidase in a simple batch reactor. In addition, CGTase was retained by a 32 kDa hollow fiber membrane and simultaneous removal of the product from the reactor.

In the second bioreactor configuration, the membrane functions both as a barrier and as a support for enzymes. The immobilization of enzymes can be achieved through covalent or non-covalent bonding or entrapment inside the pore matrix. Luo et al. investigated four different strategies for entrapment of alcohol dehydrogenase in various commercial polymeric membranes, namely normal mode (d), reverse mode (e), sandwich mode (f), switch mode (g), as shown in **Figure 1.6.2**. The highest conversion was obtained for a 30 kDa regenerated cellulose membrane configured in sandwich mode due to the highest retention of enzymes and improved biocompatibility of this membrane conformation[40].

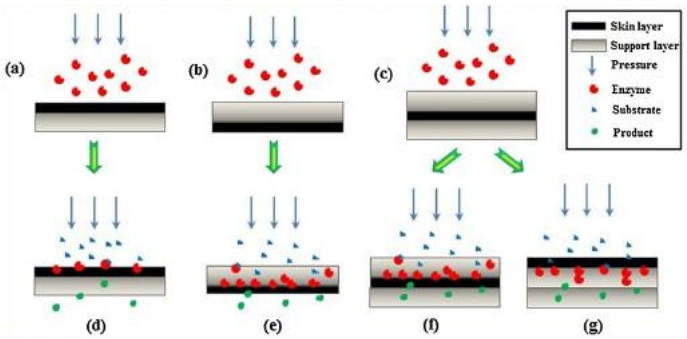

Fig. 1.6.2. Schematic diagram of membrane configurations for enzyme immobilization and subsequent catalytic reaction. (a) Enzyme immobilization in normal mode; (b) enzyme immobilization in reverse mode; (c) enzyme immobilization in "sandwich" mode; (d) enzymatic reaction in normal mode; (e) enzymatic reaction in reverse mode; (f) enzymatic reaction in "sandwich" mode; (g) enzymatic reaction in switch mode[40].

1.6.2. Fouling model

Fouling is one of the major challenges in most processes involving membrane technology and therefore membrane bioreactors. Fouling reduces the membrane performance in terms of both flux

and separation efficiency, which thus decrease during the filtration period. The adsorption or deposition of solutes in membranes could develop reversible fouling, also known as external fouling, and caused mainly by the formation of a gel or cake layer. Alternatively, irreversible fouling, also known as internal fouling, could develop due to internal pore blocking caused by complex interactions between the membrane and foulants such as hydrophobic or electrostatic adsorption, particle deposition or aggregation, hydrogen bonding, and bio-affinity. The different fouling mechanisms, such as complete blocking, standard blocking, intermediate blocking, and cake layer formation (see Table 1), can be described or evaluated by monitoring the flux and retention during filtration. Such fouling can result in significant increases in hydraulic resistance that potentially leads to transmembrane pressure (TMP) increases at constant flux or decreases of permeate flux at constant TMP.

Table 1. Summary of membrane fouling models and mechanism under constant pressure filtration.

Models	Equations	Schematic description
Complete blocking	$V = \frac{V_0}{k_b}[1 - \exp(-k_b t)]$	
Standard blocking	$V = (V_0 \mathrm{t})(1 + \frac{V_0 k_s}{A_0}\mathrm{t})^{-1}$	
Intermediate blocking	$V = \frac{1}{k_i}\ln(1 + k_i V_0 \mathrm{t})$	
Cake layer	$V = \frac{1}{V_0 k_c}(\sqrt{1 + (2k_c V_0^2 t)} - 1)$	

Nomenclature

V	filtrate volume, m^3	k_b	complete blocking constant, s^{-1}
t	filtration time, s	k_s	standard blocking constant, m^{-1}
V_0	initial volumetric flowrate, m^3/s	k_i	intermediate blocking constant,m^3
A_0	initial membrane frontal area, m^2	k_c	cake filtration blocking constant, s m^{-6}

In this study, we directed major efforts towards increasing the conversion of CO_2 and reducing the economic cost for sufficiently efficient enzymatic conversion of CO_2 to useful fuel to be of potential for industrial application. First, ILs were used as adsorbents of CO_2 in the enzymatic reaction to overcome the limitations of conventional buffer (low CO_2 solubility). Second, to attain economic feasibility, a membrane bioreactor as a novel platform provided enzymes with a microenvironment for recycling of enzyme. Furthermore, an artificial photocatalysis system for NADH regeneration was also established by using ILs as photosensitizer. Therefore we mainly focus on the use of ILs and membrane technology to achieve high conversion of CO_2 and lay the foundation of the industrial application.

Chapter 2 - Purpose, Hypotheses, and Objectives

2.1 Purpose and hypothesis

2.1.1 Conversion of CO_2 to formic acid (Paper 1)

Enzymatic hydrogenation of CO_2 to formic acid catalyzed by formate dehydrogenase (FDH) was achieved in vitro. In this system, reduced nicotinamide adenine dinucleotide (NADH) was used as the terminal electron donor for the enzymatic reaction. The low conversion is partly explained by the fact that the reaction rate of the first reaction in the sequence (CO_2 → formic acid), catalyzed by FDH, is much slower than its reverse reaction (formic acid → CO_2). In this regard, we envisioned that a higher yield of the product could be reached by increasing the concentration of substrate (CO_2) in the solution, which may drive the transformation of CO_2 to formic acid forward. Due to the high ability of ILs to capture CO_2, ILs could be promising substitutes for traditional buffers for conducting selected enzymatic reactions. ILs as co-solvent were therefore proposed as a means to increase the substrate (CO_2) of enzymatic reactions to promote reaction shift. Other questions that we tried to address in this study include the influence of ILs on enzymes and coenzymes. The general study hypotheses were the following:

- Introducing ILs enhances the conversion of CO_2 to level higher than in the traditional buffer by increasing the amount of substrate that is available.
- A proper IL concentration, in balance with enzyme activity and CO_2 concentration, can help increase the conversion of substrate into the desired products.

2.1.2 Conversion of CO_2 to methanol (Paper 2)

Another strategy to further increase conversion of CO_2 is to conduct a cascade multi-enzymatic reaction to convert CO_2 to methanol. Under such a process, the product of one reaction is converted in the subsequent reaction, switching the equilibrium to the right (CO_2 → formic acid → formaldehyde → Methanol). Sequential reduction of CO_2 to formic acid, formaldehyde, and methanol was achieved by using FDH, FaldDH, and ADH, respectively. According to the kinetic reaction reported by Luo et al., the reaction rate of the forward reaction (CO_2 → formic acid) is much lower than that of the reverse reaction (formic acid → CO_2). For the second enzyme, FaldDH, the reaction (formic acid → formaldehyde) was also found to be less efficient than the reverse reaction (formaldehyde → formic acid). However, for the third enzyme, ADH, the forward reaction (formaldehyde → methanol) was much more efficient than the reverse reaction (methanol →

formaldehyde). Thus, as regards this multi-enzymatic reaction, the first two reactions (CO_2 → formic acid, formic →acid formaldehyde) are less efficient than the third reaction (formaldehyde → methanol). Besides, the production of formaldehyde was delayed by a slow accumulation of formic acid from the first reaction (i.e. the second reaction required a threshold concentration of formic acid to be activated). Due to these two factors (unfavorable equilibrium rates and need for a minimum concentration threshold), the first reaction of this sequence (the one studied here) plays a decisive role in the conversion of CO_2 to methanol. So there is apparently still a lot of space for improvement of conversion of CO_2 to methanol. In this regard, we envisioned that a higher yield of product, either formaldehyde or methanol, could be reached by increasing the concentration of substrate (CO_2) with ILs in the solution; this modification could drive the transformation of CO_2 to formic acid forward.

As ILs are known to have a high ability for CO_2 capture, ILs are proposed as an alternative of conventional buffer for achieving high conversion of CO_2 by increasing CO_2 concentration. Most common ionic liquids for the biocatalytic reaction are imidazole-based and pyridine-based. Although they have major ability to capture CO_2, it raises some concern that they can be toxic to enzymes. Due in particular to similarities between the structure of imidazole and cofactor NADH, imidazole-based ILs easily occupy the position of NADH in enzymes, which leads to low catalytic efficiency of the enzymatic reaction. So, inspired by the biocompatibility of biological compounds and enzymes, we envisioned that ILs that were synthesized using biomolecules, such as choline and amino acids as feedstock, would probably provide a friendly environment for enzymes. Therefore four kinds of ILs choline amino acids were synthesized and evaluated in the enzymatic reaction.

In addition, it could also be helpful to further improve the reaction rate by incorporating a membrane in the system so that products would be immediately separated from the reaction, driving the equilibrium towards the formic acid. For in-situ removal of products (methanol and NAD^+) and recycling of enzymes, a separation system platform is additionally required. Inspired by membrane fouling mechanisms, we proposed a simple approach to immobilize enzymes in membranes using “reverse filtration” of the enzyme solution. In this system, enzyme immobilization was achieved by hydrogen bonding, entrapment, and hydrophobic or electrostatic adsorption. The activity of the immobilized enzymes could be maintained at approximately that of the free enzymes due to the mild and fast immobilization procedure. High enzyme loading could also be maintained, and the contact time for the substrate-enzyme complex could be controlled by changing pressure. Two general hypotheses were proposed for this study:

- The way the immobilization of the three enzymes involved in the cascade is performed influences the overall catalytic performance of the system.
- Enzyme activity and interaction enzyme-coenzyme improve when certain ILs are presented in the reaction mixture.

2.1.3 Conversion of CO_2 to methanol coupled with photocatalytic NADH regeneration.

Coenzyme (NADH) acts as a terminal electron donor and hydrogen donor in the cascade enzymatic reaction and is consumed stoichiometrically at each step. As a result, three molar equivalents of NADH are consumed to transform one molar equivalent of CO_2 in methanol. If the process is to be economically feasible, NADH regeneration is necessary. Besides, the byproduct NAD^+ was consumed for NADH regeneration, which is helpful for shifting the equilibrium of reaction forward. Inspired by the process in nature, an artificial photosynthesis system (APS) for NADH regeneration was one of the most promising solutions for utilizing limitless and renewable solar energy. For artificial photosynthesis, a photo-induced electron transfer reaction must occur via a light-harvesting photosensitizer in the presence of electron donors and an electron mediator, which can fulfill the role of both photosystems in natural photosynthesis. So far, a rhodium-based organometallic complex (**M**), like Cp*Rh(bpy)Cl (M, Cp* = pentamethylcyclodienyl; bpy = bipyridine), has been recognized as one of the most efficient mediators especially for photosynthesizing NADH from NAD^+. Although these biocatalytic APS systems have been considered as one the most promising solutions, a key factor limiting the success of APS is the lack of efficient photo-induced electron transfer within molecular systems. Furthermore, APS systems are fraught with problems such as poor photo-stability of the catalyst, a slow rate of electron transfer from the electron donor to the photosensitizer, and fast energy-wasting back-electron transfer from the catalyst to the photosensitizer.

Originating from the structural similarity between porphyrins and chlorophylls in natural photosynthesis systems, supramolecular systems containing porphyrins have been extensively explored as a biomimetic light-harvesting molecule to facilitate the generation of photo-excited electrons from an electron donor under irradiation. The natural light-harvesting pigments, porphyrins, are water-insoluble, and therefore cannot efficiently achieve high NAD^+ conversion in the presence of water-soluble electron mediators and electron donors. Recently, ionic liquids (ILs) have attracted interest in the electrochemistry field because they could reduce the energy barrier and enhance the rate of electron transfer. Inspired by this, porphyrins were therefore modified to porphyrin-based ILs, with carboxyl groups organic bromine salts, in this research. Several kinds

of porphyrin-based ILs as photosensitizer were therefore tested for their catalytic performance.

Next, we sought to develop a biocatalytic artificial photosynthesis platform for integration of cascade reduction of CO_2 to methanol coupled with photo-regeneration of NADH. In continuation of the use of the bioreactor membrane, we proposed co-deposition of dopamine with PEI on the support layer after enzyme immobilization in the membrane, and then photocatalyst was covalently bound through the amino group of dopamine and PEI. This method is simple, facile, stable, and less harmful to enzyme activity because it is biocompatible and noncovalent bonding is dominant. In addition, the polydopamine (PDA) with the PEI layer does not capture only CO_2 (the substrate of enzymatic reaction) and in-situ hydrogenation in the enzymatic system, but it also can enhance the electron layer. Therefore a membrane bioreactor as a novel platform was constructed as an integrated, biocatalyzed, artificial photosynthesis system by incorporating the photo-regeneration of NADH with the cascade reduction of CO_2 to methanol; the system may enhance photocatalysis efficiency. Three general hypotheses were proposed for this study:

- A porphyrin-based photosensitizer can be used to achieve highly efficient NADH regeneration.
- Co-deposition of layers of polydopamine and PEI should help enhance CO_2 capture, which in turn should enhance enzymatic hydrogenation of CO_2.
- Conversion of CO_2 coupled with NADH regeneration in an immobilization system provides higher conversion of CO_2 than the free enzyme system.

2.2 Research objectives

Specific objectives linked to each of the chapters are as follows:

Chapter 3 (Paper I): Ionic liquids as bifunctional cosolvents enhanced CO_2 conversion catalyzed by NADH-dependent formate dehydrogenase

- Assess the performance of different kinds of ILs in the catalytic efficiency of the cascade reaction in terms of conversion, and optimize the operational conditions of the selected ILs
- Evaluate the role of selected key variables i.e. temperature, concentration and pH on the enzymatic reaction and stability of coenzymes
- Investigate the stability of enzymes and coenzymes in selected ILs, and elucidate the mechanism of enzymatic action in such ILs

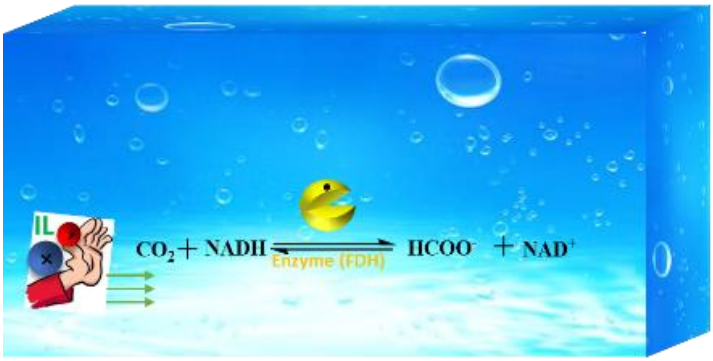

Chapter 4 (Paper II): An efficient ionic liquid–based platform for multi-enzymatic conversion of carbon dioxide to methanol

- Evaluate four kinds of biocompatible ILs in terms of catalytic performance in the cascade multi-enzymatic reaction, and also the ability of such ILs to capture CO_2
- Study the stability of the biocatalytic membrane, and the effect of pH and ILs concentration on the multi-enzymatic reaction performance
- Elucidate the mechanism of the enzymatic reaction in one of ILs that shows best catalytic performance

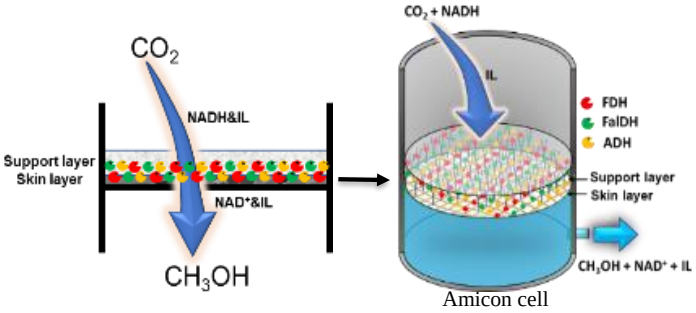

Amicon cell

Chapter 5 (Paper III): A biomimetic artificial photocatalysis membrane for the production of methanol from CO_2

- Develop a porphyrin-based IL system for photochemical NADH regeneration, and evaluate the catalytic performance of four porphyrin-based photosensitizers for NADH regeneration
- Design a photocatalysis membrane bioreactor for the cascade multi-enzymatic reaction coupled with NADH regeneration
- Elucidate the mechanism of the developed artificial photocatalysis membrane for the production of methanol from CO_2

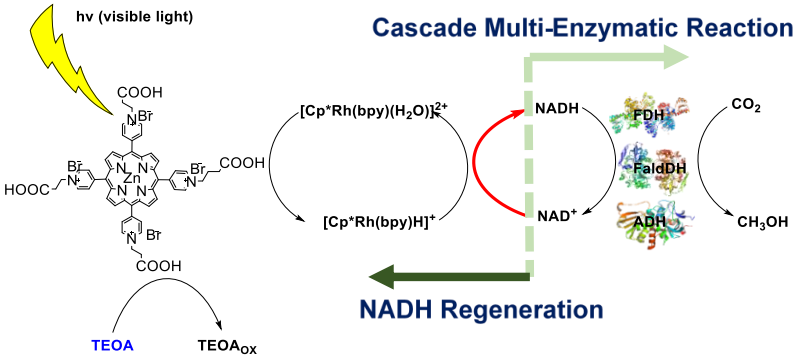

Overview of the Different Progressive Research Steps Carried out During the Thesis

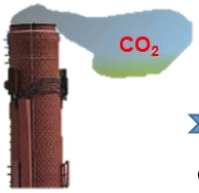

Capture CO_2 with ILs

I. Single enzymatic reaction (Paper 1)

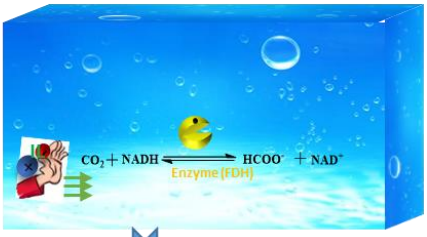

1. Paper 1

Single enzymatic reaction with ILs for increasing CO_2 concentration and stabilize coenzyme (NADH).

Conduct multi-enzymatic reaction by adding enzyme (ADH) for achieving high CO_2 conversion

II. Cascade Multi-enzymatic reaction in ILs (Paper 2)

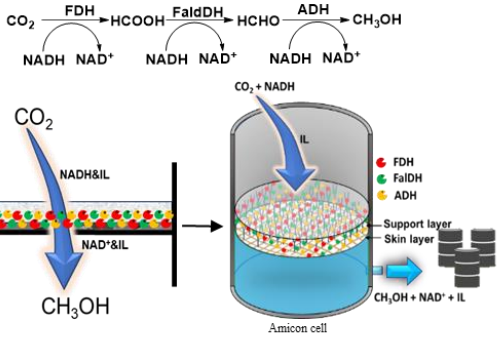

2. Paper 2

Cascade multi-enzymatic reacion using a membrane platform to overcome kinetic restrticion and ILs to increase CO_2 concentration and FDH activity.

A more economical NADH regeneration with photocatalysis

III. Cascade Multi-enzymatic reaction coupled with NADH regeneration (Paper 3)

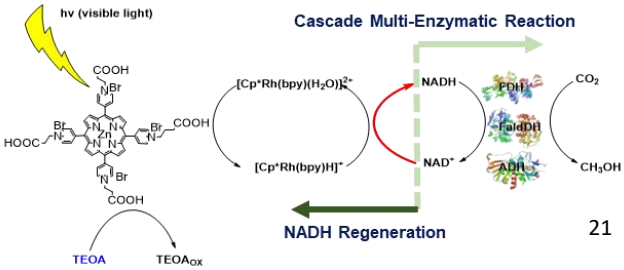

3. Paper 3

ILs as photosensitizer are used for NADH regeneration by photocatalytic reaction.

Chapter 3 – Ionic Liquids as Bifunctional Cosolvent Enhanced CO_2 Conversion Catalysed by NADH-dependent Formate Dehydrogenase

To achieve high conversion of CO_2, different kinds of ILs were evaluated in the enzymatic reaction. Detection method for formic acid is called method **N**, where the yield of formic acid is determined through quantifying the reduction of NADH. The assumption is that the formation of formic acid during the enzyme-catalyzed process would consume an equal-molar amount of NADH. Preliminary results show that Method **N** is not reliable because we found that NADH degradation occurs during enzymatic reaction. By investigating NADH degradation and its mechanism, selected ILs were shown to perform successfully to stabilize NADH and enhance conversion of CO_2. By optimizing the variables, such as IL concentration and solution pH, conversion of CO_2 in $BmimBF_4$ was increased 2-fold compared to the conversion of CO_2 in phosphate buffer.

3.1 Hypotheses

- Introducing ILs enhances the conversion of CO_2 to level higher than in the traditional buffer by increasing the amount of substrate that is available.
- A proper IL concentration, in balance with enzyme activity and CO_2 concentration, can help increase the conversion of substrate into the desired products.

3.2 Experimental considerations

In this research, two analytical methods were used for detecting the product of the enzymatic reaction. Since both analytical methods provided different results, the overestimation of the conversion determined by the method based on the degradation of NADH (so-called method N) was further investigated. The degradation mechanism of NADH was studied and the results showed that acidity in the medium was the main reason for the overestimation. Next, different kinds of ILs were tested, and the concentration of selected ILs was optimized.

Therefore this study was performed in a sequential fashion. First, the comparison between CO_2 conversion achieved by the systems with and without IL was quantified by two analytical methods. Next, once the mechanism responsible for the overestimation of one of the methods had been unraveled, the stability of the ILs was explored. Third, the enzymatic reaction with the selected ILs was conducted, and the concentration of ILs was optimized.

3.3 Highlights

The preliminary results of this study suggested that NADH was heavily degraded during enzymatic CO_2 conversion. This degradation was the cause of overestimation of the yield of the reaction and also harmed the conversion of CO_2 by reducing the amount of available cofactor. To avoid or alleviate NADH degradation, the reason for degradation was investigated, and the main reason was shown to be low pH; under acidic conditions, new species were confirmed by spectrophotometry (see **Figure 3.1**). Next, the degradation mechanism of NADH was also studied by NMR and DFT calculations, including detailed description of the structures generated during the transitional state. Finally, the NADH degradation pathway was determined (**Figure 3.2)**, confirming that the low energy barrier of the parallel reaction (leading to NADH degradation) was responsible for the loss of NADH.

Consequently, degradation of NADH in the reaction is mainly caused by the acidic gas, CO_2, which is also the substrate of the enzymatic reaction. Interestingly, ionic liquids ($BmimBF_4$) can alleviate degradation of NADH by capturing CO_2 as shown in **Figure 3.3**. Furthermore, by adjusting the concentration of ionic liquid in the buffer, maximum stabilization of NADH can be achieved along with enabling a higher CO_2 concentration for the reaction.

Since CO_2 conversion to formic acid is a bottleneck in multi-enzymatic reaction, this first reaction conversion step has to be enhanced to achieve high conversion of the cascade multi-enzymatic reaction. The study showed that, with the introduction of $BmimBF_4$ to stabilize NADH and increase CO_2 concentration, conversion of CO_2 to methanol in $BmimBF_4$ was more than two-fold compared to conversion in phosphate buffer (see **Table 3.1**).

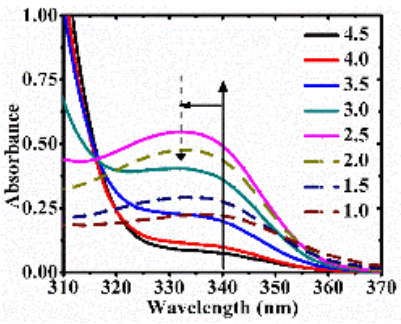

Figure 3.1 Degradation of NADH at pH 1.0 to 4.5. General conditions: NADH (1.4 mg, 2 mol); phosphate buffer (2 mL); 3h; 37 ºC

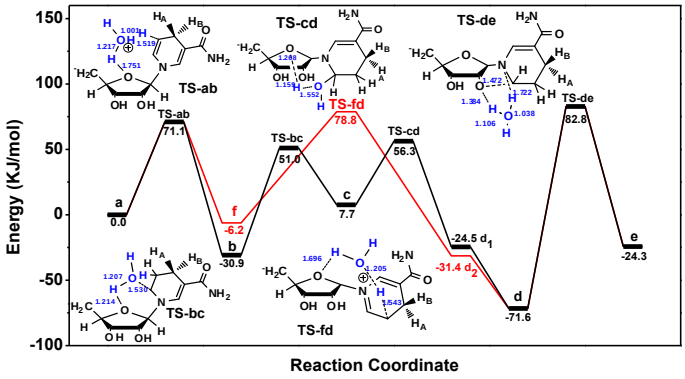

Figure 3.2 Calculated reaction pathways and energy profiles of the NADH model compound catalyzed by H_3O^+ at the B3LYP/6-311+g(d,p) level. The black and red curves denote two kinds of possible reaction pathways.

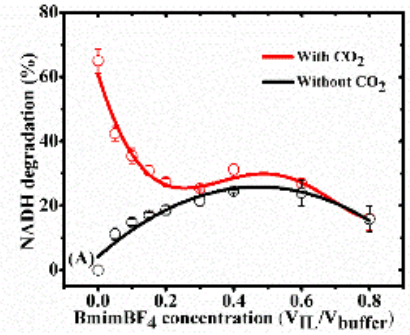

Figure 3.3 Degradation of NADH with CO_2 and without CO_2. General conditions: NADH in contained-BmimBF4 buffer for 3 hours at 37 °C; NADH (1.4 mg, 2 mol); CO_2 (1 bar); Buffer (2ml).

Table 3.1 Enzymatic conversion of CO_2 to methanol.[b]

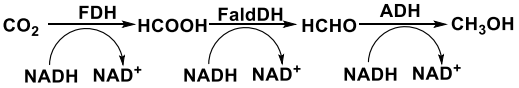

Entry	Solvent(v_{IL}/v_{buffer})	Yield of methanol (%) (SD)
1	Phosphate buffer	24.3 (± 1.2)
2	$BmimBF_4$ (10%)	20.2 (± 1.9)
3	$BmimBF_4$ (20%)	67.1 (± 2.4)
4	$BmimBF_4$ (40%)	48.3 (± 2.1)
5	$BmimBF_4$ (60%)	15.2 (± 2.6)

[b]**Reaction conditions:** FDH (3 µL, 0.075U/mL); FaldDH (0.2 mg, 0.1 U/ml); ADH (0.2 mg, 30U/ml); NADH (2 µmol, 1 mM); CO_2 (1 bar), buffer (100 mM phosphate, pH=7); 37 °C, 3h. Standard deviation (SD).

3.4 Significance of the study

This study is a significant contribution to the use of enzymes such as formate dehydrogenase in ionic liquids and paves the way for improving biocatalysts using ionic liquids. One of the main findings in this study is the degradation of NADH during the enzymatic reaction. Degradation of NADH not only contributed to the decreased conversion of CO_2 but also resulted in overestimation of CO_2 yield when measured using the typical absorbance of NADH (Method N).

To overcome the limitations of the method N, a colorimetric method (Method C) was developed for determining product concentration (formic acid). This alternative method was proven to be more direct and precise compared to method N. Therefore ILs were proposed as promising new kinds of buffers for enzymatic reactions to capture CO_2, which not only could increase the substrate (CO_2) of the enzymatic reaction but also prevent NADH degradation by CO_2. In this study, six kinds of ILs, BmimDCA, EmimOAC, $EmimBF_4$, $BmimBF_4$, BmimDMP and DBULat, were investigated. The performance of $BmimBF_4$ was excellent in the enzymatic reaction, and CO_2 conversion in this IL was more than two-fold compared to the conversion reached by the enzymatic reaction in phosphate buffer (traditional buffer).

3.5 Paper

This chapter was based on the following paper:

Ionic Liquids as Biofunctional Cosolvents Enhanced CO_2 Conversion Catalyzed by NADH-Dependent Formate Dehydrogenase

Zhibo Zhang, Bao-Hua Xu, Jianquan Luo, Nicolas von Solms, Hongyan He, Yaqin Zhang, Manuel Pinelo, and Suojiang Zhang

Published: accepted in Catalysts (3.465); Catalysts 2018, 8, 304.

catalysts

MDPI

Article

Ionic Liquids as Bifunctional Cosolvents Enhanced CO_2 Conversion Catalysed by NADH-Dependent Formate Dehydrogenase

Zhibo Zhang [1,2], Bao-hua Xu [2], Jianquan Luo [3], Nicolas Von Solms [1], Hongyan He [2], Yaqin Zhang [2], Manuel Pinelo [1,*] and Suojiang Zhang [2,*]

1 Department of Chemical and Biochemical Engineering, Building 229, Technical University of Denmark, 2800 Kgs. Lyngby, Denmark; zhiz@kt.dtu.dk (Z.Z.); nvs@kt.dtu.dk (N.V.S.)

2 Beijing Key Laboratory of Ionic Liquids Clean Process, Key Laboratory of Green Process and Engineering, State Key Laboratory of Multiphase Complex Systems, Institute of Process Engineering, Chinese Academy of Sciences, Beijing 100190, China; bhxu@ipe.ac.cn (B.-h.X.); hyhe@ipe.ac.cn (H.H.); zhangyq@ipe.ac.cn (Y.Z.)

3 State Key Laboratory of Biochemical Engineering, Institute of Process Engineering, Chinese Academy of Sciences, Beijing 100190, China; jqluo@ipe.ac.cn

* Correspondence: mp@kt.dtu.dk (M.P.); sjzhang@ipe.ac.cn (S.Z.); Tel.: +45-52-695821 (M.P.); +86-010-8262-7080 (S.Z.)

Received: 20 July 2018; Accepted: 26 July 2018; Published: 28 July 2018

Abstract: Efficient CO_2 conversion by formate dehydrogenase is limited by the low CO_2 concentrations that can be reached in traditional buffers. The use of ionic liquids was proposed as a manner to increase CO_2 concentration in the reaction system. It has been found, however, that the required cofactor (NADH) heavily degraded during the enzymatic reaction and that acidity was the main reason. Acidity, indeed, resulted in reduction of the conversion of CO_2 into formic acid and contributed to overestimate the amount of formic acid produced when the progression of the reaction was followed by a decrease in NADH absorbance (method **N**). Stability of NADH and the mechanism of NADH degradation was investigated by UV, NMR and by DFT calculations. It was found that by selecting neutral–basic ionic liquids and by adjusting the concentration of the ionic liquid in the buffer, the concentration of NADH can be maintained in the reaction system with little loss. Conversion of CO_2 to methanol in $BmimBF_4$ (67.1%) was more than twice as compared with the conversion attained by the enzymatic reaction in phosphate buffer (24.3%).

Keywords: ionic liquids; formate dehydrogenase; NADH degradation; CO_2 conversion

1. Introduction

Carbon dioxide (CO_2) emissions from combustion of fossil fuels and its greenhouse effect on climate change (i.e., global warming) are considered a current threat [1]. To minimize environmental problems and produce clean energy, efficient utilization of CO_2 and carbon regeneration has been the focus of a tremendous amount of research [2–5]. Recently, a strategy by which CO_2 may be converted enzymatically into valuable chemicals and fuels such as formate, formaldehyde and methanol has inspired many researchers [6,7]. Obert and Dave were the first to report a cascade reaction involving the three enzymes, formate dehydrogenase (FDH), formaldehyde dehydrogenase (FaldDH) and alcohol dehydrogenase (ADH), where the product of the first reaction serves as a substrate of downstream reaction. Reduced nicotinamide adenine dinucleotide (NADH) was used as the terminal electron donor for the enzymatic reaction [8]. However, enzymatic hydrogenation of CO_2 to formic acid (CH_2O_2), formaldehyde (CH_2O) and methanol (CH_3OH) is hampered by the low concentration of CO_2 that is available for the enzyme (formic acid dehydrogenase) in the reaction mixture. Such a low

concentration may account for the common poor conversion to formic acid and hence low conversions to formaldehyde and methanol [9].

CO_2 is highly soluble in ionic liquids (ILs) and solubility can be enhanced by adjusting the anion and substituents on the cation, for instance, by fluorinating the anion or cation components [10]. These components usually interact via electrostatic forces, van der Waals forces, hydrogen bonds and other physical effects, which can explain the high solubilities of CO_2 in ILs [11–13]. For instance, at just 50 bar of CO_2 pressure, CO_2 solubility was on the order of 50% mole fraction in [Bmim][PF_6] [14]. ILs have also been used in various enzymatic reactions involving enzymes such as lipases, celluloses, and alcohol dehydrogenases [15–17]. Zhao reported that ILs were successfully applied to lipase-catalysed enantioselective esterification reactions for enhancing the stability of lipase [18]. Zhu reported that cellulase showed a higher stability than cellobiase in aqueous 1-ethyl-3-methylimidazolium acetate media for cellulose hydrolysis [19].

It has therefore been promising to perform enzymatic conversion of CO_2 in an IL environment in order to obtain better conversion efficiency. For instance, Amado employed ILs as an alternative solvent for enzymatic conversion of CO_2 to methanol [20]. However, the conversion of CO_2 did not increase significantly compared to the result obtained with the conventional buffer. In addition, Nicole and Udo reported that the changes in concentration of ILs could cause FDH inactivation to different degrees [21]. Bahareh and Khosro reported that imidazolium based ILs had a severe inhibition effect on alcohol dehydrogenase [22]. Interestingly, however, the activity of enzyme was partially recovered with diluted ILs of less than 150 mM.

Former research has focused on the activity of dehydrogenase in ILs, but investigations on the interaction between ILs and coenzyme (NADH), which could play a key role in the conversion of CO_2, have been neglected. NADH is used not only as hydrogen donor in the reduction of CO_2 but is also employed for following the progression of the reaction and thus to quantify formate [23–25]. NADH has been reported to be unstable in dilute acid by Andersen and co-workers [26]. Incubation of N-substituted dihydropyridines in acid results in the addition of water across the 2–3 double bond to yield a 3-hydroxy-tetrahydropyridine. Alivisatos and co-workers have reported that the reaction of NADH in concentrated phosphate solutions first forms 3-hydroxy-tetrahydropyridine-tinamide which then subsequently rearranges to α-$O^{2'}$-3B-cyclo-tetrahydronicotinamide adenine dinucleotide [27]. Furthermore, the same mechanism of NADH degradation in acid has been demonstrated by Norman and co-workers [28]. Degradation of NADH in the enzymatic reaction not only reduced the conversion efficiency but also led to false results of high CO_2 conversion detected by method **N** (NADH UV absorption). Even though ILs were originally included in order to increase concentration of CO_2, degradation of NADH could counteract the positive effect and decrease the efficiency of the reaction. There is, therefore, a need to investigate the activity of NADH in ILs to understand the relationship between NADH and ILs. This will contribute to effectively conducting the enzymatic reaction and determining choice of ILs to be applied in the reaction. Additionally, UV–vis spectrophotometer is used for determination of the NADH concentration and yield of formate is calculated based on the amount of NADH consumed, which is defined as method **N** in this research. In order to find a precise method for detecting directly formate, a new detection method is thereby needed for determination of product (formate) in ILs in situations where NADH is degraded. The objective of present work was thus to find a suitable method to detect formate in the presence of ILs, and to investigate the activity of NADH in ILs to improve the efficiency of the enzymatic reaction and the potential for application of ILs for CO_2 capture.

2. Results and Discussion

2.1. Comparison between CO_2 Conversions with and without IL

Determining CO_2 conversion by monitoring decrease of UV–absorbance of NADH during reaction (due to conversion of NADH into NAD, method **N**) overestimated dramatically the actual conversion of

CO_2 provided by measuring formic acid concentrations (method **C**) (Table 1). The overestimation was much higher when the reaction was performed in buffer (~60 times) as compared to the reaction carried out in a 20/80 (*v*/*v*) $BmimBF_4$/buffer mixture (~8 times). The values of CO_2 conversion provided by the **C** method are within a typical range for such an enzymatic reaction under thermodynamic equilibrium, which generally has a low conversion rate (0.002 mM·min^{-1}) at the conditions at which the reaction was performed (FDH = 1.3 μg/mL, Tris-buffer, 37 °C) [9,29]. Liu and co-workers reported a higher conversion rate for the same reaction, however the final yield of formate was at the same level (less than 1%) [30]. The higher values of CO_2 conversion by the method **N** suggested a possible degradation of NADH during reaction, which was further investigated.

Table 1. Enzymatic Conversion of CO_2 to Formate [a].

$$CO_2 + NADH \xrightleftharpoons{\text{FDH (cat.)}} HCOO^- + NAD^+$$

Entry	IL (V_{IL}/V_{buffer})	NADH Conv. (%) (SD)	Yield of Formate (%) (SD)
		Method N	Method C
1	Phosphate buffer (Blank)	64.6 (±3.6)	1.1 (±0.5)
2	$BmimBF_4$ (20%)	25.4 (±3.2)	2.9 (±0.4)

[a] Reaction conditions: FDH (3 μL, 0.075 U/mL), NADH (2 μmol, 1 mM), CO_2 (1 bar), buffer (100 mM phosphate, pH = 7); 37 °C, 3 h. Standard deviation (SD).

2.2. Stability of NADH in ILs

In order to evaluate the effect of temperature on NADH degradation, aqueous mixtures of NADH with $BmimBF_4$ (5.0 equiv.) were monitored over a temperature range of 10–80 °C (Figure 1A). NADH degradation curves were obtained by in-situ UV–vis spectroscopy. A remarkable reduction of NADH was observed at temperatures higher than 40 °C, whereas such reduction was alleviated at lower temperature. At 37 °C, the kinetics approximated to a first order, with a degradation energy *Ea* of 59.5 kJ mol^{-1} (Figure S5) and a degradation rate constant of 6.2 × 10^{-3} (min^{-1}). Degradation decreased exponentially with time, with 90% loss of NADH after 4 h (Figure 1B), suggesting that the decrease of the NADH concentration in the presence of FDH was not only due to CO_2 conversion, but also due to spontaneous degradation under the reaction conditions. Degradation of NADH does not only contribute to overestimate the final CO_2 conversion, but also has a direct impact in the actual conversion of CO_2 into formic acid, as it also plays a role as a substrate in the CO_2 reduction. In order to find likely structure-performance relationships and verify whether NADH degradation occurs in a wide range of ionic liquids, degradation was evaluated in five imidazolium-based ILs, including $BmimBF_4$ (Table 2). Results showed that the stability of NADH was not only dependent on temperature, but also highly dependent on the pH value of the reaction mixture. Under neutral–basic conditions, almost no degradation of NADH was detected (entry 1). In contrast, the concentration of NADH diminished markedly at lower pH values, even under weakly acidic conditions (entry 2). Notably, under strongly acidic conditions, the absorption at 340 nm assigned to NADH disappeared coincidently with the appearance of a blue-shifted peak at 332 nm (entries 3~5 and Figure S8). Finally, when DBULat (known to be a strong basic IL) was employed rather than imidazolium-based ILs (entry 6), only traces of degradation of NADH were observed (non-statistically significant).

Table 2. Stability of NADH in aqueous ILs. [a]

Entry	IL	Residue$_{(NADH)}$ (%) (SD)	pH (SD)
1	BmimDCA	100.0 (±0.1)	7.8 (±0.20)
2	EmimOAc	12.8 (±3.1)	5.3 (±0.12)
3	EmimBF$_4$	0	2.8 (±0.18)
4	BmimBF$_4$	0	2.6 (±0.18)
5	BmimDMP	0	2.3 (±0.16)
6	DBULat	99.7 (±0.6)	9.3 (±0.14)

[a] General conditions: V_{IL}/V_{H2O}: 20%; NADH (1 mM); incubation time (3 h); temperature (37 °C); Residue$_{(NADH)}$ (%) determined by absorption at 340 nm through UV–vis spectrum. Standard deviations (SD).

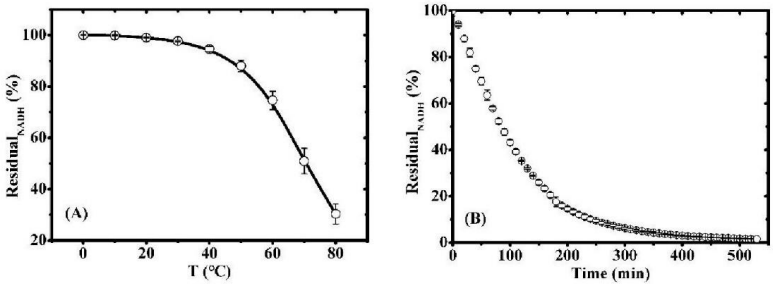

Figure 1. Study of the degradation of NADH in the presence of BmimBF$_4$. (**A**) Temperature-course plot (time interval: 10 min); (**B**) Time-course plot of degradation at 37 °C; General conditions: NADH (1.4 mg, 2 μmol); BmimBF$_4$ (2 μL, 5.0 equiv.); H_2O (2 mL).

2.3. Mechanism Discussion for NADH Degradation

2.3.1. Effect of Acidity on the Degradation of NADH

For better identification of the role of acidity on the stability of NADH during enzymatic conversion, the pH of the phosphate buffer was adjusted within the range 1.0–7.0 by the addition of proper amounts of phosphoric acid. In the absence of FDH, NADH degraded steadily with decreasing pH from 4.5 to 7.0 (Figure S6). At pH 4.5 (Figure 2), complete degradation of NADH was observed after incubation at 37 °C for 3 h. With further reduction of pH to 2.5, a new band appeared at 332 nm, and the intensity of this band gradually increased within the pH range from 2.5 to 4.5 (Figure 2). Such variation of NADH degradation with increasing acidity is consistent with our observations for the aqueous IL system in Table 2. However, the newly formed species referenced at 332 nm was not stable under extreme acid conditions, as indicated by decrease in absorbance at this wavelength over the pH range from 1.0 to 2.0.

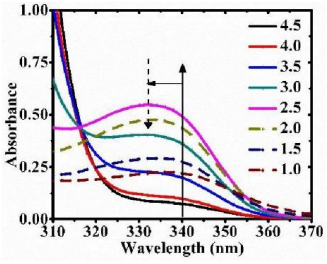

Figure 2. Degradation of NADH at pH 1.0 to 4.5. General conditions: NADH (1.4 mg, 2 μmol); phosphate buffer (2 mL); 3 h; 37 °C.

2.3.2. Proposed Mechanism of NADH Degradation

Next, a buffer solution (2 mL) of $BmimBF_4$ (V_{IL}/V_{buffer} = 20%) and NADH (2 μmol) was prepared separately for in-situ UV–vis detection at 37 °C. Initially, the presence of two typical peaks assignable to NADH at 340 and 260 nm, respectively, were observed. Upon incubation at 37 °C for 3 h, an apparent decrease of absorption intensity at 340 nm and a simultaneous increase of absorption at 260 nm were observed (Figure S7). Such variation was once referred to conversion of NADH to NAD^+ [31]. However, subsequent ^1H NMR studies indicated that a new compound besides NAD^+ was formed. Typical signals of the 1.4-dihyropyridine unit in NADH (δ: ppm), such as $C(1)H_2$ (2.80, 2.89), C(3)H (6.00) and C(4)H (6.95), were fully diminished (Figure 3, Figure S10, and Table S2). On the other hand, representative C-H signals of pyridinium in NAD^+ arising from hydride abstraction of NADH were not formed.

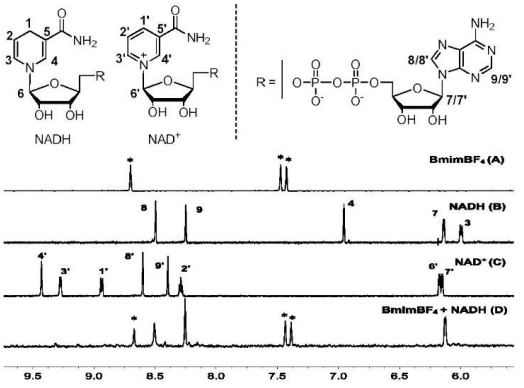

Figure 3. ^1H NMR (600 MHz, D_2O, 298 K) (δ: ppm) study. (**A**) $BmimBF_4$; (**B**) NADH; (**C**), NAD^+; (**D**) a mixture of NADH and $BmimBF_4$ (molar ratio = 1:1); * signals for imidazolium $C(sp^2)$-H.

DFT calculations were performed to better unravel the mechanisms of NADH degradation in acid conditions [32]. On the basis of previous literature and from our results, α-$O^{2'}$-3B-cyclo-tetrahydronicotinamide adenine dinucleotide was most likely to be the final product and two potential pathways for such conversion were evaluated (Figure S9) [28]. In pathway 1 (denoted by black curve in the Figure 4), the decomposition of NADH started with protonation of N-contained 6-membered ring at the β-position, with leading to **b**. Subsequent configuration isomerization from **b** to $\mathbf{d_1}$ occurred through ring opening of O-contained 5-memered ring. Specifically, nucleophilic addition of H_2O to the iminium cation in **b** at the α-position and C-O bond breaking of the O-contained 5-membered ring in the presence of acid affords **c**. Next, dehydrogenation of **c** at the α-position of N-contained 6-membered ring readily proceeded to generate $\mathbf{d_1}$ denoted as an α configuration, wherein the N-contained heterocycle and hydroxyl group sit at the same side of O-contained 5-memered ring (the β configuration in **b** represents two substituents sit at the opposite position). Optimization of the position of H_2O in the structure of $\mathbf{d_1}$ is found favourable in energy. A ternary hydrogen-bonding interaction system -OH/H_2O/C=O was found in the relatively stable structure **d**. Finally, the intra-molecular nucleophilic attack of OH to iminium cation of **d** affords the product **e**, coincidently with one equivalent of proton being released. In comparison to pathway 1, configuration isomerization occurred directly in pathway 2 (denoted by a red curve in the Figure 4) through an O-contained ring opening intermediate **f**. As a result, $\mathbf{d_2}$ with α configuration was formed, which is slightly different from $\mathbf{d_1}$ in pathway 1 imposed by the interaction mode towards H_2O. Subsequently, $\mathbf{d_2}$ follows the same route as $\mathbf{d_1}$ to eventually provide **e**. All structures of transitional state for both pathways are also optimized (Table S1). It suggests that the reaction leading to **d** is more likely following pathway 1 since its energy barrier step (**b**→**c**) is 3.1 kJ/mol lower as compared with that (**f**→$\mathbf{d_2}$) in pathway 2.

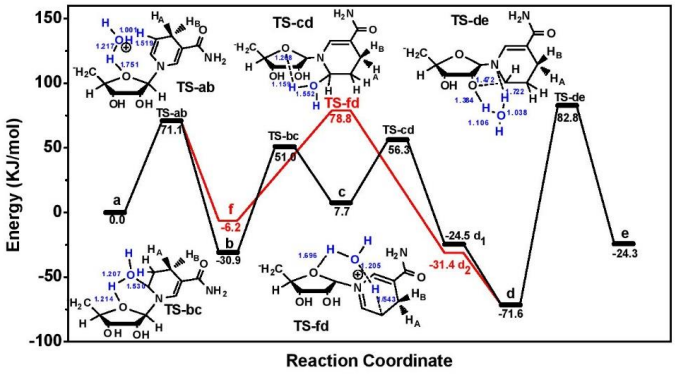

Figure 4. Calculated reaction pathways and energy profiles of the NADH model compound catalyzed by H_3O^+ at the B3LYP/6-311+g(d,p) level. The black and red curves denote two kinds of possible reaction pathways.

2.4. Enzymatic Reaction in BmimBF$_4$ and BmimDCA

2.4.1. Effect of NADH Degradation in BmimBF$_4$ and BmimDCA

pH was found to be the most crucial factor leading to NADH degradation. However, variation of pH value cannot be avoided given the intrinsic nature of the reaction. For instance, both the absorption of CO_2 into the aqueous solution and the formation of formic acid will result in a more acidic environment [33]. Interestingly, the results indicated that with CO_2, NADH degradation is significantly prevented in the presence of contained-BmimBF$_4$ buffer (Table 1, method **N**). To clarify and rationally understand this phenomenon, the influence of CO_2 absorption with and without BmimBF$_4$ on NADH degradation and pH variation were evaluated and compared. Experiments of NADH degradation were conducted in an aqueous solution with a range of volume ratio of BmimBF$_4$ to buffer in the presence or absence of CO_2 (Figure 5A). The degradation concentration-course plot (in black) in the case of without CO_2 offers a downward parabola. It demonstrated that the maximum degradation of NADH in a combination of BmimBF$_4$ and buffer is 22% when a volume ratio of 40% (V_{IL}/V_{buffer}) is reached. The in-situ pH evaluation of the solution (Figure 5B) indicated this degradation follows a function of pH value variation, with maximum degradation appearing at the lowest pH value. The pH value variation was attributed to the hydrolysis of BmimBF$_4$, which may occur with a different extent under these conditions [34]. On the other hand, a significant degradation of NADH was detected in the buffer as soon as CO_2 (1 bar) was introduced (Figure 5A, plot in red). Interestingly, such a degradation was gradually relieved with loading BmimBF$_4$ from 0 to 20% (V_{IL}/V_{buffer}). The stabilization has been attributed to the formation of ternary aggregates (CO_2/IL/H_2O), wherein the amphipathic BmimBF$_4$ could self-assemble at the interface between the nonpolar CO_2 and the aqueous phase [35]. In this manner, formation of carbonic acid was therefore avoided. Specifically, both hydrolysis of BmimBF$_4$ and the formation of carbonic acid will be inhibited when a higher ratio of V_{IL}/V_{buffer} was launched, with less NADH degradation.

In contrast, NADH is much more stable in the presence of a weakly basic BmimDCA (Figure 6A, plot in black), with less than 10% degradation of NADH occurring at maximum. The pH value of the solution progressively increased when the ratio of BmimDCA was increased (Figure 6B). A similar stabilization of NADH with IL functioning as the surface-active molecule was also observed when CO_2 was introduced (Figure 6A, plot in red).

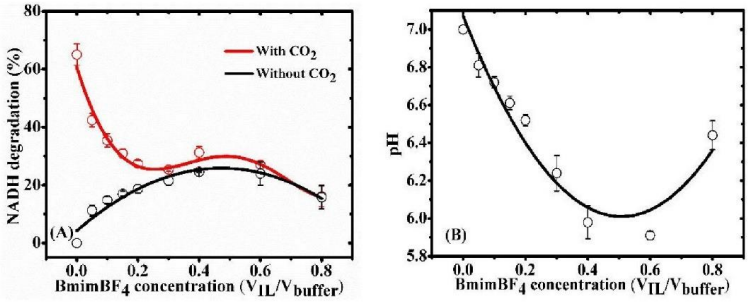

Figure 5. Effect of CO_2 on the degradation of NADH in $BmimBF_4$. (**A**) Degradation of NADH with CO_2 and without CO_2; (**B**) pH of solution at different concentrations of $BmimBF_4$; General conditions: NADH in contained-$BmimBF_4$ buffer for 3 h at 37 °C; NADH (1.4 mg, 2 μmol); CO_2 (1 bar); Buffer (2 mL).

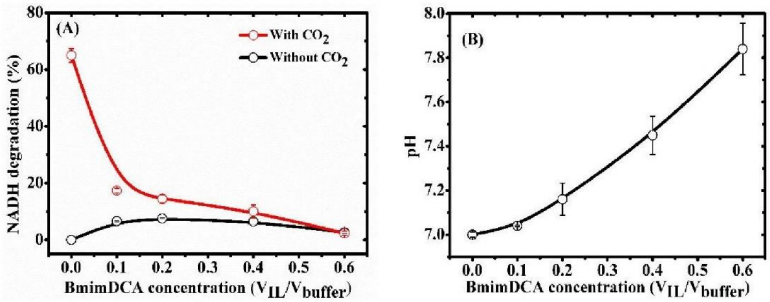

Figure 6. Effect of CO_2 on degradation of NADH in BmimDCA. (**A**) Degradation of NADH with CO_2 and without CO_2; (**B**) pH of solution at different concentrations of BmimDCA; General conditions: NADH in contained-BmimDCA buffer for 3 h at 37 °C; NADH (1.4 mg, 2 μmol); CO_2 (1 bar); Buffer (2 mL).

2.4.2. Enzymatic Reaction in $BmimBF_4$ and BmimDCA

Enzymatic conversion of CO_2 to formate in phosphate buffer systems (IL/buffer) consisting of two alternative ILs at different ratios was subsequently conducted (Table 3). As indicated by experiments of NADH degradation (Figure 5A), it will lead to not only the formation of a ternary aggregates (CO_2/IL/H_2O) but also hydrolysis of $BmimBF_4$ when the concentration of $BmimBF_4$ was increased within a range (V_{IL}/V_{buffer} < 50%), which actually has an opposite effect towards the degradation of NADH. Therefore, taking these premises into consideration, to find a proper concentration of $BmimBF_4$ is required to attain an optimized conversion with least NADH being degraded (entry 3). In contrast to the acidic $BmimBF_4$, NADH was more stable in the presence of basic BmimDCA. And the conversion of NADH monotonously decreased when the concentration of BmimDCA was increased (entries 6~9), but the yield of formate increased with the concentration of BmimDCA from 10% to 40%, and dropped to the lowest at 60% BmimDCA.

It is well known that water with small amounts of salts is considered to be the best media for proteins. However, high concentration of ILs (salts) can cause conformational changes of peptide chains that can result in enzyme denaturation [36]. Crystallisation and aggregation behaviour of proteins change dramatically upon increasing concentrations of ILs. Indeed, in pure ILs, enzymes can hardly be dissolved in homogenous phase without denaturation. In this enzymatic reaction, increasing concentration of IL to absorb CO_2 is expected to influence negatively the activity of the enzyme. This can explain that CO_2 conversion achieved the highest value when only a 20% of $BmimBF_4$ was used.

Table 3. Enzymatic Conversion of CO_2 to Formate [a].

Entry	Solvent (*v*/*v*)	NADH Conv. (%) (SD)	Yield of Formate (%) (SD)	pH (SD)	
		Method N	Method C	Before	After
1	Phosphate buffer	64.6 (±3.6)	1.1 (±0.5)	7.0 (±0.04)	5.6 (±0.08)
2	10% $BmimBF_4$	46.8 (±2.3)	0.2 (±0.3)	6.7 (±0.08)	6.2 (±0.12)
3	20% $BmimBF_4$	25.4 (±3.2)	2.9 (±0.4)	6.5 (±0.06)	6.0 (±0.16)
4	40% $BmimBF_4$	36.3 (±2.0)	2.3 (±0.4)	6.0 (±0.05)	5.8 (±0.18)
5	60% $BmimBF_4$	24.6 (±3.0)	0.6 (±0.3)	5.9 (±0.05)	5.6 (±0.19)
6	10% BmimDCA	34.0 (±3.9)	0.4 (±0.2)	7.0 (±0.04)	6.6 (±0.12)
7	20% BmimDCA	16.2 (±1.3)	1.5 (±0.5)	7.2 (±0.06)	6.5 (±0.14)
8	40% BmimDCA	4.9 (±2.8)	1.8 (±0.5)	7.5 (±0.08)	6.5 (±0.19)
9	60% BmimDCA	1.6 (±1.4)	0.2 (±0.2)	7.8 (±0.09)	6.8 (±0.20)

[a] Reaction conditions: FDH (3 µL, 0.075 U/mL), NADH (2 µmol, 1 mM), CO_2 (1 bar), buffer (100 mM (Na_2HPO_4:NaH_2PO_4 = 39:61 (mol/mol)), 2 mL); 37 °C, 3 h. [a] Enzymatic reaction was repeated three times and standard deviations (SD) were calculated that presented in the Table 3. pH value of reaction mixture was added before and after saturating CO_2.

2.4.3. Multi-Enzymatic Reaction of Converting CO_2 to Methanol in $BmimBF_4$

Sequential reduction of CO_2 to formic acid, formaldehyde and finally methanol is limited by the low reaction rate of the first reaction in the sequence (CO_2 → formic acid), which is much lower than that of the reverse reaction (formic acid → CO_2) [9]. Indeed formic acid oxidation was 30 times faster than CO_2 reduction catalyzed by FDH [29]. For the second enzyme, FaldDH, the reaction (formic acid → formaldehyde) was also found to be less efficient than the reverse reaction (formaldehyde → formic acid). However, for the third enzyme, ADH, the forward reaction (formaldehyde → methanol) is much more favorable than the reverse reaction (methanol → formaldehyde). Therefore, to make this multi-enzymatic reaction efficient, formic acid and formaldehyde have to be consumed by the next sequential reaction, in order to shift the equilibrium of the cascade reaction and eventually achieving high conversion of CO_2 to methanol (Table 4, entry 1).

Table 4. Enzymatic Conversion of CO_2 to Methanol [b].

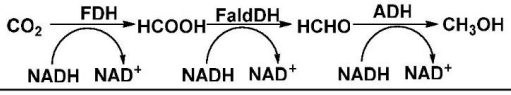

Entry	Solvent (v_{IL}/v_{buffer})	Yield of Methanol (%) (SD)
1	Phosphate buffer	24.3 (±1.2)
2	$BmimBF_4$ (10%)	20.2 (±1.9)
3	$BmimBF_4$ (20%)	67.1 (±2.4)
4	$BmimBF_4$ (40%)	48.3 (±2.1)
5	$BmimBF_4$ (60%)	15.2 (±2.6)

[b] Reaction conditions: FDH (3 µL, 0.075 U/mL), FalDH (0.2 mg, 0.1 U/mL), ADH (0.2 mg, 30 U/mL), NADH (2 µmol, 1 mM), CO_2 (1 bar), buffer (100 mM phosphate, pH = 7); 37 °C, 3 h. Standard deviation (SD).

Another strategy to further increase conversion of CO_2 to methanol is to enhance CO_2 solubility, as low CO_2 solubility in water would also result in low formic acid concentration. As a consequence, production of formaldehyde is prevented, as the second sequential reaction requires a threshold concentration of formic acid to be activated [24]. Both factors (unfavourable equilibrium rates and need of a minimum concentration threshold) make the first reaction of the sequence (the one studied here) to play a decisive role on conversion of CO_2 to methanol. Addition of $BmimBF_4$ helps enhance the conversion in the first reaction by both stabilizing NADH and also increasing CO_2 solubility. Indeed, the yield of methanol when the reaction was conducted in 20% $BmimBF_4$ was two times higher than in the phosphate buffer.

Other authors followed other strategies to increase conversion. For example, Ober and Dave immobilized the three enzymes in silica sol-gel matrixes, confining and reducing the volume of the

phosphate solution (pH = 7). NADH (1 mM) in these buffers was separately incubated at 37 °C for 3 h. Residue NADH is measured at 340 nm by an in-situ UV–vis spectroscopy (Figures 2 and S6).

3.6. NMR for NADH Degradation in $BmimBF_4$

Equimolar of NADH and $BmimBF_4$ was mixed in deuteroxide. The mixture was heated at 50 °C for 3 h and then the product was purified through extraction of methylene dichloride. After removing methylene dichloride in a vacuum oven at 50 °C for 3 h, solid powder was obtained and detected by NMR.

3.7. Effect of NADH Degradation in $BmimBF_4$ and BmimDCA

Solutions (2 mL) of $BmimBF_4$ with phosphate buffer in different concentration were prepared, namely, 0%, 5%, 10%, 15%, 20%, 30%, 40%, 60%, and 80% (V_{IL}/V_{buffer}). In the reactor, NADH (1 mM) in the prepared solution was bubbled with CO_2 for 5 min to remove the residual air, after which the pressure was adjusted to 1 bar. The reactor was positioned in water bath at 37 °C for 3 h. Without CO_2, it is no need to press CO_2 in the reactor. In the same way, solutions (2 mL) of BmimDCA with phosphate buffer in different concentrations were prepared, namely, 0%, 10%, 20%, 30%, 40%, and 60% (V_{IL}/V_{buffer}). In the reactor, NADH (1 mM) in the solution was bubbled with CO_2 for 5 min to remove the residual air, after which the pressure was adjusted to 1 bar. The reactor was positioned in water bath at 37 °C for 3 h. Furthermore, pH value of each solution was measured by pH meter (298.5 K, Mettler Toledo FE20, Mettler Toledo, Zurich, Zurich State, Switzerland) before starting reaction.

3.8. Enzymatic Reaction in $BmimBF_4$ and BmimDCA

Solutions (2 mL) of $BmimBF_4$ with phosphate buffer in different concentrations were prepared, namely, 0%, 10%, 40%, and 60% (V_{IL}/V_{buffer}). Solutions (2 mL) of $BmimBF_4$ with phosphate buffer were prepared in the same way. Procedure of enzymatic reaction is as same as described above (General procedure).

3.9. Analytical Method

Two methods, NADH (named as **N**) and colorimetric detection (named as **C**), were evaluated to determine the yield of formate product. The details of these methods are as follows:

*3.10. Method **N** for Determination Concentration of NADH*

Method **N** is an indirect method where the yield of formate is determined through quantifying reduction of NADH. It can be easily monitored by UV–vis spectroscopy at 340 nm referenced to NADH [23]. The assumption is that formation of formate during the enzyme-catalysed process would consume an equal-molar amount of NADH. The concentration of NADH was quantified by absorbance measurements, which was monitored at 340 nm by an in-situ UV–vis spectroscopy. After the enzymatic conversion to formate was completed, 0.5 mL of sample was taken and diluted with 1.5 mL of water. After dilution of NADH solution, absorbance at 340 nm is below 2 that is more precise. Then 2 mL of the solution was pipetted into a 10 mm quartz cell. The photometric measurement was monitored at 340 nm using a UV–vis spectrophotometer (Shimadzu UV, 2550 spectrophotometer Shimadzu Corporation, Tokyo, Tokyo metropolitan, Japan). The standard calibration curve is presented in Figure S1.

3.11. Method C for Determination Concentration of Formate

Method **C** was originally used for detecting formate in products from fermentation [37]. The assumption is that a complex compound, recorded at 515 nm using UV–vis spectroscopy, would be formed by the reaction of formate with a mixture of citric acid, isopropanol, acetic anhydride, sodium acetate in an appropriate ratio [38]. The yield of formate is then directly determined. First, 3.5 mL of 100% acetic anhydride, 50 µL of 30% (*w*/*v*) sodium acetate, and 1 mL of 2-propanol solution

containing 0.5% (*w*/*v*) citric acid and 10% (*w*/*v*) acetamide were added in a 10 mL vial. Then 0.5 mL of sample was added to this assay solution and incubated for 90 min at 25 °C. Finally, the absorbance was determined at 515 nm using a UV–vis spectrophotometer. The formate standard calibration curve was prepared against the appropriate concentrations of formate (Figures S2–S4). 500 µL of sample was used for the colorimetric assay.

3.12. GC for Determination Concentration of Methanol

A Hewlett Packard HP6890 gas chromatograph (Hewlett-Packard Company, Palo Alto, CA, USA) (GC) equipped with a FID (250 °C) and a Restek XTI-5 column (30 m × 0.25 mm i.d., film thickness 0.25 mm) was used for methanol concentration by using ethyl acetate as an internal standard. The carrier gas was N_2 with a flow rate of 0.4 mL min^{-1}. The injector temperature was 150 °C and the injection volume was 1 mL. Methanol GC chromatograms were calibrated with 0.01–1 mM methanol solution in 0.1 M pH 7.0 phosphate buffer.

3.13. ^1H Nuclear Magnetic Resonance Measurements

Spectra were recorded at 298 K on a Bruker av-600 MHz spectrometer (Bruker, Bilka, MA, USA) operating at 600 MHz. Deuterium oxide was as solvent.

4. Conclusions

In summary, we demonstrated that NADH degradation is unavoidable due to the presence of acid gas during enzymatic CO_2 conversion, which impedes the CO_2 conversion and overestimates the conversion when the absorbance of NADH is used as a method of detection. The mechanism of NADH degradation was investigated by UV, NMR, and DFT calculation and all methods suggested that the occurrence of acid in the reaction mixture is the main contributing factor to the degradation observed. By selecting neutral–basic ionic liquids and adjusting the concentration of ionic liquids in the buffer, stabilization of the cofactor (NADH) can be achieved, along with enabling a higher CO_2 concentration in the buffer. Finally, CO_2 conversion was more than twice as compared with the conversion reached by the enzymatic reaction in a phosphate buffer (traditional buffer). This study is a significant contribution to the use of enzymes like formate dehydrogenase in ionic liquids and paves the way for improving biocatalysts using ionic liquids.

Supplementary Materials: The following are available online at http://www.mdpi.com/2073-4344/8/8/304/s1, **Figure S1**. Standard calibration curve for NADH method. **Figure S2**. Standard calibration of formate for colorimetric method in buffer. **Figure S3**. Standard calibration curve of formate for colorimetric method in BmimBF4. **Figure S4**. Standard calibration curve of formate for colorimetric method in BmimDCA. **Figure S5**. Arrhenius plots for degradation of NADH in BmimBF4 as temperature increases. **Figure S6**. NADH degrades in phosphate buffer whose pH in range from 7.0 to 4.5. **Figure S7**. NADH degrades in contained-BmimBF4 reaction. **Figure S8**. NADH degrades in ILs. **Figure S9**. Two possible pathway (red and black) for NADH degradation mechanism proposed by the Norman and co-worker. **Figure S10.** 1H NMR (600 MHz, D2O, 298K) (δ: ppm). (a) BmimBF4; (b) NADH; (c), NAD+; (d) a mixture of NADH and BmimBF4 (molar ratio = 1:1); D2O was used as the solvent. **Table S1** Structure for the NADH and its derivatives. **Table S2**. Summary of chemicals NMR data.

Author Contributions: Z.Z., B.-h.X. and J.L. conceived and designed the experiment, performed the experiments, and analysed the data. M.P., N.V.S. and S.Z. wrote the paper and reviewed drafts of the paper. H.H. and Y.Z. conceived and designed the simulation experiment, analysed the data and reviewed drafts of the paper.

Acknowledgments: The authors are thankful for support from National Science Foundation of China (U1704251) and (U1662133), CAS 100-Talent Program (2014).

Conflicts of Interest: The authors declare no conflict of interest.

References

1. Shi, J.F.; Jiang, Y.J.; Jiang, Z.Y.; Wang, X.Y.; Wang, X.L.; Zhang, S.H.; Han, P.P.; Yang, C. Enzymatic conversion of carbon dioxide. *Chem. Soc. Rev.* **2015**, *44*, 5981–6000. [CrossRef] [PubMed]

2. He, M.Y.; Sun, Y.H.; Han, B.X. Green carbon science: Scientific basis for integrating carbon resource processing, utilization, and recycling. *Angew. Chem. Int. Ed.* **2013**, *52*, 9620–9633. [CrossRef] [PubMed]
3. Xu, B.H.; Wang, J.Q.; Sun, J.; Huang, Y.; Zhang, J.P.; Zhang, X.P.; Zhang, S.J. Fixation of CO_2 into cyclic carbonates catalyzed by ionic liquids: A multi-scale approach. *Green Chem.* **2015**, *17*, 108–122. [CrossRef]
4. Cui, G.K.; Wang, J.J.; Zhang, S.J. Active chemisorption sites in functionalized ionic liquids for carbon capture. *Chem. Soc. Rev.* **2016**, *45*, 4307–4339. [CrossRef] [PubMed]
5. Hao, L.D.; Zhao, Y.F.; Yu, B.; Yang, Z.Z.; Zhang, H.Y.; Han, B.X.; Gao, X.; Liu, Z.M. Imidazolium-based ionic liquids catalyzed formylation of amines using carbon dioxide and phenylsilane at room temperature. *ACS Catal.* **2015**, *5*, 4989–4993. [CrossRef]
6. Dominguez-Benetton, X.S.S.; Satyawali, Y.; Vanbroekhoven, K.; Pant, D. Enzymatic electrosynthesis: An overview on the progress in enzyme-electrodes for the production of electricity, fuels and chemicals. *J. Microb. Biochem. Technol.* **2013**, *S6*, 007.
7. Srikanth, S.G.Y.A.; Vanbroekhoven, K.; Pant, D. Enzymatic electrosynthesis of formic acid through carbon dioxide reduction in a bioelectrochemical system: Effect of immobilization and carbonic anhydrase addition. *ChemPhysChem* **2017**, *18*, 3174–3181. [CrossRef] [PubMed]
8. Obert, R.; Dave, B.C. Enzymatic conversion of carbon dioxide to methanol: Enhanced methanol production in silica sol-gel matrices. *J. Am. Chem. Soc.* **1999**, *121*, 12192–12193. [CrossRef]
9. Luo, J.Q.; Meyer, A.S.; Mateiu, R.V.; Pinelo, M. Cascade catalysis in membranes with enzyme immobilization for multi-enzymatic conversion of CO_2 to methanol. *New Biotechnol.* **2015**, *32*, 319–327. [CrossRef] [PubMed]
10. Zhang, X.P.; Zhang, X.C.; Dong, H.F.; Zhao, Z.J.; Zhang, S.J.; Huang, Y. Carbon capture with ionic liquids: Overview and progress. *Energy Environ. Sci.* **2012**, *5*, 6668–6681. [CrossRef]
11. D'Alessandro, D.M.; Smit, B.; Long, J.R. Carbon dioxide capture: Prospects for new materials. *Angew. Chem. Int. Ed.* **2010**, *49*, 6058–6082. [CrossRef] [PubMed]
12. Kenarsari, S.D.; Yang, D.L.; Jiang, G.D.; Zhang, S.J.; Wang, J.J.; Russell, A.G.; Wei, Q.; Fan, M.H. Review of recent advances in carbon dioxide separation and capture. *RSC Adv.* **2013**, *3*, 22739–22773. [CrossRef]
13. Zhao, Z.J.; Dong, H.F.; Zhang, X.P. The research progress of CO_2 capture with ionic liquids. *Chin. J. Chem. Eng.* **2012**, *20*, 120–129. [CrossRef]
14. Blanchard, L.A.; Gu, Z.Y.; Brennecke, J.F. High-pressure phase behavior of ionic liquid/CO_2 systems. *J. Phys. Chem. B* **2001**, *105*, 2437–2444. [CrossRef]
15. Lau, R.M.; van Rantwijk, F.; Seddon, K.R.; Sheldon, R.A. Lipase-catalyzed reactions in ionic liquids. *Org. Lett.* **2000**, *2*, 4189–4191.
16. Datta, S.; Holmes, B.; Park, J.I.; Chen, Z.W.; Dibble, D.C.; Hadi, M.; Blanch, H.W.; Simmons, B.A.; Sapra, R. Ionic liquid tolerant hyperthermophilic cellulases for biomass pretreatment and hydrolysis. *Green Chem.* **2010**, *12*, 338–345. [CrossRef]
17. Eckstein, M.; Villela, M.; Liese, A.; Kragl, U. Use of an ionic liquid in a two-phase system to improve an alcohol dehydrogenase catalysed reduction. *Chem. Commun.* **2004**, 1084–1085. [CrossRef] [PubMed]
18. Zhao, R.H.; Zhang, X.W.; Zheng, L.; Xu, H.; Li, M. Enantioselective esterification of (*R*,*S*)-flurbiprofen catalyzed by lipase in ionic liquid. *Green Chem. Lett. Rev.* **2017**, *10*, 23–28. [CrossRef]
19. Zhu, C.H.; Guo, F.; Guo, X.Q.; Li, X.K. In situ saccharification of cellulose using a cellulase mixture and supplemental beta-glucosidase in aqueous-ionic liquid media. *Bioresources* **2016**, *11*, 9068–9078. [CrossRef]
20. Amado, V.C.F. *"One-Pot" Enzymatic Conversion of CO_2 to Methanol*; Faculdade de Ciências e Tecnologia: Caparica, Portugal, 2013.
21. Kaftzik, N.; Wasserscheid, P.; Kragl, U. Use of ionic liquids to increase the yield and enzyme stability in the beta-galactosidase catalysed synthesis of *N*-acetyllactosamine. *Org. Process Res. Dev.* **2002**, *6*, 553–557. [CrossRef]
22. Dabirmanesh, B.; Khajeh, K.; Ranjbar, B.; Ghazi, F.; Heydari, A. Inhibition mediated stabilization effect of imidazolium based ionic liquids on alcohol dehydrogenase. *J. Mol. Liq.* **2012**, *170*, 66–71. [CrossRef]
23. Lu, Y.; Jiang, Z.Y.; Xu, S.W.; Wu, H. Efficient conversion of CO_2 to formic acid by formate dehydrogenase immobilized in a novel alginate-silica hybrid gel. *Catal. Today* **2006**, *115*, 263–268. [CrossRef]
24. Wang, X.; Li, Z.; Shi, J.; Wu, H.; Jiang, Z.; Zhang, W.; Song, X.; Ai, Q. Bioinspired approach to multienzyme cascade system construction for efficient carbon dioxide reduction. *ACS Catal.* **2014**, *4*, 962–972. [CrossRef]
25. Liu, A.H.; Feng, R.R.; Liang, B. Microbial surface displaying formate dehydrogenase and its application in optical detection of formate. *Enzyme Microb. Technol.* **2016**, *91*, 59–65. [CrossRef] [PubMed]

26. Anderson, A.G.; Berkelhammer, G. A study of the primary acid reaction on model compounds of reduced diphosphopyridine nucleotide. *J. Am. Chem. Soc.* **1958**, *80*, 992–999. [CrossRef]
27. Alivisatos, S.G.; Ungar, F.; Abraham, G.J. Spontaneous reactions of 1,3-substituted 1,4-dihydropyridines with acids in water at neutrality.I. Kinetic analysis and mechanism of reactions of dihydronicotinamide—adenine dinucleotide with orthophosphates. *Biochemistry* **1965**, *4*, 2616–2630.
28. Oppenheimer, N.J.; Kaplan, N.O. Structure of the primary acid rearrangement product of reduced nicotinamide adenine dinucleotide (NADH). *Biochemistry* **1974**, *13*, 4675–4685. [CrossRef] [PubMed]
29. Ruschig, U.; Muller, U.; Willnow, P.; Hopner, T. CO_2 reduction to formate by nadh catalyzed by formate dehydrogenase from pseudomonas-oxalaticus. *Eur. J. Biochem.* **1976**, *70*, 325–330. [CrossRef] [PubMed]
30. Wang, Y.Z.; Li, M.F.; Zhao, Z.P.; Liu, W.F. Effect of carbonic anhydrase on enzymatic conversion of CO_2 to formic acid and optimization of reaction conditions. *J. Mol. Catal. B-Enzym.* **2015**, *116*, 89–94. [CrossRef]
31. Rover, L.; Fernandes, J.C.B.; Neto, G.D.; Kubota, L.T.; Katekawa, E.; Serrano, S.H.P. Study of nadh stability using ultraviolet-visible spectrophotometric analysis and factorial design. *Anal. Biochem.* **1998**, *260*, 50–55. [CrossRef]
32. Frisch, M.J.T.G.W.; Schlegel, H.B.; Scuseria, G.E.; Robb, M.A.; Cheeseman, J.R.; Scalmani, G.; Barone, V.; Mennucci, B.; Petersson, G.A.; Nakatsuji, H.; et al. *Gaussian 09, Revision d. 01*; Gaussian, Inc.: Wallingford, CT, USA, 2013.
33. Baltrusaitis, J.; Grassian, V.H. Carbonic acid formation from reaction of carbon dioxide and water coordinated to al(oh)(3): A quantum chemical study. *J. Phys. Chem. A* **2010**, *114*, 2350–2356. [CrossRef] [PubMed]
34. Freire, M.G.; Neves, C.M.S.S.; Marrucho, I.M.; Coutinho, J.A.P.; Fernandes, A.M. Hydrolysis of tetrafluoroborate and hexafluorophosphate counter ions in imidazolium-based ionic liquids. *J. Phys. Chem. A* **2010**, *114*, 3744–3749. [CrossRef] [PubMed]
35. Carrete, J.; Mendez-Morales, T.; Cabeza, O.; Lynden-Bell, R.M.; Gallego, L.J.; Varela, M.L. Investigation of the local structure of mixtures of an ionic liquid with polar molecular species through molecular dynamics: Cluster formation and angular distributions. *J. Phys. Chem. B* **2012**, *116*, 5941–5950. [CrossRef] [PubMed]
36. Yuki Kohno, H.O. Ionic liquid/water mixtures: From hostility to conciliation. *Chem. Commun.* **2012**, *48*, 7119–7130. [CrossRef] [PubMed]
37. Sleat, R.; Mah, R.A. Quantitative method for colorimetric determination of formate in fermentation media. *Appl. Environ. Microb.* **1984**, *47*, 884–885.
38. Denning, D.M.; Thum, M.D.; Falvey, D.E. Photochemical reduction of CO_2 using 1,3-dimethylimidazolylidene. *Org. Lett.* **2015**, *17*, 4152–4155. [CrossRef] [PubMed]

Chapter 4 - Efficient Ionic Liquid–based Platform for Multi-Enzymatic Conversion of Carbon Dioxide to Methanol

In our previous step, the research mainly focused on the single enzymatic reaction (FDH). In this chapter, we describe use of three strategies to promote the switching of the equilibrium of the reaction to the product side. First, ADH (the enzyme of the sequence that transforms formaldehyde into methanol) is known to be highly efficient. Therefore a cascade multi-enzymatic reaction with three enzymes (i.e. formate dehydrogenase, formaldehyde hydrogenase, and alcohol dehydrogenase) was established in the next step of the research aimed at achieving high CO_2 conversion via removal of the product from the previous reactions. Sequential reduction of CO_2 to formic acid, formaldehyde, and methanol can be achieved by using formate dehydrogenase (FDH), formaldehyde dehydrogenase (FaldDH), and alcohol dehydrogenase (ADH) sequentially. The second strategy consisted of introducing an IL capable of capturing CO_2 and therefore increasing its solubility so that the first reaction catalyzed by FDH is enhanced to shift equilibrium to the product side. Since the activity of FDH could be either positively or negatively affected by the occurrence of ILs, the selection of the right IL is crucial. Third, to further promote the reaction rate, a separation membrane was incorporated in the system so that products would be immediately separated from the reaction and thus drive the equilibrium towards the formic acid. Four kinds of ILs as co-solvents were evaluated in a biocatalytic membrane reactor by passing a mixture of CO_2, IL, and cofactor through the enzyme-loaded membrane.

4.1 Hypotheses

- The way the immobilization of the three enzymes involved in the cascade is performed influences the overall catalytic performance of the system.
- Enzyme activity and interaction enzyme-coenzyme improve when certain ILs are presented in the reaction mixture.

4.2 Experimental considerations

For this study, it is important to have a robust platform for enzyme immobilization to enable enzyme recycling and product removal for avoiding product inhibition. Therefore the research strategy in this case was as follows. First, four kinds of biocompatible ILs were synthesized for capturing CO_2 in the enzymatic reaction, and the solubility of the gas in each kind was tested. Second, three enzymes (i.e. FDH, FaldDH, and ADH) were co-immobilized

in the membrane by using reverse filtration methods. Third, four kinds of ILs were evaluated in the enzymatic reaction with immobilized enzymes, and stability of biocatalytic membrane was tested. Lastly, the mechanism of enzymatic reaction involving ionic liquids (i.e. [CH][Glu]) was unraveled by using molecular simulation and ITC (isothermal titration calorimetry).

4.3 Highlights

The results obtained in this study suggest that the IL ([CH][Glu]) as co-solvent was good not only for capturing CO_2 but also keeps FDH in a productive conformation (as seen by molecular simulation). First, based on the CO_2 solubility in the pure ILs shown in **Figure 4.1 (a)**, CO_2 concentration in the four kinds of 20% ILs was calculated to be in the range 467 to 714 mM, which is far higher than CO_2 solubility in water (33 mM). The maximum methanol yield achieved using [CH][Glu] was ~3.5 times higher than the results of multi-enzymatic reactions in Tris-HCl buffer. The same reaction was also examined in the same way for the other three ILs, but the conversion of CO_2 was not significantly improved compared to reactions in Tris-HCl buffer.

The yield of methanol was clearly increased with increasing [CH][Glu] from 10% to 20%, as shown in **Figure 4.1 (b)**. CO_2 captured in the solution was noticeably increased by increasing [CH][Glu] concentration, which probably shifted the reaction equilibrium towards the production of methanol. However, the yield of methanol declined with further increase of [CH][Glu] concentration from 20% to 60%. This result apparently shows that a large amount of [CH][Glu] (above 20% concentration) starts to have a negative effect on enzyme catalysis performance even though more CO_2 is captured, which should benefit product formation. Finally, methanol yield could be improved almost three-fold by increasing the CO_2 concentration 15 times in the [CH][Glu] system compared to the reaction performed in Tris-HCl buffer.

To evaluate the stability of the biocatalytic membrane, FDH, FaldDH, and ADH were co-immobilized in the 10 kDa regenerated cellulose membrane, and six 30-minute reaction cycles were performed. The yield of methanol in the Tris-HCl buffer was maintained at 20% - 40% for six runs **(Figure 4.2)**, which confirmed that enzyme leakage was acceptable and that enzyme activity was not lost during immobilization. In the presence of [CH][Glu], the yield of methanol increased and was between 60% to 75% during the six runs.

The active site of FDH, which binds the CO_2 molecule in all solvent systems, was inspected by MD simulations, as shown in **Figure 4.3**. As a measure of this surface opening, the distance of the amino acid side chain OH-group of Tyr73 and the Cζ of the side-chain

of Phe285 was recorded over the simulation time. The 20% [CH][Glu] exhibited significantly different behavior compared to the other solvent systems and had a mean distance of 4.7 Å, while that of the other solvent systems ranged from 6.9 – 8.5 Å (Figure 7b). The amino acid side chains of Asn119, Arg258, and His311, in particular, showed a significantly lower fluctuation over the MD simulation time in 20% [CH][Glu] compared to the other solvent systems. To explain the high yield of methanol in 20% [CH][Glu], we hypothesized that the increased rigidity of the FDH increased protein stability on its own and additionally led to an increased residence time of CO_2 in the active site. This prolonged TS-like residence time of CO_2 in the active site may have increased the probability of a productive positioning of the reactants for the formation of formic acid, thus resulting in a shift of the reaction equilibrium towards the less favored reduction of CO_2 to formic acid.

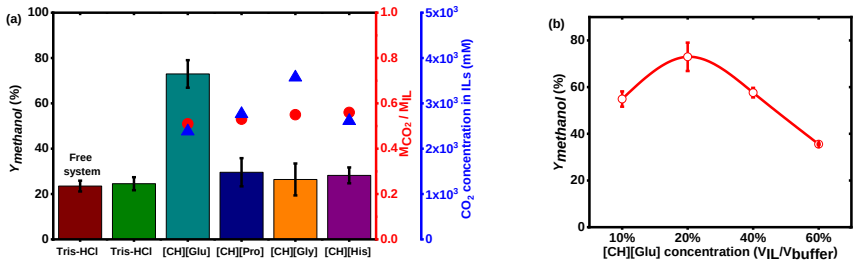

Figure 4.1. (a) The **y**ield of methanol in free enzyme Tris-HCl (pH=7.0) and in four kinds of 20% ILs (left); solubility of CO_2 in the absolute ILs with molar ratio of CO_2 to the IL (M_{CO2}/M_{IL}) (left, red circle); CO_2 concentration in ILs (left, blue triangle). (b) Methanol production at different concentrations of [CH][Glu].

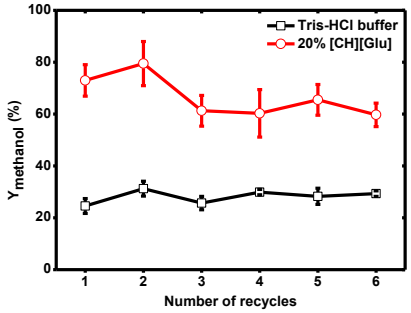

Figure 4.2. Stability of biocatalytic membrane in Tris-HCl buffer and 20% [CH][Glu].

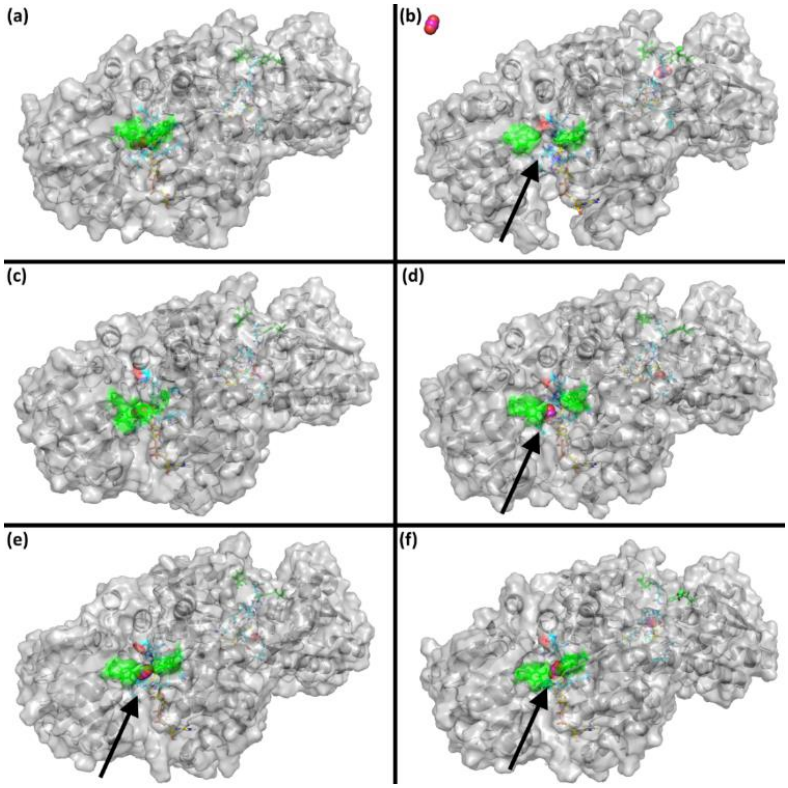

Figure 4.3. Surface representation of formate dehydrogenase (PDB 5DN9) at the beginning (A) and end (B-F) of MD simulation in different solvent systems: H_2O (B), 20% [Ch][Glu] (C), 20% [Ch][Gly] (D), 20% [Ch][His] (E), 20% [Ch][Pro] (F). For clarity, the bulk solvent is not shown. The NADH cofactor is shown as yellow sticks, the catalytically important Arg is shown as cyan sticks, Tyr73 and Phe285 are highlighted as greens ticks and green surface, CO_2 is shown as cyan spheres. The solvent accessible active sites are highlighted with the black arrows.

4.4 Significance of the study

Ever since Overt and Dave reported the possibility of converting CO_2 to methanol by using a sequence of three enzymes in 1999, many researchers have attempted to use the principle. Large-scale implementation of such cascade reactions has, however, been hindered by the extremely low yield attained, regardless of the enhancing strategy used e.g. enzyme immobilization, molecular enzyme modification, etc. One of the limitations for the reaction to proceed is the low solubility of CO_2 in water, which makes the first reaction in the sequence highly inefficient.

The discovery of new ionic liquids compatible with enzyme activity and capable of solubilizing high levels of CO_2 could open new doors in terms of increasing yields. Previous studies have shown that the first reaction of the sequence, conversion of CO_2 to formic acid, plays a decisive role in the conversion of CO_2 to methanol and represents the “bottleneck”

that determines the progress of the whole reaction. In this research we demonstrated that, in addition to increasing CO_2 solubility, ionic liquids can modify the conformation of the passage to the active site of the enzyme, so that the interaction between the active site and the CO_2 molecule (which needs to penetrate this passage to access the active site) becomes more efficient and results in increased conversion. In addition, the straightforward enzyme loading approach inspired by membrane fouling mechanisms provided a novel platform for conducting a sequential enzyme reaction in the presence of ILs. The biocatalytic system had a promising capacity for enzyme loading and showed high stability after several experimental cycles. The system that offered the best conversion results was an aqueous mixture of 20% [CH][Glu] in which CO_2 concentration was around 15 times higher than in Tris-HCl buffer as the control.

This discovery can be a breakthrough not only for this particular conversion of CO_2 to methanol, but also for other enzymatic reactions in which conversion is limited by ineffective conformations around the enzyme active site.

4.5 Paper

This chapter was based on the following paper:

Efficient Ionic Liquid–based platform for Multi-Enzymatic Conversion of Carbon Dioxide to Methanol

Zhibo Zhang, Jan Muschiol, Yuhong Huang, Sigyn Björk Sigurdardóttir, Nicolas von Solms, Anders Egede Daugaard, Jiang Wei, Jianquan Luo, Bao-Hua Xu, Suojiang Zhang and Manuel Pinelo

Published: accepted in Green Chemistry (8.586); Green Chemistry, 2018, 20, 4339-4348.

Green Chemistry

PAPER

View Article Online
View Journal | View Issue

Cite this: *Green Chem.*, 2018, **20**, 4339

Efficient ionic liquid-based platform for multi-enzymatic conversion of carbon dioxide to methanol†

Zhibo Zhang, [a,b] Jan Muschiol, [a] Yuhong Huang,[a] Sigyn Björk Sigurdardóttir,[a] Nicolas von Solms,[a] Anders E. Daugaard, [a] Jiang Wei,[a] Jianquan Luo, [c] Bao-Hua Xu, [b] Suojiang Zhang *[b] and Manuel Pinelo*[a]

Received 18th July 2018,
Accepted 25th August 2018

DOI: 10.1039/c8gc02230e

rsc.li/greenchem

Low yields commonly obtained during enzymatic conversion of CO_2 to methanol are attributed to low CO_2 solubility in water. In this study, four selected ionic liquids with high CO_2 solubility were separately added to the multi-enzyme reaction mixture and the yields were compared to the pure aqueous system (control). In an aqueous 20% [CH][Glu] system, yield increased *ca.* 3.5-fold compared to the control (*ca.* 5-fold if NADH regeneration was incorporated). Molecular dynamics simulation revealed that CO_2 remains for longer in a productive conformation in the enzyme in the presence of [CH][Glu], which explains the marked increase of yield that was also confirmed by isothermal titration calorimetry – lower energy (ΔG) binding of CO_2 to FDH. The results suggest that the accessibility of CO_2 to the enzyme active site depends on the absence/presence and nature of the ionic liquid, and that the enzyme conformation determines CO_2 retention and hence final conversion.

Introduction

One of the greatest environmental challenges we face today is the emission of enormous amounts of carbon dioxide (CO_2) into the atmosphere each year, which contributes to global warming, ocean acidification, melting of icebergs and the energy crisis.[1,2] Ideally, CO_2 ought to be converted to useful chemical and fuels (*e.g.* methanol) for renewable energy utilization and simultaneous alleviation of the problem of CO_2 emissions. Therefore extensive efforts have been made to bring about catalytic hydrogenation of CO_2 *via* chemistry, electrochemistry, photochemistry and enzymatic conversions.[3–5] Due to the inherent thermodynamic stability and low reactivity of CO_2, production of methanol by enzymatic conversion has significant advantages over conventional techniques owing to the high selectivity, high efficiency, mild experimental conditions, and environmental friendliness of enzymatic catalysis.[6]

Inspired by the biological metabolic pathway, sequential reduction of CO_2 to formic acid, formaldehyde and methanol can be achieved by using formate dehydrogenase (FDH), formaldehyde dehydrogenase (FaldDH), and alcohol dehydrogenase (ADH), respectively.[7] However, the yield of methanol achieved in this type of system is only 43.8%.[7] The low conversion is partly explained by the fact that the reaction rate of the first reaction in the sequence (CO_2 → formic acid), catalysed by FDH, is much slower than its reverse reaction (formic acid → CO_2). Indeed, Rusching *et al.* reported that formic acid oxidation was 30 times faster than CO_2 reduction catalyzed by FDH.[8] Thus the CO_2 → formic acid step is likely to contribute to the low performance reduction of CO_2 to methanol. In this regard, we envisioned that a higher yield of product, either formaldehyde or methanol, could be reached by increasing the concentration of substrate (CO_2) in the solution, which may drive the transformation of CO_2 to formic acid forward. Indeed, a certain threshold concentration of formic acid is required for the second step reaction to proceed.[9] In addition, it could also be helpful to further promote the reaction rate by incorporating a membrane in the system so that products would be immediately separated from the reaction, driving the equilibrium towards the formic acid.

Ionic liquids (ILs) have great capacity to capture CO_2 *via* electrostatic forces, van der Waals forces, hydrogen bonds and other physical effects.[10] Amine functionalized cation-tethered ILs have been used for CO_2 capture, in which 0.5 mol CO_2 per mol

[a]*Department of Chemical and Biochemical Engineering, Building 229, Technical University of Denmark, DK-2800 Kgs. Lyngby, Denmark. E-mail: mp@kt.dtu.dk*
[b]*Beijing Key Laboratory of Ionic Liquids Clean Process, Key Laboratory of Green Process and Engineering, State Key Laboratory of Multiphase Complex Systems, Institute of Process Engineering, Chinese Academy of Sciences, Beijing 100190, P. R. China. E-mail: sjzhang@ipe.ac.cn*
[c]*State Key Laboratory of Biochemical Engineering, Institute of Process Engineering, Chinese Academy of Sciences, Beijing 100190, PR China*
†Electronic supplementary information (ESI) available. See DOI: 10.1039/c8gc02230e

of IL could be absorbed through a carbamate mechanism.[11] Amino acid ILs could capture almost 1 mol CO_2 per mol of IL by forming carbamic acid rather than carbamate.[12] Furthermore, the high potential of CO_2 electronic reduction could be lowered by ILs to achieve a lower energy barrier.[13,14] To date, ILs have been used in various enzymatic reactions, *e.g.* with cellulases and ADH.[15–18] Recently, several biocompatible and environmentally friendly ILs have been identified which are composed of naturally-derived materials such as sugars, amino acids, and choline.[19] Several proteins have been successfully dissolved in choline dihydrogenphosphate [CH][DHP] without denaturation.[20] 70% of the initial redox activity of Cytochrome C remained more than one year after dissolving in a mixture of [CH][DHP] and water.[21] Amino acid-based ILs as benign media have been also reported in biomedical applications.[22,23] ILs could thus be promising substitutes of traditional buffers for conducting selected enzymatic reactions.

For *in situ* removal of products (methanol and NAD^+) and recycling of enzymes, a separation system platform is additionally required. Recently, inspired by membrane fouling mechanisms, we proposed a simple approach to immobilize enzymes in membranes using "reverse filtration" of the enzyme solution.[24] In this system, enzyme immobilization was achieved by hydrogen bonding, entrapment and hydrophobic or electrostatic adsorption.[25] The activity of the immobilized enzymes could be maintained to approximately that of the free enzymes due to the mild and fast immobilization procedure. High enzyme loading could also be maintained and the contact time for the substrate–enzyme complex could be controlled by changing pressure. However, to produce one mole of methanol in such a cascade reaction, three moles of reduced nicotinamide adenine dinucleotide (NADH) are stoichiometrically consumed, as the cofactor (NADH) acts as a hydrogen and electron donor at each step of the reduction reaction.[9] Converting the oxidized form of the cofactor (NAD^+) to NADH is essential for reducing cost and enhancing methanol production. Normally, NADH regeneration is accomplished by chemical, photochemical, and electrochemical methods, but such regeneration can be also attained by adding another enzyme system which requires NAD^+ to proceed (Scheme 1).[26]

In this study, biocompatible ILs composed of choline and amino acids (*i.e.* [CH][Glu], [CH][Pro], [CH][Gly], and [CH][His]) were designed and synthesized in order to increase CO_2 solubility and stabilize FDH. These ILs were incorporated in a membrane reactor system which enabled *in situ* removal of products from the reaction, as illustrated in Fig. 1. Four

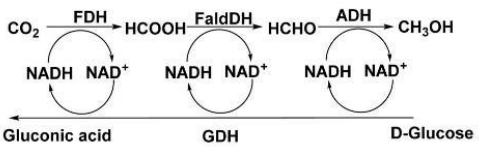

Scheme 1 Multi-enzyme system for methanol synthesis from CO_2 with *in situ* regeneration of NADH.

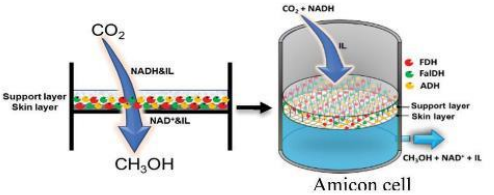

Fig. 1 The immobilization strategy of enzymes in membrane for multi-enzymatic cascade reaction.

kinds of ILs as co-solvent were evaluated in the biocatalytic membrane reactor by passing a mixture of CO_2, IL and cofactor through the enzyme-loaded membrane. To our knowledge, this is the first report of multi-enzymatic conversion of CO_2 to methanol in ILs with NADH regeneration. This integration of ILs and biocatalytic membrane provides a promising avenue for a practical CO_2-based sustainable chemistry.

Experimental

Materials

Glycine (Gly), L-proline (Pro), L-histidine (His), L-glutamic acid (Glu), choline hydroxide (aqueous solution 46 wt%), were purchased from Sigma Aldrich (St Louis, MO, USA). Methanol and acetonitrile were analytical grade and used without any further purification. Double-distilled water was used in all experiments. Formate dehydrogenase (EC 1.2.1.2, homo-dimer, 76 kDa) from Candida boidinii (FDH), formaldehyde dehydrogenase (EC 1.2.1.46, homo-dimer, 150 kDa) from *Pseudomonas* sp. (FaldDH), alcohol dehydrogenase (EC 1.1.1.1, homo-tetramer, 141 kDa) from *Saccharomyces cerevisiae* (ADH), and glucose dehydrogenase (EC 1.1.1.118, homo-hexamer, 300 kDa) from *Pseudomonas* sp. (GDH) were purchased from Sigma–Aldrich (St Louis, MO, USA). These commercial powders or liquids are not pure enzymes and the protein content was determined by Bradford protein assay. β-Nicotinamide adenine dinucleotide reduced form (NADH, >97 wt%), β-nicotinamide adenine dinucleotide hydrate (NAD^+), trizma base, hydrochloric acid (37%) D-glucose, and methanol (≥99.9%) were purchased from Sigma Aldrich (St Louis, MO, USA). All the enzyme and substrate solutions were prepared using 0.1 M Tris-HCl buffer (pH = 7.0) unless otherwise stated. CO_2 gas (>99.5%) in a cylinder was purchased from AGA A/S (Denmark). Commercial UF membranes (PLGC, Millipore) used in this work have a regenerated cellulose skin layer on a polypropylene support, and their molecular weight cut-off is 10 kDa.

Synthesis of [Ch][AA] ILs

ILs were prepared and purified according to the literature.[27] [Ch][OH] aqueous solution (about 4 M) was added dropwise under cooling to an amino acid aqueous solution or suspension (0.06 mol) to obtain a slight excess (about 10 mol%) of amino acid. The mixture was stirred at about 3 °C overnight in

the dark. Water was then removed under reduced pressure at 50 °C using a rotavapor. Acetonitrile/methanol (9 : 1, v/v) was then added under vigorous stirring to precipitate the excess of amino acid. The mixture was left stirring overnight and the excess of amino acid was then filtered off. The filtrate was evaporated to remove solvents at 50 °C. The product was dried under vacuum for 72 h at 60 °C. Characterizaiton data of ILs can be found in ESI.†

Experimental set-up and procedure

The dead-end filtrations and enzymatic reaction were performed in a stirred cell (Amicon 8050, Millipore, USA) and descriptions of equipment and procedure can be found in previous work.[24] The PLGC membranes (10 kDa) were placed on the membrane holder in 'sandwich' mode (with their own support layer facing the feed and an extra polypropylene support beneath the skin layer). The membrane was first soaked in a 5% NaCl solution for 30 min and then filtered with deionized water for another 30 min at 1 bar (procedures according to the manufacturers' instructions). Next, the water permeability of the membranes was measured at 2 bar with buffer for 30 min. Then each enzyme solution (30 mL) was poured into the cell with a 10 kDa membrane for enzyme immobilization. The prepared solution was bubbled with CO_2 through a syringe needle (0.6 mm × 25 mm) before entering the reactor. The flow rate of gas (measured by the speed of bubble emission) was controlled in the same manner in all the experiments by controlling the pressure valve.

Solubility experimental apparatus and procedure

The gas solubility experimental apparatus and procedure are similar to the work of Shang *et al.* In the experiment CO_2 of ambient pressure was bubbled at a flow rate of about 60 mL min^{-1} through about 4.0 g of the IL in a glass tube with an inner diameter of 12 mm. The glass tube was partly immersed in a water bath of desired temperature. The weight of the IL solution was determined at regular intervals by an electronic balance (OHAUS Corp. AR2140, USA) with a resolution of 0.0001 g.

Enzyme immobilization

Three enzymes of 100 μL liquid FDH, 1.0 mg solid FaldDH, and 1.5 mg solid ADH were immobilized in the 10 kDa regenerated cellulose membrane. Enzyme immobilization was carried out at a pressure of 2 bar, and permeate was collected in precision cylinders for analysis. The cylinders were replaced manually for every 4 mL. At the end of filtration, the 'fouled' membrane was washed with 10 mL of buffer at a pressure of 2 bar, and then rinsed 3 times with buffer without pressure. The amount of immobilized enzyme (loading) was calculated from the mass balance equation, and the immobilization efficiency was expressed as enzyme loading efficiency $\left(\text{loading efficiency} = \frac{m_i}{m_t}\right)$ where m_i and m_t are amount of immobilized and total enzyme, respectively.

Enzymatic reaction with immobilized enzymes

NADH solution (5 mM) was prepared with 0.1 M Tris-HCl buffer and ILs which had been pre-bubbled with CO_2 for 30 min. 4 mL NADH solution with saturated CO_2 was added to the stirred cell equipped with 10 kDa regenerated cellulose membrane. The applied pressure was controlled manually to ensure that 4 mL permeate was obtained in 30 min. For the enzyme reuse experiment, when 4 mL of permeate had been obtained, the filtration was paused and another 4 mL of fresh NADH solution with saturated CO_2 was added for the next cycle (each cycle lasted about 30 min).

Enzymatic reaction with NADH regeneration

2 mg of glucose dehydrogenase (GDH) for NADH regeneration was immobilized together with the other three enzymes (*i.e.* FDH, FaldDH, ADH) in the 10 kDa regenerated cellulose membrane, following the immobilization procedure given above. The 4 ml NADH solution with saturated CO_2 containing 5 mM NADH and 50 mM D-glucose as substrate for glucose dehydrogenase was run through the membrane. The obtained permeate was recycled as feed solution in the next reaction cycle and this operation was repeated for six times.

Analytical methods

The concentration of enzymes was measured as protein concentration using the Bradford protein assay (PerkinElmer lambda20 UV/VIS, Germany). A Hewlett Packard HP6890 gas chromatograph (GC) equipped with a FID (250 °C) and a Restek XTI-5 column (30 m × 0.25 mm i.d., film thickness 0.25 mm) was used for methanol concentration. The carrier gas was N_2 with a flow rate of 0.4 mL min^{-1}. The injector temperature was 150 °C and the injection volume was 1 μL. Methanol GC chromatograms were calibrated with 0.01–1 mM methanol solution in 0.1 M pH 7.0 Tris-HCl buffer. Scanning electron microscopy (SEM) was performed in an FEI Helios EBS3 dual beam electron microscope. The skin and support samples were prepared by cutting a small square of the membrane, which was then attached to an aluminium stub by means of double sided sticky carbon tape. The edges of the sample were mounted on the aluminium stub by means of copper tape. After freezing the membrane sample by plunging in liquid nitrogen, cross sections of the membrane skin and the support were cut from the with a pair of scissors. The cross sections were mounted on a slotted specimen stub and fixed with copper tape. All samples were coated with Pt for 2 s at 80 mA in a Cressington 208HR Sputter Coater, which gave an approximate thickness of 4 nm. The micrographs were obtained with an Everhart Thornley detector at low magnifications and with a Thru-the-Lens detector at high magnifications, in high vacuum at 5 keV acceleration voltage and 43 pA current. ^{1}H NMR and ^{13}C NMR measurements. Spectra were recorded at 298 K on NMR spectrometer (av-600 MHz, D_2O, Bruker, Switzerland). Solutions were prepared by dissolving 20–30 mg of IL in 0.7 mL of D_2O. Elemental analysis of C, H, and N (Elementar Vario EL, Germany) indicated that the

elemental ratio of ILs agrees well with their predicted structure.

Isothermal titration calorimetry

The titration experiments were performed using a Nano ITC low volume titration calorimeter (TA instruments, New Castle, DE, USA). Titrations were performed at 25 °C and consisted of enzyme (FDH) and 4.0 μL injections of ligand ($NaHCO_3$, sodium formate, NADH, or NAD^+) at 300-second intervals. All solutions were filtered, degassed to avoid bubble formation, and equilibrated to the corresponding temperature before each experiment. The syringe was inserted into the reaction cell, stirring (250 rpm) was initiated, and the instrument was equilibrated at 25 °C until the base line was flat and stable. The titration data were analyzed with Nano Analyze software (TA Instruments) using an independent model to obtain the curve fitting and thermodynamic binding data. Enthalpy of binding was determined for three titrations of each experiment and average values were compared. The intrinsic molar enthalpy change (ΔH), the binding stoichiometry (n) and binding constant (K) for the binding process were obtained from the best fit of the calorimetric data. Gibbs free energy of binding and K_d were calculated from binding affinity measurements, using $\Delta G = -R(T)\ln(1/K_d)$, where R is the universal gas constant and T is temperature in kelvin. Entropy of binding was then estimated with $\Delta S = (\Delta H - \Delta G)/T$, where ΔH was the average enthalpy of binding.

MD simulations

MD simulations were carried out to study the effect of the employed IL water mixtures on FDH. Therefore the structure of FDH from *Candida biodinii* (pdb code 5DN9) in complex with NAD^+ and azide was downloaded from the PDB database. In preparation for the MD simulations the azide was replaced with a CO_2 molecule in both monomers of the enzyme using the *replace* function of YASARA 16.9.23 (YASARA Biosciences GmbH, Vienna, Austria).[28] Next, the program was used to clean the structure and optimize the hydrogen bonding network. To run the simulation in a mixed solvent system, a cubic simulation cell extending 10 Å around all atoms was created and the AMBER15IPQ force field was chosen.[29] A cell neutralization and pK_a prediction experiment at pH 6.85 was carried out to neutralize the simulation cell and assign correct protonation states of the amino acid side-chains. For creation of the mixed solvent system, all water molecules were deleted from the soup and the solvent density was estimated using weighted densities of the pure compounds as found in the literature.[30] The specific IL molecules were created using the *Build* function of YASARA to fill the simulation cell with an aqueous ionic liquid. In the next step the cell was filled with the created molecule using the respective densities specified in Table S3.† The rest of the cell was filled with water molecules by temporarily removing the IL molecules, filling the cell with water using the specified density (Table S3†), and adding the removed IL molecules back again. To remove all bumps between solvent molecules, the protein was fixed and an energy minimization experiment was carried out. Then all atoms were freed again and the resulting scene was saved as solvent system for the MD simulations. The simulations themselves were done using the YASARA macro md_run with the pressure control mode "Manometer", pH 6.85 and 298 K over a time of 18.1 ns. The resulting simulation snapshots were analysed using the YASARA macros md_analyze and md_analyzeres. For visualization in PyMOL (The PyMOL molecular Graphics System, Version 1.1 Schrodinger, Cambridge, MA, USA), the simulation file was converted to pdb using the YASARA macro md_convert. The movies were prepared using OBS Studio (https://obsproject.com).

Results and discussion

Fabrication of biocatalytic membrane

The immobilization was performed in a membrane assembled in a so-called sandwich mode (polypropylene layer–skin layer–polypropylene support) so that the membrane support layer was positioned to face the feed, while underneath the skin layer an extra polypropylene support was placed to act as a cushion to alleviate membrane compression and peeling of the skin layer (Fig. 1). Based on the "fouling-induced immobilization" method, the three enzymes (*i.e.* FDH, FaldDH and ADH) were simultaneously immobilized in the membrane. During enzyme loading in the membrane, the permeate was collected over time, as presented in Fig. S1.† The mechanism of membrane fouling induced by the enzyme solution filtration was categorized into four fouling models which are presented in Table S1† and identified as standard, intermediate, complete blocking, and cake layer models.[31,32] The cake layer model, showing a high correlation coefficient, was found to best describe the loading mechanism. In the initial stage of the filtration process, only the cake layer model fitted the experimental data, which indicated that most enzymes are deposited on the skin layer of the membrane. As filtration time increased, the experimental data also correlated well with other models because the fouling layer created by the enzymes acts as an additional membrane.[24] The morphology of the enzyme-immobilized membrane was characterized by SEM, and is shown in Fig. 2. The figure shows the skin layer, which is made up of regenerated cellulose (Fig. 2a), and some enzyme aggregates adsorbed on the surface of the polypropylene support fibres (Fig. 2b and c). From the mathematical modelling and characterization by SEM, the fouling-induced enzyme immobilization was found to involve at least two mechanisms: entrapment and adsorption. In Fig. 2c it can be seen that some enzymes were bound to the support fibres by hydrophobic adsorption (additional SEM pictures can be found in Fig. S3†). Based on mass balance calculations by Bradford assay, 2.66 mg of protein was immobilized in the membrane, which corresponds to enzyme loading efficiency of 76%. Accordingly, the permeability dropped to 3.04 L m^{-2} h^{-1} bar^{-1} after enzyme loading, which is around 100 times lower than that of virgin membrane (330 ± 6 L m^{-2} h^{-1} bar^{-1}).

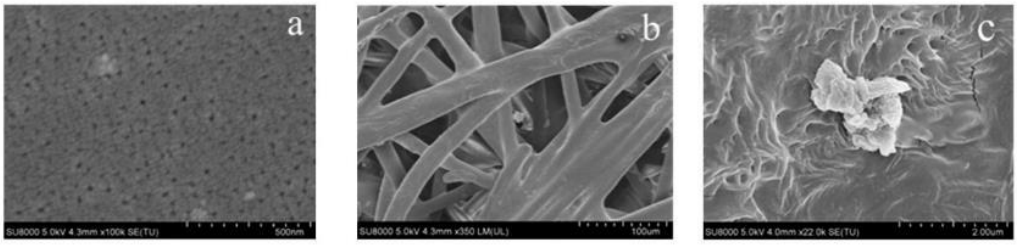

Fig. 2 SEM images of (a) membrane skin layer (regenerated cellulose); (b) support layer (nonwoven polypropylene); (c) view of support layer after enzyme immobilization.

The synthesis of methanol from CO_2 catalyzed by the three-enzyme cascade reaction in Tris-HCl buffer was performed with the membrane loaded with enzymes. According to the reaction route, three moles of NADH are stoichiometrically consumed to produce one mole of methanol in the cascade reaction. Therefore the methanol yield ($Y_{methanol}$) based on NADH may be calculated using the following equation.

$$Y_{methanol}\,(\%) = \frac{C_{methanol} \times 3}{C_{NADH,initial}} \times 100$$

where $C_{methanol}$ is the methanol concentration (mM), and $C_{NADH,initial}$ is the initial NADH concentration (mM).

After 30 min reaction, a methanol yield of 24.5% was obtained for the immobilized system, whilst practically the same yield (23.5%) was obtained for an equivalent free enzyme system (using the same amount of enzymes in free form) (Fig. 3a). The similar yield obtained confirmed that no enzyme activity was sacrificed during immobilization. The low yield of methanol obtained was explained by the kinetics of the reaction, as reported by Luo *et al.*[24] As explained above, the reaction rate of the forward reaction (CO_2 → formic acid) is much lower than that of the reverse reaction (formic acid → CO_2). For the second enzyme, FaldDH, the reaction (formic acid → formaldehyde) was also found to be less efficient than the reverse reaction (formaldehyde → formic acid). However, for the third enzyme, ADH, the forward reaction (formaldehyde → methanol) was much more efficient than the reverse reaction (methanol → formaldehyde). Additionally, Luo *et al.* suggested that in order to be activated, the second reaction required a threshold concentration of formic acid. Therefore the first reaction from CO_2 to formic acid probably plays a decisive role in this cascade reaction.

Multi-enzymatic reaction in the ILs with co-immobilization of enzymes

The four selected ILs have a high capacity to absorb CO_2, where one mole of IL can chemically absorb half a mole of CO_2. The adsorption of half a mole of CO_2 by each mole of IL was proposed by Han *et al.*, and similar mechanisms of CO_2 adsorption by ILs were also reported by other authors.[33,34] Han *et al.* also demonstrated that [CH][AA] can be repeatedly recycled for CO_2 adsorption, since CO_2 can be desorbed from the IL by bubbling with N_2. Therefore, the process of CO_2 adsorption is reversible, and ILs can provide FDH with a high enough CO_2 concentration with a slow-releasing system, as required by FDH. As illustrated in Fig. 3a (red points), the measured molar ratio of CO_2 to the ILs could slightly exceed 0.5. The minor excess in the CO_2: IL molar ratio suggests that physical adsorption also contributes to the uptake of CO_2. Based on the CO_2 solubility in the pure ILs, the CO_2 concen-

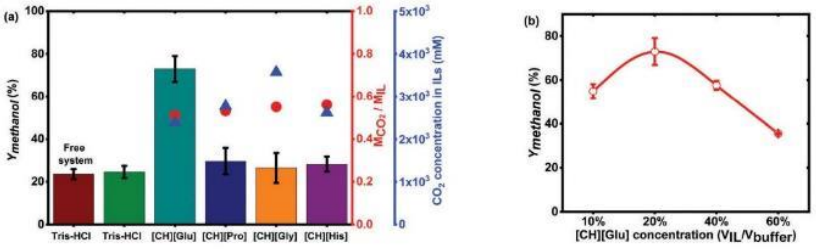

Fig. 3 (a) Yield of methanol in free enzyme Tris-HCl (pH = 7.0) and in four kinds of 20% ILs (left); solubility of CO_2 in the absolute ILs with molar ratio of CO_2 to the IL (M_{CO_2}/M_{IL}) (left, red circle); CO_2 concentration in ILs (left, blue triangle). All the enzymatic reactions were conducted in the membrane except "Free system". (b) Methanol production at different concentrations of [CH][Glu]. An enzymatic membrane reactor equipped with a 10 kDa regenerated cellulose membrane (skin layer facing feed) was used. Recycling of immobilized enzymes was conducted using fresh NADH solution in Tris-HCl buffer and containing 20% [CH][Glu] buffer (NADH = 5 mM).

tration in the four kinds of 20% ILs was calculated to be in the range from 467 to 714 mM, which is far higher than the CO_2 solubility in water (33 mM).[35] Furthermore, the CO_2 adsorption rate in an aqueous IL solution is faster than in the pure IL. Indeed, CO_2 adsorption equilibrium is reached after 20 minutes in aqueous 5 wt% [CH][AA], whilst the saturation of CO_2 in pure [CH][AA] will take at least 4 h.[36] Therefore aqueous ILs may be ideal media for enzymatic reactions.

CO_2 reduction to methanol with the enzyme-loaded membrane (*i.e.* FDH, FaldDH, and ADH) was performed in the presence of 20% ILs (V_{IL}/V_{buffer} = 20%) (Fig. 3a). The maximum methanol yield was achieved using [CH][Glu] and was ~3.5 times higher than the results of multi-enzymatic reactions in Tris-HCl buffer. The same reaction was similarly examined for the other three ILs, but conversion of CO_2 was not significantly improved compared to the reactions in Tris-HCl buffer. In previous work, Liu *et al.* increased the pressure during operation as an additional strategy to achieve high CO_2 concentration in solution. They found that the reaction rate increased from $(1.20 \pm 0.09) \times 10^{-3}$ to $(2.17 \pm 0.07) \times 10^{-3}$ μmol min^{-1} when CO_2 pressure was increased from 0.2 MPa to 0.5 MPa, but almost no change was detected when pressure was further increased to 1.0 MPa.[37] The stable yield detected when pressure was increased above 0.5 MPa was attributed to the fact that NADH concentration probably became the limiting factor. In our case, methanol yield could be improved almost three fold by increasing the CO_2 concentration 15 times in the [CH][Glu] system compared to reactions in Tris-HCl buffer.

To further improve the efficiency of CO_2 conversion, the [CH][Glu] concentration was studied over the range from 10% to 60%. The yield of methanol was clearly increased with increasing [CH][Glu] from 10% to 20%. CO_2 captured in the solution was noticeably increased by increasing [CH][Glu] concentration, thus shifting the reaction equilibrium towards the production of methanol. However, the yield of methanol declined with further increase of the [CH][Glu] concentration from 20% to 60%. Such decrease can be explained by the negative role that large amounts of [CH][Glu] exert on the enzyme activity, which has been attributed to the change of electrostatic balance between charges in proteins when subjected to high salt (IL) concentrations. Additionally, stability, crystallization and aggregation tendency of proteins have been also reported to change dramatically with increasing concentration of ILs in aqueous media.[38–40] As a matter of fact, it has been reported that enzymes lose all activity when in pure ILs.[41,42] Therefore, a balance between increasing CO_2 solubility and maintaining enzyme performance has to be found. Water-based solvents with small amounts of salts (water-rich IL mixtures) have been indeed reported to be the best media for proteins, which is consistent with our results.[41]

pH effect on enzyme activity

Liu *et al.* reported that the optimal pH for reduction of CO_2 to formic acid by FDH was 6.0.[42] However, the highest yield of formaldehyde catalysed by FaldDH was produced at pH 7.0. ADH, the third enzyme in the sequence, was reported to have an optimal activity at pH 8.1 by Sarcar *et al.*[43] In our case, the optimum pH value when the reaction took place in buffer (without ionic liquids) was 6.5, which is similar to the optimum pH of FDH (Fig. 4a); this result suggests that the first reaction (CO_2 → formic acid) plays a decisive role in the performance of the whole reaction. The relative activity was also found to significantly decrease when the pH value of the buffer was either below 6.5 or above 7.5, which suggests a reduced enzyme activity under either acid or alkali conditions. Previous studies suggested that the activity and structure of the enzymes might be affected by strongly acidic or alkaline media.[44] Our results showed that the pH of the 20% [CH][Glu] mixture (pH 6.85) was lower than the pH of the other ILs screened, which could also have influenced the higher conversion of the former compared to the ILs evaluated. Unfortunately, these ILs were synthesized by acid–base neutralization of choline and amino acids. Therefore lowering the pH of the other ILs was not be possible because a change of pH would have resulted in decomposition and amino acid precipitation from the solution; thus no direct comparison among the four ILs at the same pH could be performed.

Recycle of the biocatalytic membrane

To evaluate the recyclability of the biocatalytic membrane, FDH, FaldDH and ADH were co-immobilized in the 10 kDa regenerated cellulose membrane and fresh substrate was fed to the reactor after each of the six 30-minutes reaction cycles. The yield of methanol in the Tris-HCl buffer was maintained at

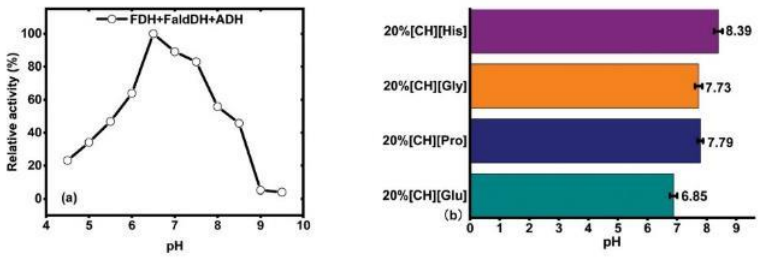

Fig. 4 (a) Activity of the three enzymes at different pH from 4.5 to 9.5; (b) pH values in different kinds of 20% ILs (V_{IL}/V_{Buffer}) after 30 min bubbling with CO_2.

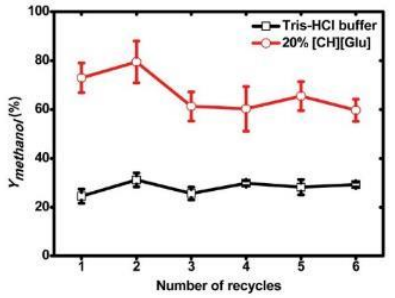

Fig. 5 Stability of biocatalytic membrane in Tris-HCl buffer and 20% [CH][Glu]. One-way ANOVA statistical analysis showed that $Y_{methanol}$ did not change during the three hours of reaction.

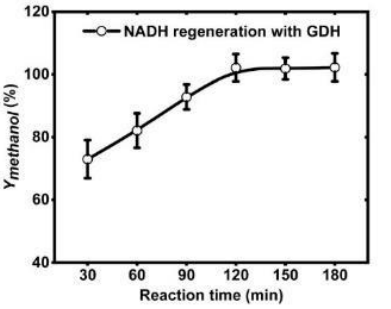

Fig. 6 Methanol production as a function of reaction time with coupled GDH for cofactor (NADH) regeneration.

20%–40% for six runs (Fig. 5), which confirmed that enzyme leakage was low and that enzyme activity was not lost during immobilization. In the presence of [CH][Glu], the yield of methanol increased and was between 60% to 75% during the six runs. A slight decrease in the yield (albeit not statistically significant) was observed after the second run, but no further decrease was observed during the remaining four runs. The decrease of yield observed after the second cycle could be anyway ascribed to the decrease of available NADH due to adsorption in the fouling layer.[24]

Cofactor (NADH) regeneration with glucose dehydrogenase

NADH acts as a terminal electron donor and hydrogen donor in the cascade enzymatic reaction and is consumed stoichiometrically at each step. As a result, three molar equivalents of NADH are consumed to transform one molar equivalent of CO_2 in methanol. Efficient regeneration of NADH is crucial for such a cascade enzymatic reaction since the cost of NADH is very high and *in situ* generated NAD^+ will in turn inhibit the reduction of CO_2 and promote the reverse oxidative reaction. In the current study, glucose dehydrogenase (GDH) was used for NADH regeneration and the enzymatic reaction was coupled to the main cascade enzymatic reaction. Therefore GDH was immobilized together with the three enzymes (FDH, FaldDH, ADH) in the 10 kDa regenerated cellulose membrane. D-Glucose (50 mM) as the GDH substrate was mixed with NADH solution (4 mL) containing 20% [CH][Glu], which was pre-bubbled with CO_2 for 30 minutes. As seen in Fig. 6, the yield of methanol increased from 73% to 100% after 30 to 120 min reaction and then reached equilibrium after 120 min. The result indicates that NADH was efficiently regenerated with high activity of GDH. A number of researchers have also reported that the yield of methanol increased with increasing NADH concentration.[45–47] Total turnover number (TTN) of up to 10 000 has been obtained by using GDH for the regeneration of NAD^+, as reported by Obón.[48] The reduction rate from NAD^+ to NADH catalysed by GDH is faster than the oxidation of NADH to NAD^+ by ADH, as reported by Marpani *et al.*[26] The reaction rate for the reaction from NAD^+ to NADH catalysed by GDH was 6.3 μmol mg^{-1} min^{-1}, while the reaction rate for the reaction from NADH to NAD^+ catalysed by ADH was 4.7 μmol mg^{-1} min^{-1}. Furthermore, converting NADH to NAD^+ catalysed by ADH was much more efficient than with the other two enzymes (FDH and FaldDH).[24] The reaction rate for the cascade reaction is limited by the slowest reaction. Therefore the reaction rate for converting NAD^+ to NADH is far higher than the oxidation of NADH by the three enzymes. Lastly, after two hours there was no further improvement in yield of methanol. Probably, due to product inhibition by high methanol concentration in the solution, the reversible enzymatic reaction would not progress any further.

Molecular dynamics (MD) simulations

MD simulations on FDH with different solvents (*i.e.* water, 20%[CH][Gly], 20%[CH][Glu], 20%[CH][His] and 20% [CH][Pro]) were performed in order to evaluate the effect of the aqueous IL on the enzyme. As depicted in Fig. 7a, all simulations using aqueous ILs showed a similar trend with respect to the root mean square deviation (RMSD) value of the Cα backbone over the MD simulation time, with the exception of 20% [CH][Glu] which approached a lower maximum value. The average RMSD values for the simulation in water and using the aqueous ILs (except [CH][Glu]) ranged from 1.7 to 1.9 Å (Fig. S2†). In contrast, the average RMSD values for the 20% [CH][Glu] simulation of 1.3 Å were markedly lower compared to the other solvents (Fig. S2†). These results might also indicate a stabilizing effect of the aqueous 20% [CH][Glu] on protein structural integrity and therefore be another explanation for the good performance of the 20% [CH][Glu] as solvent for the reaction system.

Closer inspection of the MD simulations revealed that in all solvent systems (except 20% [CH][Glu]) the active site, which binds the CO_2 molecule, quickly became solvent accessible (Fig. 8, Movies S1–5†). This was especially pronounced in the simulation with water as solvent where one of the CO_2 molecules has left the active site after 12.5 ns (Fig. 8b, Movie S1†). As a measure of this surface opening, the distance of the amino acid side chain OH-group of Tyr73 and the Cζ of the

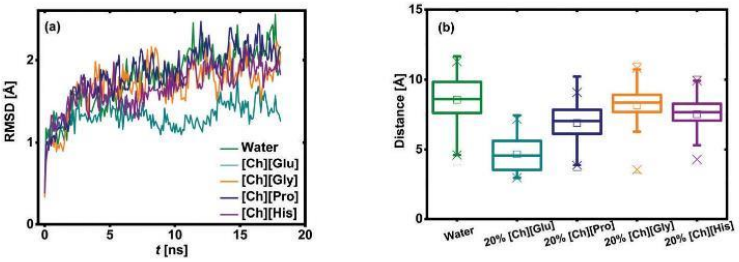

Fig. 7 (a) RMSD time course during the molecular dynamics simulations using H_2O (black line), 20% [Ch][Gly] (blue line), 20% [Ch][Glu] (red line), 20% [Ch][His] (green line) and 20% [Ch][Pro] (pink line) in water as solvents. (b) Distance of the Tyr73 OH-group and Phe 285 Cζ over the MD simulation time.

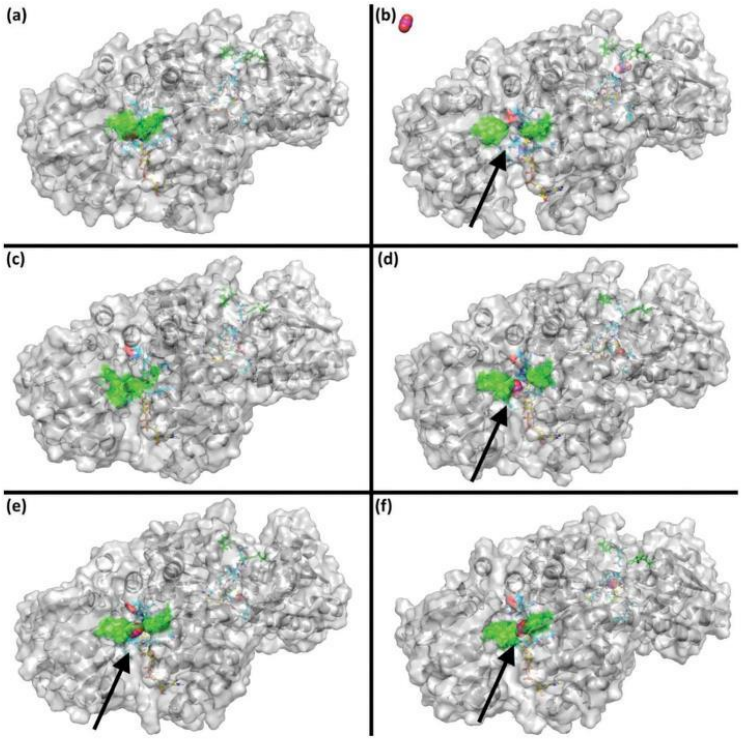

Fig. 8 Surface representation of formate dehydrogenase (PDB 5DN9) at the beginning (A) and end (B–F) of MD simulation in different solvent systems: H_2O (B), 20% [Ch][Glu] (C), 20% [Ch][Gly] (D), 20% [Ch][His] (E), 20% [Ch][Pro] (F). For clarity the bulk solvent is not shown. The NADH cofactor is shown as yellow sticks, the catalytically important Arg is shown as cyan sticks, Tyr73 and Phe285 are highlighted as greens ticks and green surface, CO_2 is shown as cyan spheres. The solvent accessible active sites are highlighted with the black arrows.

side-chain of Phe285 was recorded over the simulation time. The 20% [CH][Glu] exhibited significantly different behaviour compared to the other solvent systems and had a mean distance of 4.7 Å while that of the other solvent systems ranged from 6.9–8.5 Å (Fig. 7b). Furthermore, detailed analysis of distance between residues and ligands involved in formation of the enzyme transition state (TS, Fig. 9A), as reported by Castillo, *et al.*,[49] revealed clearly that formation of the TS would be favoured far more in the 20% [CH][Glu] system than in all the other systems (Table S4†). This effect was also

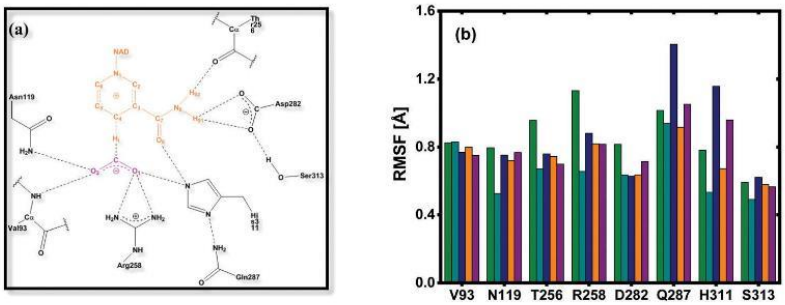

Fig. 9 (A) Transition state of the FDH catalyzed reaction as proposed by Castillo *et al.* The NADH cofactor is highlighted in orange and the substrate CO_2 in pink. (B) RMSF values for the amino acid residues involved in substrate and co-factor binding as well as TS formation over MD simulation time for the different solvent systems: H_2O (olive bars), 20% [CH][Glu] (cyan bars), 20% [CH][Pro] (blue bars), 20% [CH][Gly] (orange bars), 20% [CH][Pro] (purple bars).

reflected in the root mean square fluctuation (RMSF) values of the residues involved in positioning the CO_2 molecule inside the active site (Fig. 9B). The amino acid side chains of Asn119, Arg258 and His311 in particular showed a significantly lower fluctuation over the MD simulation time in 20% [CH][Glu] compared to the other solvent systems. As an explanation for the high yield of methanol in 20% [CH][Glu] we hypothesize that the increased rigidity of the FDH on the one hand also increases protein stability itself and on the other hand leads to an increased residence time of CO_2 in the active site in a more TS-like conformation than in the other studied solvent systems. This prolonged TS-like residence time of CO_2 in the active site increases the probability of a productive positioning of the reactants for the formation of formic acid, which thus could result in a shift of the reaction equilibrium towards the less favoured reduction of CO_2 to formic acid.

For further validation of the MD simulation, isothermal titration calorimetry (ITC) was carried out to elucidate the interaction of FDH with CO_2 in the different solvents (*i.e.* water and 20% [CH][Glu]). Adsorption heat due to interaction between FDH with CO_2 in water and [CH][Glu] was fitted with the Nano-Analyze software (TA Instruments) using an independent model to obtain the Gibbs free energy (ΔG). As shown in Table S1,† the ΔG value of CO_2 interactions with FDH in water was -17.12 kJ mol^{-1}, which is higher than that of CO_2 and FDH interaction in the presence of [CH][Glu] (-18.75 kJ mol^{-1}). This indicates the binding of CO_2 due to lower enzyme flexibility in 20% [CH][Glu].

Conclusions

A straightforward enzyme loading approach inspired by membrane fouling mechanisms provided a novel platform for conducting a sequential enzyme reaction in the presence of ILs. The biocatalytic system had a promising capacity for enzyme loading and showed high stability after several experimental cycles. Previous studies have shown that the first reaction of the sequence, conversion of CO_2 to formic acid, plays a decisive role in conversion of CO_2 to methanol and represents the "bottleneck" that determines the progress of the whole reaction. A strategy to enhance the conversion of this reaction step was attempted by increasing the concentration of CO_2 in the reaction system through adding ionic liquids as a co-solvent. The system that offered the best conversion results was an aqueous mixture 20% [CH][Glu] in which CO_2 concentration was around 15 times higher than in Tris-HCl buffer as the control.

Though CO_2 concentration achieved was similar in the other ionic liquids selected, the reaction yield significantly increased only when [CH][Glu] was used. The reason for this difference was further investigated. We found that pH might play a significant role in the reaction, because slightly acidic pH seems to favour the conversion. The most convincing explanation, however, was provided by molecular simulation dynamics. While CO_2 easily diffuses out of the active site in the other ILs tested, and especially in water, the conformation of FDH in the presence of [CH][Glu] is such that CO_2 stays for a longer time in the vicinity of the active site of the enzyme. Such longer retention times may therefore result in higher conversion of CO_2.

Further systematic research on this topic must provide more specific information about the mechanisms and specific functional groups of ionic liquids, which are responsible for the kinds of conformational enzyme changes that can support higher conversions.

Conflicts of interest

The authors declare no conflict of interest.

Acknowledgements

The authors are thankful for support from National Science Foundation of China (U1704251) and (U1662133), CAS 100-Talent Program (2014).

References

1 X. Z. Lim, *Nature*, 2015, **526**, 628–630.
2 Y. M. Al-Saleh, G. Vidican, L. Natarajan and V. V. Theeyattuparampil, *Futures*, 2012, **44**, 105–115.
3 X. D. Xu and J. A. Moulijn, *Energy Fuel*, 1996, **10**, 305–325.
4 W. B. Hou, W. H. Hung, P. Pavaskar, A. Goeppert, M. Aykol and S. B. Cronin, *ACS Catal.*, 2011, **1**, 929–936.
5 H. Li, P. H. Opgenorth, D. G. Wernick, S. Rogers, T. Y. Wu, W. Higashide, P. Malati, Y. X. Huo, K. M. Cho and J. C. Liao, *Science*, 2012, **335**, 1596–1596.
6 J. F. Shi, Y. J. Jiang, Z. Y. Jiang, X. Y. Wang, X. L. Wang, S. H. Zhang, P. P. Han and C. Yang, *Chem. Soc. Rev.*, 2015, **44**, 5981–6000.
7 R. Obert and B. C. Dave, *J. Am. Chem. Soc.*, 1999, **121**, 12192–12193.
8 U. M. Ulrich Rusching, P. Willnow and T. Höpner, *Eur. J. Biochem.*, 1976, **70**, 325–330.
9 X. L. Wang, Z. Li, J. F. Shi, H. Wu, Z. Y. Jiang, W. Y. Zhang, X. K. Song and Q. H. Ai, *ACS Catal.*, 2014, **4**, 962–972.
10 G. K. Cui, J. J. Wang and S. J. Zhang, *Chem. Soc. Rev.*, 2016, **45**, 4307–4339.
11 E. D. Bates, R. D. Mayton, I. Ntai and J. H. Davis, *J. Am. Chem. Soc.*, 2002, **124**, 926–927.
12 B. E. Gurkan, J. C. de la Fuente, E. M. Mindrup, L. E. Ficke, B. F. Goodrich, E. A. Price, W. F. Schneider and J. F. Brennecke, *J. Am. Chem. Soc.*, 2010, **132**, 2116–2117.
13 B. A. Rosen, W. Zhu, G. Kaul, A. Salehi-Khojin and R. I. Masel, *J. Electrochem. Soc.*, 2013, **160**, H138–H141.
14 D. T. Whipple and P. J. A. Kenis, *J. Phys. Chem. Lett.*, 2010, **1**, 3451–3458.
15 W. Hussain, D. J. Pollard, M. Truppo and G. J. Lye, *J. Mol. Catal. B: Enzym.*, 2008, **55**, 19–29.
16 S. Datta, B. Holmes, J. I. Park, Z. W. Chen, D. C. Dibble, M. Hadi, H. W. Blanch, B. A. Simmons and R. Sapra, *Green Chem.*, 2010, **12**, 338–345.
17 M. Eckstein, M. Villela, A. Liese and U. Kragl, *Chem. Commun.*, 2004, 1084–1085, DOI: 10.1039/b401065e.
18 R. M. Lau, F. van Rantwijk, K. R. Seddon and R. A. Sheldon, *Org. Lett.*, 2000, **2**, 4189–4191.
19 K. D. Weaver, H. J. Kim, J. Z. Sun, D. R. MacFarlane and G. D. Elliott, *Green Chem.*, 2010, **12**, 507–513.
20 K. Fujita and M. Forsyth, *Chem. Commun.*, 2005, **38**, 4804–4806.
21 K. Fujita, D. R. MacFarlane, R. W. Reid and G. D. Elliott, *Biotechnol. Bioeng.*, 2006, **94**, 1209–1213.
22 F. A. E. Silva, F. Siopa, B. F. H. T. Figueiredo, A. M. M. Goncalves, J. L. Pereira, F. Goncalves, J. A. P. Coutinho, C. A. M. Afonso and S. P. M. Ventura, *Ecotoxicol. Environ. Saf.*, 2014, **108**, 302–310.
23 M. Petkovic, J. L. Ferguson, H. Q. N. Gunaratne, R. Ferreira, M. C. Leitao, K. R. Seddon, L. P. N. Rebelo and C. S. Pereira, *Green Chem.*, 2010, **12**, 643–649.
24 J. Q. Luo, A. S. Meyer, R. V. Mateiu and M. Pinelo, *New Biotechnol.*, 2015, **32**, 319–327.
25 J. Q. Luo, F. Marpani, R. Brites, L. Frederiksen, A. S. Meyer, G. Jonsson and M. Pinelo, *J. Membr. Sci.*, 2014, **459**, 1–11.
26 F. Marpani, Z. Sarossy, M. Pinelo and A. S. Meyer, *Biotechnol. Bioeng.*, 2017, **114**, 2762–2770.
27 S. De Santis, G. Masci, F. Casciotta, R. Caminiti, E. Scarpellini, M. Campetella and L. Gontrani, *Phys. Chem. Chem. Phys.*, 2015, **17**, 20687–20698.
28 E. Krieger and G. Vriend, *Bioinformatics*, 2014, **30**, 2981–2982.
29 K. T. Debiec, D. S. Cerutti, L. R. Baker, A. M. Gronenborn, D. A. Case and L. T. Chong, *J. Chem. Theory Comput.*, 2016, **12**, 3926–3947.
30 L. del Olmo, I. Lage-Estebanez, R. Lopez and J. M. G. de la Vega, *J. Phys. Chem. B*, 2016, **120**, 10327–10335.
31 A. Affandy, E. Keshavarz-Moore and H. K. Versteeg, *J. Membr. Sci.*, 2013, **437**, 150–159.
32 L. Palacio, C. C. Ho and A. L. Zydney, *Biotechnol. Bioeng.*, 2002, **79**, 260–270.
33 X. Y. Li, M. Q. Hou, Z. F. Zhang, B. X. Han, G. Y. Yang, X. L. Wang and L. Z. Zou, *Green Chem.*, 2008, **10**, 879–884.
34 S. Z. Jianmin Zhang, K. Dong, Y. Zhang, Y. Shen and X. Lv, *Chem. – Eur. J.*, 2006, **12**, 4021–4026.
35 J. A. Dean, *Lange's Handbook of Chemistry*, McGraw Hill, 1979.
36 Y. C. Shengjuan Yuan, X. Ji, Z. Yang and X. Lu, *Fluid Phase Equilib.*, 2017, **445**, 14–24.
37 Y. Z. Wang, M. F. Li, Z. P. Zhao and W. F. Liu, *J. Mol. Catal. B: Enzym.*, 2015, **116**, 89–94.
38 C. C. Hermann Weingärtner and C. Herrmannc, *Phys. Chem. Chem. Phys.*, 2012, **14**, 415–426.
39 M. S. P. Marc, L. Pusey, M. B. Turner and R. D. Rogers, *Cryst. Growth Des.*, 2007, **7**, 787–793.
40 C. J. B. Natalie Debeljuh, L. Hendersonb and N. Byrne, *Chem. Commun.*, 2011, **47**, 6371–6373.
41 H. O. Yuki Kohno, *Chem. Commun.*, 2012, **48**, 7119–7130.
42 W. F. Liu, Y. H. Hou, B. X. Hou and Z. P. Zhao, *Chin. J. Chem. Eng.*, 2014, **22**, 1328–1332.
43 S. Sarcar, T. K. Jain and A. Maitra, *Biotechnol. Bioeng.*, 1992, **39**, 474–478.
44 F. S. Baskaya, X. Y. Zhao, M. C. Flickinger and P. Wang, *Appl. Biochem. Biotechnol.*, 2010, **162**, 391–398.
45 Y. J. Qianyun Sun, Z. Jiang, L. Zhang, X. Sun and J. Li, *Ind. Eng. Chem. Res.*, 2009, **48**, 4210–4215.
46 D. D. Bilal El-Zahab and P. Wang, *Biotechnol. Bioeng.*, 2007, **99**, 508–514.
47 J. D. Rémi Cazelles, F. Fajula, O. Ersen, S. Moldovanb and A. Galarneau, *New J. Chem.*, 2013, **37**, 3721–3730.
48 A. Manjón, J.M. Obón and J. L. Iborra, *Biotechnol. Bioeng.*, 1998, **57**, 510–517.
49 M. O. R. Castillo, S. Martí and V. Moliner, *J. Phys. Chem. B*, 2008, **32**, 10012–10022.

Chapter 5 - Integration of a Biomimetic Artificial Photocatalysis Membrane for the Production of Methanol from CO_2

NADH acts as a terminal electron donor and hydrogen donor in the cascade enzymatic reaction and is consumed stoichiometrically at each step. As a result, three molar equivalents of NADH are consumed to transform one molar equivalent of CO_2 to methanol. Considering the economic cost, NADH regeneration catalyzed by photocatalysis is a promising solution for cutting costs as well as combating excessive CO_2 emission by utilizing limitless solar energy rather than fossil fuels. However, conventional photosensitizers suffer from poor stability and a slow rate of electron transfer from the electron donor to the photosensitizer as well as transfer from the photosensitizer to the catalyst. It is therefore crucial to develop efficient photosensitizers for establishing an artificial photosynthesis system. Inspired by the natural light-harvesting pigments, the porphyrins, porphyrin-based photosensitizers were designed and synthesized for NADH regeneration. In addition, in order to integrate multi-enzymatic reaction and NADH regeneration, 10 kDa regenerated cellulose was used as a platform for immobilizing enzymes, photosensitizer and electron mediator.

5.1 Hypotheses

- A porphyrin-based photosensitizer can be used to achieve highly efficient NADH regeneration.
- Co-deposition of layers of polydopamine and PEI should help enhance CO_2 capture, which in turn should enhance enzymatic hydrogenation of CO_2.
- Conversion of CO_2 coupled with NADH regeneration in an immobilization system provides higher conversion of CO_2 than the free enzyme system.

5.2 Experimental considerations

In the artificial photosynthesis process, the photosensitizer is crucial for regenerating NADH for achieving efficient photocatalysis. First, four kinds of porphyrin-based photosensitizers were designed and synthesized, namely HTPyP, HTPyBr, ZnTPyP, and ZnTPyPBr. The four porphyrin-based ionic solids were examined for the efficiency of their electron transfer in photochemical NADH regeneration under visible light. Second, the photocatalytic membrane was fabricated with immobilizing enzymes, electron mediator, and codeposition of PEI with DPA. Third, multi-enzymatic reactions were carried out in the photocatalytic membrane to select the photosensitizer which had the best catalytic performance on NADH regeneration.

5.3 Highlights

Four synthesized photosensitizers, ZnTPyPBr, ZnTpyP, HTPyPBr, and HTPyP were evaluated for NADH regeneration. The results showed that ionic liquids (ZnTPyPBr) with the insertion of zinc at the core of porphyrin and with the functional group carboxyl gave the best catalytic performance, indicating that performance is highly related to the zinc and the carboxyl. Furthermore, the electron mediator reduction potential **M** (Ered: -0.3 V vs. Ag/Pt) was higher than those of the ZnTCPyPBr (E_{red}: -1.25 V vs. Ag/Pt), hence enabling the transfer of electrons from ZnTCPyPBr porphyrins to **M**.

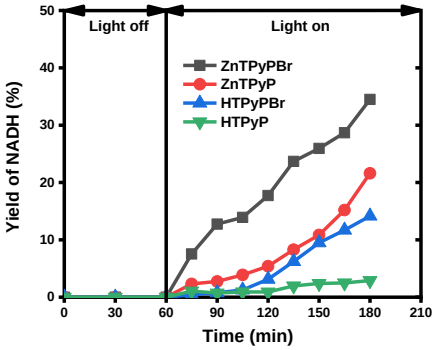

Figure 5.3.1. Visible-light driven NADH regeneration by porphyrins in a degassed phosphate buffer containing 0.5 mM porphyrin, 0.5 mM M, 1 mM NAD^+, and 15 wt% TEOA.

The photocatalytic membrane was fabricated with immobilizing redox enzymes, electron mediator, and codeposition of layers of PEI and dopamine for enzyme sealing. First, as shown in Figure 5.3.2, the morphology of the enzyme-immobilization was enlarged from left to right in sequence, and some enzyme aggregates obviously adsorbed on the surface of the polypropylene support fibers. Second, Energy-Dispersive X-ray Spectroscopy (EDS) elemental mapping of rhodium (Rh) and Zinc (Zn), which are characteristic elements in the electron mediator (M) and photosensitizer (EY), respectively, clearly confirmed their uniform assembly on the surface of the hollow nanofibers or microcapsules in **Figure 5.3.2**. Third, the morphology of PDA-PEI coating was observed by SEM in **Figure 5.3.2**, which clearly demonstrates that a PDA-PEI layer covered the surface of PPE. After coating PDA-PEI on the surface of PPE, the contact angle on their surface was changed from 113.0 to 23.1℃. All these results confirm a successful coating of PDA-PEI on the PPE fiber.

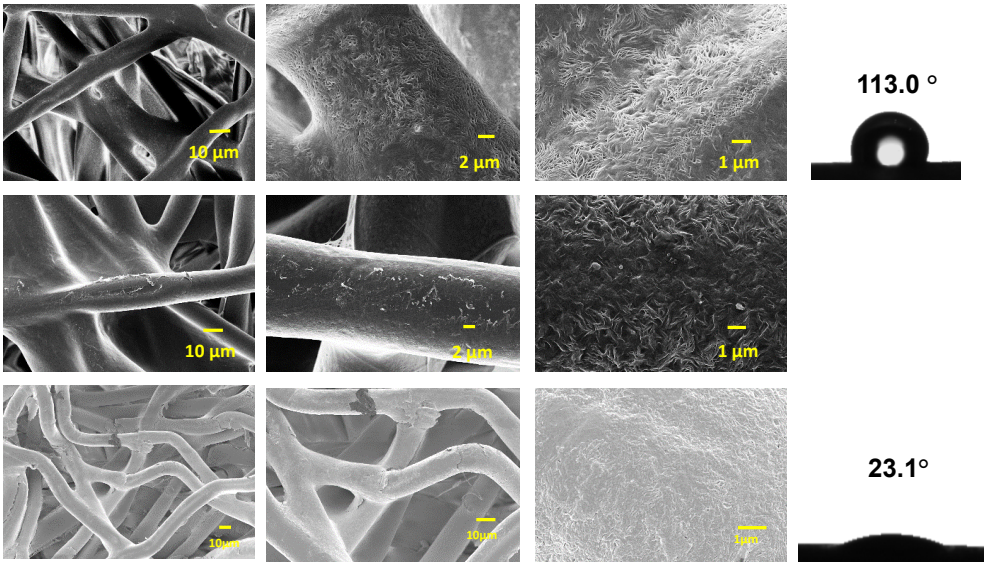

Figure 5.3.2. SEM images of the support layer (nonwoven polypropylene) before enzyme immobilization in the first line, and a view of the support layer after enzyme immobilization in the second line.

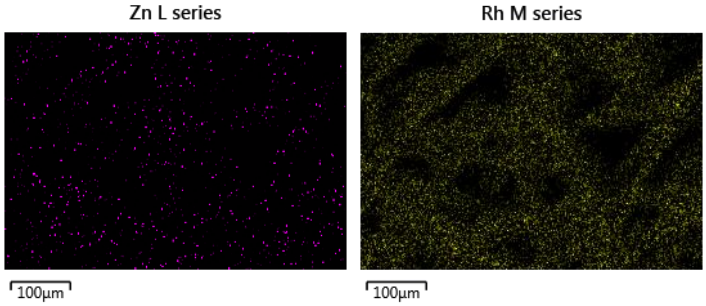

Figure 5.3.3. The distribution of Rh and Zn elements on the hollow nanofibers and microcapsules were mapped after self-assembly of the M and EY layers, respectively.

5.4 Significance of the study

The economic cost is probably a bottleneck for industrial application of conversion of CO_2 to methanol catalyzed by enzymes. A large amount of cofactor NADH is consumed during the synthesis of methanol from CO_2, which leads to high cost. In this study, advanced ionic liquid photosensitizers were developed and successfully applied for NADH regeneration under the visible-light driven system. The ionic liquid photosensitizer with low potential can efficiently activate electron transfer from photosensitizer to electron mediator under visible light, thus ensuring that NADH regeneration can be successfully carried out. This step lays a foundation for an artificial photosynthetic system.

An artificial photosynthetic system was established using membrane technology. Based on the membrane fouling mechanism, the redox enzymes were immobilized to a large degree in

the surface of the fibers. Subsequently, co-deposition of layers of PEI and dopamine was performed for sealing enzymes, and to recycle enzymes. Next, the photosensitizer and electron mediator were immobilized on the co-deposition of layers. This is the first time an artificial photosynthetic system has been established in a membrane according to previous reports. Finally, we demonstrated the synthesis of methanol from CO_2 catalyzed by enzymes incorporating visible light-driven regeneration of NADH. This research offers the possibility of industrial application of synthesis of methanol from CO_2 catalyzed by enzymes.

5.5 Paper

This chapter was based on the following paper:

A Biomimetic Photocatalytic Membrane for the Production of Methanol from CO_2

Zhibo Zhang, Jiahuan Tong, Xianglei Meng, Yingjun Cai, Wenjing Zhang, Mingbo Ji, Nicolas von Solms, Jianquan Luo, Bao-Hua Xu, Suojiang Zhang and Manuel Pinelo

Submitted to: Green Chemistry

A Biomimetic Photocatalytic Membrane for Enzymatic Production of Methanol from CO_2

Zhibo Zhang, [a, b] Jiahuan Tong,[a] Xianglei Meng, [a] Yingjun Cai, [a] Wenjing Zhang,[b] Mingbo Ji, [a] Nicolas von Solms, [b] Jianquan Luo, [c] Bao-Hua Xu, [a] Suojiang Zhang [a]* and Manuel Pinelo [b]*

[a] *Beijing Key Laboratory of Ionic Liquids Clean Process, Key Laboratory of Green Process and Engineering, State Key Laboratory of Multiphase Complex Systems, Institute of Process Engineering, Chinese Academy of Sciences, Beijing 100190, P. R. China.*
[b] *Department of Chemical and Biochemical Engineering, Building 229, Technical University of Denmark, DK-2800 Kgs. Lyngby, Denmark.*
[c] *State Key Laboratory of Biochemical Engineering, Institute of Process Engineering, Chinese Academy of Sciences, Beijing 100190, PR China*
E-mail: sjzhang@ipe.ac.cn; mp@kt.dtu.dk

NADH is a cofactor required for hydrogenation of CO_2 to formic acid, formaldehyde, and methanol, but the high costs of NADH deter its large scale application. Photochemical NADH regeneration is a promising solution that utilizes limitless solar energy. The success of photochemical NADH regeneration depends on photosensitizer which, however, suffers from poor stability and a slow rate of electron transfer, from electron donor to photosensitizer and from photosensitizer to catalyst. Inspired by chlorophyll, ionic porphyrins were developed for efficient NADH regeneration. The results show that NADH was most efficiently *in-situ* regenerated using ZnTPyPBr as photosensitizer. Furthermore, compared to the free system (control), yield of methanol was increased almost three-fold by using membrane technology to integrate cascade enzymatic reaction and NADH regeneration.

Introduction.

Reduction of carbon dioxide (CO_2) is becoming a global strategy due to the worsening greenhouse effect.[1] Green conversion of CO_2 to useful chemicals and fuels has attracted great interest for renewable energy utilization and simultaneous alleviation of the problem of CO_2.[2, 3] Recently, redox biocatalysts have also become popular for reduction of CO_2, owing to the mild conditions, high selectivity, and environment-friendly characteristic.[4]

Sequential reduction of CO_2 to formic acid, formaldehyde, and methanol can be achieved by using formate dehydrogenase (FDH), formaldehyde dehydrogenase (FaldDH), and alcohol dehydrogenase (ADH), respectively.[5] However, three molar equivalents of NADH are consumed to transform one molar equivalent of CO_2 to methanol, which leads to high cost and deters large scale application. Therefore, in order to cut down costs, NADH regeneration by photocatalysis is a promising solution that can utilize limitless solar energy.[6] In natural photosynthesis, the reaction occurs via multi-step electron-transfer and generation of a reducing agent (i.e. NADPH), as illustrated in **Scheme 1A**. The process is known as the Calvin cycle, and in photosynthesis a key role is played by chlorophyll as photosensitizer. In contrast,

artificial photosynthesis mimics natural photosynthesis is much simpler. A redox enzymatic reaction was carried out, coupled with photochemical regeneration of cofactors.[7, 8] As illustrated in **Scheme 1B,** NAD^+ is reduced to NADH catalyzed by electron mediator **M** (catalyst). In the meanwhile, photosensitizer receives electrons from an electron donor (triethanolamine, TEOA), and the electrons are excited by photosensitizer irradiated by solar energy. Then the excited electrons are transferred from photosensitizer to **M,** providing a high reduction equivalent for efficient photo-regeneration of NADH. Therefore the photosensitizer plays a key role in exciting electron and transferring electrons to **M** under visible light and determines whether efficient NADH regeneration can be achieved in artificial photosynthesis.

During the past decade, many efforts have been made in developing efficient photosensitizer for establishing artificial photosynthesis system.[9, 10] Some inorganic species such as semiconductors, graphene-based material, and metal nanoparticles are usually applied as photosensitizers for cofactor regeneration in artificial photosynthesis.[11-13] But they suffer poor stability and a slow rate of electron transfer from the electron donor to the photosensitizer, and fast energy-wasting back-electron transfer from the electron mediator (**M**) to the photosensitizer.[14] Inspired by chlorophyll, the porphyrins and porphyrin derivatives with similar structures have attracted great interests and have been explored as biomimetic light-harvesting molecules to facilitate the generation of photo-excited electrons from an electron donor under irradiation. This is possible because the porphyrin ring as the active site can effectively absorb photons and transfer electrons to the electron mediator (**M**).[15] Kim and Park et al. report that Zn-tetrakis(4-carboxyphenyl) porphyrin as the light-harvesting molecule was used for regenerating NADH utilizing solar energy, and NADH conversion could be achieved to 20% after 60 minutes.[16] 5,10,15,20-tetrakis(3-hydroxyphenyl)- 21H,23H-porphine (mTHPP) was encapsulated in raw material from plants for NADH regeneration was reported by Lee and Park et al.[17] In addition, Liu and Wang et al. report that Zn-tetrakis(4-carboxyphenyl)porphyrin was applied as a photosensitizer for NADH regeneration under visible light.[18] However, the porphyrins owing to their hydrophobic properties were mostly applied together with various immobilization methods using support materials and structures. Since NADH regeneration and the enzymatic reaction occurs in aqueous solution with water-soluble electron mediator and the electron donor, the limited solubility of porphyrins results in a phase interface between the undissolved part and the aqueous phase; this interface is a potential barrier of photo-generated electron transport.[17] Therefore, to increase the hydrophilicity and polarity of porphyrins, porphyrins were proposed to modify to ionic liquids (ILs) and with grafting a carboxyl group. Furthermore, ionic porphyrins were also expected to reduce the energy barrier and enhance the rate of electron transfer due to ionic liquids properties applied in electrochemistry.[19] Therefore

four porphyrin-based photosensitizers were evaluated for NADH regeneration in this study. For NADH regeneration, the reaction system also included electron mediator rhodium complex **M** ($[Cp^*Rh(bpy)H_2O)]^{2+}$) and electron donor (TEOA), which have been recognized as one of the most popular and efficient electron mediator and electron donor for specifically photosynthesizing NADH from NAD^+.[20, 21]

Next, we sought to develop a biocatalytic artificial photosynthesis platform for integration of cascade reduction of CO_2 to methanol coupled with photo-regeneration of NADH. Based on our previous research, enzyme immobilization in membranes can be achieved by using "reverse filtration" of the enzyme solution.[22] Enzymes were immobilized by physical adsorption, where the enzymatic membrane reactor can make possible to reuse enzymes in continuous mode and improve enzyme stability, and the product can be extracted to relieve the product inhibition effect. In this study, the immobilization method was further developed by grafting electron mediator (**M**) and co-deposition of polydopamine (PDA) with polyethyleneimine (PEI). After enzyme immobilization followed by PDA/PEI coating, PDA/PEI under weakly alkaline conditions forms a stable self-polymerized coating layer on various supports, which has been widely used for enzyme immobilization.[23] Furthermore, PDA/PEI layer can be improved catalytic efficiency by adsorbing and enriching substrates (CO_2).[24] In nest step, for grafting electron mediator **M**, **M** can be grafted on the surface of PDA/PEI layer by electrostatic force. Since the polymer PDA/PEI takes negative charge in pH 7 solution, the positive charge **M** can be grafted on to PDA/PEI when the two are mixed in solution. This method is simple, facile, stable, and shows less harm to enzyme activity because it is biocompatible and the noncovalent bonding dominant.

In this work, four kinds of porphyrins, i.e. HTPyP, HTPyBr, ZnTPyP, and ZnTPyPBr (see Fig. S1), were evaluated for their performance of NADH regeneration. An integrated biocatalytic photosynthesis system was constructed to incorporate solar-driven NADH regeneration and cascade reduction of CO_2 to methanol.

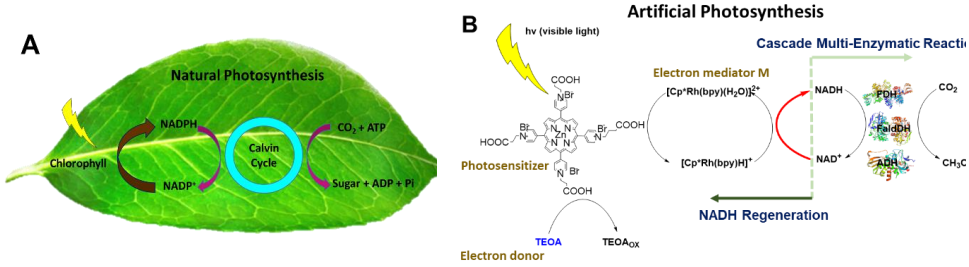

Scheme 1. An illustrative description of natural photosynthesis (**A**) and artificial photosynthesis (**B**). In both systems, organic dye as photosensitizer is used for regenerating NADH and providing cofactor in a reduced form for enzymatic synthesis.

2. Experimental

2.1 Materials

Formate dehydrogenase from *Candida boidinii* (FDH, EC.1.2.1.2, homo-dimer, 76 kDa), formaldehyde dehydrogenase from *Pseudomonas sp*. (FaldDH, EC.1.2.1.46, homo-dimer, 150 kDa), yeast alcohol dehydrogenase (ADH, EC 1.1.1.1, 141 kDa), reduced and oxidized nicotinamide adenine dinucleotide (NADH/NAD^+, 98wt%), methanol, Dopamine hydrochloride (DA), Poly(ethyleneimine) (PEI), ether, triethanolamine (TEOA), fluorescein isothiocyanate (FITC), 3-Bromopropionic acid (97 wt%), 2,2-bipyridine, dichloro-(pentamethylcyclopentadienyl) rhodium (III) dimer ($[Cp^*RhCl_2]_2$), 5,10,15,20-Tetra(4-pyridyl)-21H,23H-porphine (HTPyP 97%), Zinc 5,10,15,20-tetra(4-pyridyl)-21H,23H-porphine (ZnTPyP), were all were purchased from Sigma Aldrich (St. Louis, MO, USA). CO_2 gas (>99.5%) in a cylinder was purchased from AGA A/S (Denmark). Commercial UF membranes (PLGC, Millipore) used in this work have a regenerated cellulose skin layer on polypropylene support and a molecular weight cut-off of 10 kDa.

2.2 Synthesis of ionic porphyrins.

1 mM dark blue powder of porphyrins (HTPyP or ZnTPyP) and 4 mM 3-bromopropionic acid were added to 10 mL DMF with magnetic stirring in the dark, and then the mixture was heated up to 100 °C and kept under N_2 atmosphere for 8 h. After cooling to room temperature, the resultant purple solids were successively washed with deionized water and anhydrous ethanol and then dried in a vacuum oven for 3 h at 50 °C.

2.3 Synthesis of electron mediator (M) $[Cp^*Rh(bpy)(H_2O)]^{2+}$

The electron mediator (**M**), [Cp*Rh(bpy)Cl]Cl, (Cp* 5-C5Me5, bpy 2,2-bipyridyl) was synthesized as described in the literature.[18] In brief, the general procedure for the synthesis was as follows: $[Cp^*RhCl_2]_2$, (61.808 mg) was added to 4 mL of anhydrous methanol, where it did not dissolve but rather was dispersed in the anhydrous methanol. Upon addition of 2,2-bipyridine (31.238 mg), the suspension cleared almost immediately, and a yellowish solution was formed. From this mixture, **M** was precipitated after addition of anhydrous ether. The NMR of electron mediator **M** can be seen in the supporting information (Figure S3).

2.4 Immobilization of Enzymes (FDH, FaldDH, and ADH).

Three enzymes of 100 mL liquid FDH, 1.0 mg solid FaldDH, and 1.5 mg solid ADH were immobilized in the 10 kDa regenerated cellulose membrane. Enzyme immobilization was

carried out at a pressure of 2 bar and permeate was collected in precision cylinders for analysis. The cylinders were replaced manually for every 4 mL. At the end of filtration, the 'fouled' membrane was washed with 10 mL of buffer at a pressure of 2 bar and then rinsed 3 times with buffer without pressure. The amount of immobilized enzyme (loading) was calculated from the mass balance equation. The immobilization efficiency was expressed as enzyme loading efficiency (loading efficiency = m_i/m_t) where m_i and m_t are the amount of immobilized and total enzyme, respectively.

2.5 PDA/PEI deposition and electron mediator (M) grafting on the support layers of the membrane.

After enzyme immobilization, the support layer of the UF membrane was co-deposited with PDA and PEI. PDA and PEI with a mass ratio of 1:1 were added in Tris-HCl buffer (50 mM, pH 8.5) under magnetic stirring (100 rpm) at 28 °C, and finally concentration of both PDA and PEI are 2 mg mL^{-1}. After stirring for 2 h, the brown suspension and precipitates were washed out with deionized water. Then the electron mediator **M** was immobilized on the surface of the PDA/PEI modified support layer of the membrane. **M** powder (4 mg) was first dissolved in 4 mL deionized water to make a 1.3 mM solution, which was then stirred for 5 min in the dark. At certain time intervals, the change in the absorbance value at 280 nm (typical absorbance peak of **M**) was monitored using a UV-vis spectrophotometer, and the loading capacity of **M** was then calculated. Subsequently, the membranes were stored in 10 mL of phosphate buffer (pH 7) overnight.

2.6 NADH regeneration.

NADH regeneration was performed in a quartz reactor (Nmerry, China) in an Ar atmosphere at room temperature. 1 mM NAD^+ and 0.5 mM **M** were dissolved in a degassed phosphate buffer (100 mM, pH 7.5) containing 15 w/v% TEOA. In an Ar atmosphere, degassed phosphate buffer can prevent the oxidation of NADH to NAD^+. We then dissolved 0.5 mM porphyrin in the reaction solution, which was exposed to light from a 450 W Xe research arc lamp source (Nmerry, China) (62 mW cm^{-2}) with a 420 nm cut-off filter. The concentration of NADH was measured using a spectrophotometer (Biospec Mini, Shimadzu Co., Japan) at an absorbance of 340 nm.

2.7 Multi-enzymatic reaction.

The conversion of CO_2 to methanol was performed in aqueous solution with free or

photocatalytic NADH regeneration in a quartz cuvette reactor in an Ar atmosphere at room temperature, using a 450-W Xenon lamp with a 420-nm cut-off-filter as the light source. 10 mL of buffer solution (100 mM phosphate buffer, pH 7.0) was bubbled with N_2 and CO_2 gas for 0.5 h. The mixture solution of 0.5 mM porphyrin, 1 mM NAD^+, and 15 wt% TEOA was added in the reactor and mixed with the photocatalytic membrane. For the free system, a mixture solution of 100 μL liquid FDH, 1.0 mg solid FaldDH, 1.5 mg solid ADH, and 1 mM NADH was used in all enzymatic reactions. According to the reaction route, three moles of NADH are stoichiometrically consumed to produce one mole of methanol in the cascade reaction. Therefore the methanol yield ($Y_{methanol}$) based on NADH can be calculated using the following equation.

$$Y_{methanol}\ (\%) = \frac{C_{methanol*3}}{C_{NADH,initial}} * 100$$

Where $C_{methanol}$ is the methanol concentration (mM), and $C_{NADH,initial}$ is the initial NADH concentration (mM).

2.8 Analytical methods.

A Hewlett Packard HP6890 gas chromatograph (GC) equipped with a FID (250 ℃) and a Restek XTI-5 column (30 m × 0.25 mm i.d., film thickness 0.25 mm) was used for methanol concentration. The carrier gas was N_2 with a flow rate of 0.4 mL min^{-1}. The ethyl acetate is as internal standard substance, injector temperature was 150 ℃, and the injection sample volume was 1 μL. Scanning electron microscopy (SEM) was performed using an FEI Helios EBS3 dual beam electron microscope. The skin and support samples were prepared by cutting a small square of the membrane, which was then attached to an aluminium stub by means of double-sided sticky carbon tape. The edges of the sample were mounted on the aluminium stub by means of copper tape. After freezing the membrane sample by plunging in liquid nitrogen, cross sections of the membrane skin and the support were cut with a pair of scissors. The cross sections were mounted on a slotted specimen stub and fixed with copper tape. All samples were coated with Pt for 2 s at 80 mA in a Cressington 208HR Sputter Coater to give, an approximate coating thickness of 4 nm. The micrographs were obtained with an Everhart Thornley detector at low magnification and with a Thru-the-Lens detector at high magnification, in a high vacuum at 5 keV acceleration voltage and 43 pA current. 1H NMR spectra were recorded at 298 K on an NMR spectrometer (av-600 MHz, D_2O, Bruker, Switzerland). Solutions were prepared by dissolving 20–30 mg of sample in 0.7 mL of D_2O. A linear sweep voltammogram was carried out by using CHI 660E electrochemical working station with a conventional three-electrode system. Platinum wire was used as the working electrode and the counter electrode. The

reference electrode was a silver wire. The scanning rate was 10 mVs^{-1}. Fourier-transform infrared (FT-IR) spectra of samples were collected using a JASCO FT-IR-6100 spectrometer (JASCO Inc., Tokyo, Japan) at a resolution of 2 cm^{-1}. Confocal laser scanning microscopy (CLSM) was performed using a Leica TCS SP5 microscope (Leica Camera AG, Germany). The laser was excited FITC at a wavelength of 488 nm, and the emitted fluorescent light was detected at 545 nm. Elemental mapping was carried out by energy dispersive X-ray spectroscopy (EDS) (Inca X-MAX, Oxford, UK), which was directly connected to a scanning electron microscope (JSM-7001F). The wettability of the nanofi ber membranes was evaluated using a contact-angle instrument (DSA100, Kruss, Germany). A droplet of water with controlled volume was deposited on the membrane surface. The shape evolution of the droplet was monitored using a high-speed camera operating at 250 frames per second. Analyses of the droplet shape and contact-angle measurements were performed using the accompanying software of the instrument.

3. Results and discussions

3.1 Comparison of four photosensitizers in NADH regeneration.

Four porphyrin-based ILs, i.e. HTPyP, HTPyBr, ZnTPyP, and ZnTPyPBr (see Fig. S1), were examined as photosensitizer for the efficiency of their electron transfer in photochemical regeneration of NADH from NAD^+. As shown in **Figure 1**, NAD^+ was not reduced to NADH at all in the dark stage (the first 60 minutes) and then, under irradiation of visible light, the yield of NADH increased over time in the four kinds of photosensitizer systems. The yields of NADH for HTPyP (2.9%), HTPyBr (14.1%), ZnTPyP (21.6%), and ZnTPyPBr (34.5%) were obtained at 180 minutes. It is clear from **Figure 1** that the photocatalytic efficiency of HTPyP, HTPyBr, ZnTPyP, and ZnTPyPBr increase in turn. Zinc-containing porphyrins (ZnTPyPBr and ZnTCPyP) are distinctly superior for NADH regeneration compared to porphyrins without zinc (HTPyBr and HTPyP). The high and efficient performance of Zn-containing porphyrin can be explained by their electronegativity and aggregation behavior. After inserting zinc in the porphyrin ring (i.e. HTPyBr → ZnTPyPBr, HTPyP → ZnTCPyP), the electronegativity of porphyrin is further decreased, which enhances the electron-accepting ability of Zn-containing porphyrin from the electron donor (TEOA).[25] Furthermore, based on Zhang and Ye et al.'s report, porphyrin molecules are easily aggregated in aqueous solution, which harms to their photocatalytic efficiency.[26] In contrast, Zn-containing porphyrins are able to avoid the aggregation of porphyrin molecules by forming delocalization π bonds between the metal ions (zinc) and the porphyrins; this interaction also contribute to efficient transfer of electrons.[16]

After modifying non-ionic porphyrins (HTPyP and ZnTPyP) to ionic porphyrins (HTPyBr and ZnTPyPBr) as well as grafting on an extra carboxyl group, ionic porphyrins are catalytically better for NADH regeneration compared to non-ionic porphyrins accordingly. Since the ionic form of porphyrin is much more polar and the functional carboxyl group is hydrophilic, the solubility of ionic porphyrin in the water is significantly increased compared to the porphyrin molecule. In contrast, limited solubility of non-ionic porphyrins in aqueous solution results in a phase interface between the undissolved part and the aqueous phase, and this interface is a potential barrier of photo-generated electron transport.[27] To confirm that electrons transferred from ionic photosensitizer to **M**, the reduction potential of **M** and of the ionic photosensitizers was measured in water. The reduction potential of **M** (E_{red}: -0.31 V vs. Ag/Pt) was higher than those of the HTCPyPBr (E_{red}: -0.92 V vs. Ag/Pt) and ZnTCPyPBr (E_{red}: -0.97 V vs. Ag/Pt), which enables the electron transfer from ionic porphyrins to **M**. Since the functional group carboxyl in the porphyrin has the function of electron-withdrawing, it enhances the separation of the excited electron-hole pairs in the porphyrin ring.[28] Moreover, the electric potential difference between ZnTCPyPBr and **M** is greater than the potential difference between HTCPyPBr and **M**, which indicates that electron transfer more easily from photosensitizer to **M** in the ZnTCPyPBr system. Therefore porphyrin functionalized with a carboxyl group and zinc atom (ZnTPyPBr) shows best catalysis performance in terms of yield of NADH.

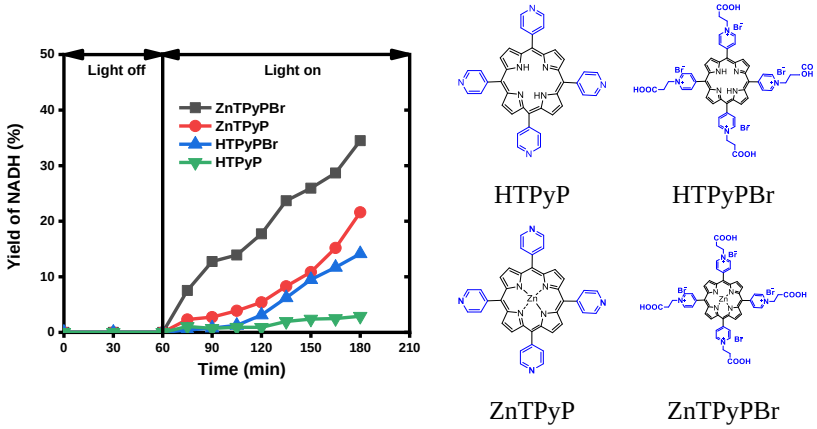

Figure 1. Four kinds of photosensitizers are tested separately in visible-light driven NADH regeneration: ZnTPyPBr (gray), ZnTPyP (red), HTPyPBr (blue), HTPyP (green). Each reaction contains 0.5 mM photosensitizer, 0.5 mM electron mediator **M**, 1 mM NAD^+, and 15 wt% TEOA in a degassed phosphate buffer (pH 7).

3.2 Fabrication and characterization of the photocatalytic membrane.

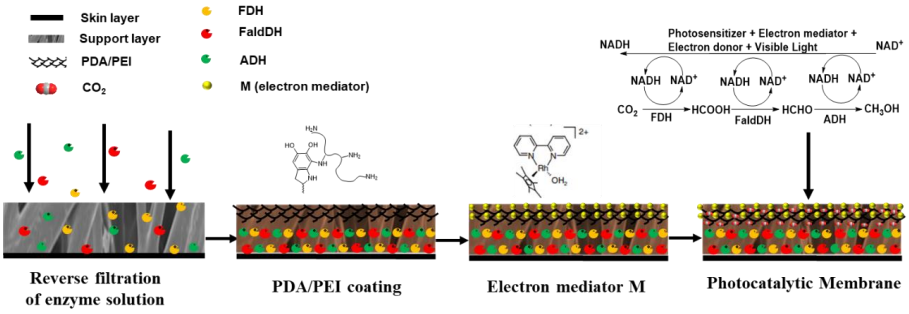

Figure 2. Schematic illustration of the synthesis of a photocatalytic membrane

In order to establish a biocatalytic artificial photosynthesis system, a biocatalytic photosynthesis membrane was fabricated according to a specific sequence of steps. As shown in **Figure 2**, enzymes were first immobilized in the support layer of the membrane. Then PDA and PEI were co-deposited on the surface of the support layer for sealing the enzymes to prevent leaking. Last, electron mediator **M** was grafted on the PDA/PEI layer for NADH regeneration.

Three enzymes, FDH, FaldDH, and ADH, were first co-immobilized in the support layer of the membrane by using "reverse filtration" of the enzyme solution. As the enzymes were loaded, permeate flux dropped from 330 ± 6 L m^{-2} h^{-1} bar^{-1} to 3.04 L m^{-2} h^{-1} bar^{-1} and the permeate volume was recorded over time, see **Figure S2**. Based on the membrane fouling mechanism induced by the enzymes, four fouling models were categorize, which refer to the standard, intermediate, complete blocking, and cake layer models presented in **Table S1**.[29] As a result, the cake layer model, which had a high correlation coefficient, was the best description of the loading mechanism and indicated that most enzymes were entrapped in the support layer. The morphology of membrane before and after enzyme immobilization was characterized by scanning electron microscope (SEM), as shown in **Figure 3**. Some enzyme aggregates clearly adsorbed on the surface of the polypropylene support fibers (**b1, b2, b3** in **Figure 3**). Furthermore, three enzymes were further detected by confocal laser scanning microscopy (CLSM) images by dying the enzymes for distinguishing with the possible existence of impurity (see **Figure 4**). Use of the membrane fouling model and characterization by SEM and CLSM indicated that enzymes were successfully immobilized and the fouling-induced enzyme immobilization involved at least two mechanisms: entrapment and adsorption.

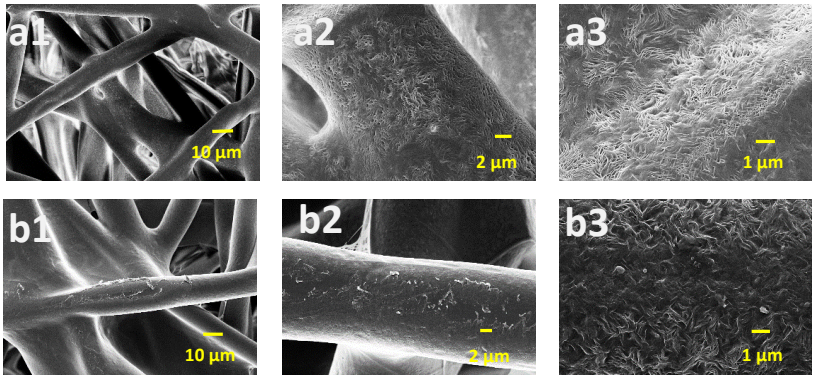

Figure 3. SEM images of the support layer (nonwoven polypropylene) of the membrane before enzyme immobilization in the first row (**a1, a2, a3**), and view of the support layer after enzyme immobilization in the second row (**b1, b2, b3**). The images are zoomed from left to right.

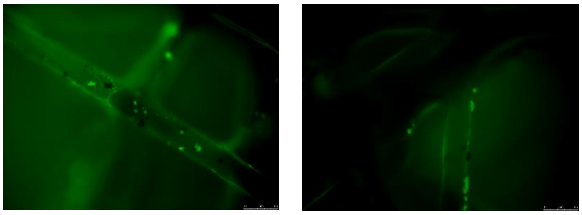

Figure 4. CLSM image of FITC-labeled FDH, FaldDH, and ADH immobilized on the surface of support fibers.

For deposition of PDA/PEI on the support layer, FTIR spectra of PPE (a), PDA/PEI (b), and PPE + PDA/PEI (c) are presented in **Figure 5.** For the virgin support layer in **Figure 5 (a)**, the peaks at 3000-2800 and 1460 cm^{-1} were attributed to the stretching vibration of methylene and the bending vibration of C-H, respectively. After coating PDA/PEI on the support layer, strong absorbance peaks at 3332 and 1640 cm^{-1} in **Figure 5 (c)** separately correspond to the characteristic peak of N-H and C=O in PDA/PEI, which shows a slightly red-shift compared to the peaks in **Figure 5 (b)**. Besides, the peaks at 1016 cm^{-1} could be ascribed to the vibration of C-N, which is consistent with the peaks in **Figure 5 (b)**. Furthermore, the morphology of PDA/PEI coating was observed by SEM in **Figure 6**, where it is clearly seen that a PDA/PEI layer covered the surface of the polypropylene fibers. After deposition of PDA/PEI on the polypropylene fibers, contact angle was changed from 113.0° to 23.1°, which is beneficial for the entry of substrate and cofactor into the active center of the enzyme as well as beneficial for separation of product from enzymes.

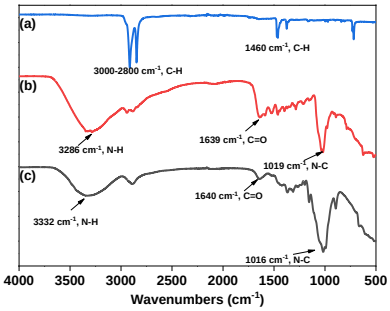

Figure 5. FTIR spectra of (a) PPE (Polypropylene, virgin support layer, VSL), (b) PDA/PEI, (c) VSL + PDA/PEI.

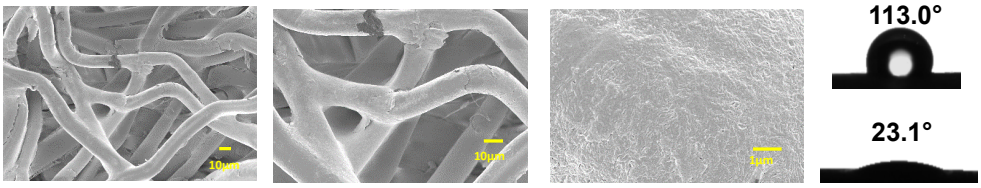

Figure 6. SEM images of the support layer (nonwoven polypropylene) of the membrane after enzymes immobilization and deposition of PDA/PEI. Contact angle of the support layer of the membrane before (113.0°) and after (23.1°) deposition of PDA/PEI (right).

After deposition of PDA/PEI, electron mediator **M** was grafted on the surface of the PDA/PEI layer by electrostatic forces. Since the weak alkali of polymer PDA/PEI shows negative charge, electrostatic interaction occurs when the positively charged **M** was mixed in the solution. As shown in **Figure 6,** the characteristic element Rh in the electron mediator **M** measured by energy-dispersive X-ray spectroscopy (EDS) was clearly present on the surface of membrane fiber, which is accordance with the picture of the support layer detected by SEM. Surprisingly, the characteristic element Br in the ionic porphyrins can be partly adsorbed on the surface of PDA/PEI layer, which is probably caused by interaction between carboxyl groups in the ionic photosensitizer and the amino group in PDA/PEI layer. Co-immobilization of the electron mediator and photosensitizer in one layer may enhance electron transfer to the electron mediator **M**.

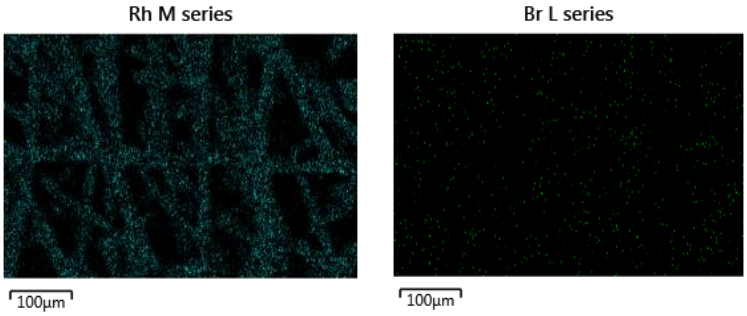

Figure 6. The distribution of Rh (left) and Br (right) elements on the surface of support fibers covered by polymer PDA/PEI.

3.3 Multi-enzymatic reaction with NADH regeneration.

Four kinds of photosensitizers were separately applied in photochemical NADH regeneration for sequential reduction of CO_2 to methanol. The free system without NADH regeneration was used as a control in a batch reactor. As shown in **Figure 7**, the yield of methanol in the contained-ZnTPyPBr system, which gave the best catalytic performance, reached 73.6% after 300 minutes. In contrast, the yield of methanol in the contained-HTPyP system was the lowest at 6.9% after 300 minutes. Such results comply with the sequence of photocatalytic performance of photosensitizer (see **Figure 1**) and indicate that increase in NADH concentration leads to more product generation. Indeed, Razieh et al. report that increase of NADH was favorable for the formic acid production in enzymatic conversion of CO_2.[30] However, the yield of methanol in the free system was 25.4% after 300 minutes and achieved the highest NADH concentration (1 mM) that can be considered as complete transformation of NAD^+ to NADH at the start of the reaction. Based on the Razieh et al. report, an inhibitory effect was observed at higher concentrations of NADH, and optimum values for maximum FDH activity of 0.45mM and 0.51mM were obtained, respectively, by free and immobilized enzymes.[30] Thus, in the current work, by introducing the photocatalytic NADH regeneration step, NADH was regenerated *in-situ* from NAD^+ at a low concentration in the beginning of the multi-enzymatic reaction. As the NADH accumulation, NADH was consumed by enzymes to maintain favorable balance of NADH concentration for the enzymes, which can decrease the inhibition effect of FDH and achieve the best catalytic performance of enzymes.

The low yield of methanol in the free system may be explained by the low solubility of CO_2 in water. Based on our previous research, the first reaction (CO_2 → formic acid) catalyzed by FDH plays a decisive role in cascade reduction of CO_2 to methanol, and efficient conversion of CO_2 to formic acid is limited by low CO_2 concentration made available by FDH. Therefore low

concentration of formic acid generation leads to low generation of formaldehyde and methanol because the second reaction (formic acid → formaldehyde) requires a threshold concentration of formic acid to be activated, as reported by Luo and Manuel et al.[31] In contrast, by adopting the PDA/PEI coating layer in our study, a large amount of amino group was grafted for capturing CO_2 and providing FDH with a higher local CO_2 concentration that contributed to CO_2 conversion. Indeed, Wang and Liu et al. reported that the reaction rate of enzymatic CO_2 hydrogenation was increased from 0.280 to 6.90 μM/min by grafting PEI on the surface of the support to capture CO_2.[24] In this regard, Ober and Dave immobilized the three enzymes in silica sol-gel matrixes, confining and reducing the volume of the enzymes in such a manner that the local concentration of reactants (CO_2) was enhanced.[5] Jiang followed a similar strategy (increasing local CO_2 concentration) and was able to increase the yield of methanol by breaking the unfavorable equilibrium by switching it to the right (formic acid) is a favorable manner to enhance the overall conversion.[32] To sum up, by using *in-situ* NADH regeneration and increasing local concentration of CO_2 around FDH, the yield of methanol was increased three-fold compared to the free system. Therefore the solar-energy driven synthesis of methanol from CO_2 using a biomimetic artificial photocatalytic membrane developed in this study may be considered all the more promising.

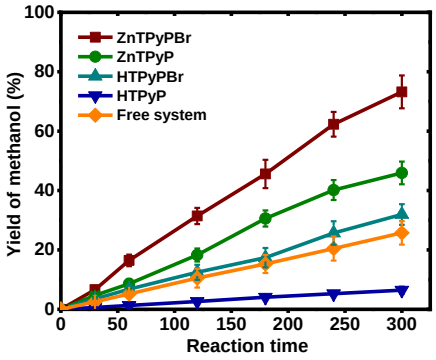

Figure 7, Photo-enzymatic synthesis of methanol from CO_2 catalyzed by enzymes (i.e. FDH, FaldDH, and ADH) either coupled with different photosensitizers for NADH regeneration or without NADH regeneration. ZnTPyP system (wine), ZnTPyP (olive), HTPyPBr (dark cyan), HTPyP (blue), free system (orange). For NADH regeneration, 0.5 mM porphyrin, 0.5 mM **M**, 1 mM NAD^+, and 15 wt% TEOA. For the free system: 1 mM NADH. Three enzymes, 100 μL liquid FDH, 1.0 mg solid FaldDH, and 1.5 mg solid ADH, were used in all enzymatic reactions.

Conclusions

ZnTPyPBr was shown to be the most suitable ionic porphyrin for efficient light harvesting and electron transfer for NADH regeneration. The development of an integrated artificial photosynthetic system using membrane technology provides a novel photocatalytic platform for cascade reduction of CO_2 to methanol and simultaneous NADH regeneration. With this system an almost three-fold increase in yield of methanol was obtained compared to the free system. Such integrated artificial photosynthesis is facilely fabricated under mild conditions and is environmentally friendly. This process it therefore expected to offer a useful platform for photo-enzymatic reaction systems that enable efficient and sustained production of a broad range of chemicals and fuels from sunlight.

List of Abbreviation

NADH: Reduced nicotinamide adenine dinucleotide

NAD^+: Nicotinamide adenine dinucleotide

FDH: Formate dehydrogenase

FaldDH: Formaldehyde dehydrogenase

ADH: Alcohol dehydrogenase

M: Pentamethylcyclopentadienyl rhodium dichloride dimer

TEOA: Triethanolamine

HTPyP: 5,10,15,20-Tetra(4-pyridyl)-21H,23H-porphine

HTPyPBr: 5,10,15,20-Tetra(4-pyridyl)-21H,23H-porphine tetrabromide

ZnTPyP: Znic 5,10,15,20-Tetra(4-pyridyl)-21H,23H-porphine

ZnTPyPBr: Znic 5,10,15,20-Tetra(4-pyridyl)-21H,23H-porphine tetrabromide

Conflicts of interest

There are no conflicts to declare.

Notes and references

1. C. D. Allen, A. K. Macalady, H. Chenchouni, D. Bachelet, N. McDowell, M. Vennetier, T. Kitzberger, A. Rigling, D. D. Breshears, E. H. Hogg, P. Gonzalez, R. Fensham, Z. Zhang, J. Castro, N. Demidova, J. H. Lim, G. Allard, S. W. Running, A. Semerci and N. Cobb, *Forest Ecology and Management*, 2010, **259**, 660-684.
2. C. Costentin, M. Robert and J. M. Saveant, *Chem Soc Rev*, 2013, **42**, 2423-2436.
3. C. Costentin, S. Drouet, M. Robert and J. M. Saveant, *Science*, 2012, **338**, 90-94.
4. J. F. Shi, Y. J. Jiang, Z. Y. Jiang, X. Y. Wang, X. L. Wang, S. H. Zhang, P. P. Han and C. Yang, *Chem Soc Rev*, 2015, **44**, 5981-6000.
5. R. Obert and B. C. Dave, *J Am Chem Soc*, 1999, **121**, 12192-12193.
6. S. H. Lee, J. Ryu, D. H. Nam and C. B. Park, *Chem Commun*, 2011, **47**, 4643-4645.
7. H. Imahori, Y. Mori and Y. Matano, *Journal of Photochemistry and Photobiology C-Photochemistry Reviews*, 2003, **4**, 51-83.
8. H. Imahori, T. Umeyama and S. Ito, *Accounts Chem Res*, 2009, **42**, 1809-1818.
9. S. K. Kuk, R. K. Singh, D. H. Nam, R. Singh, J. K. Lee and C. B. Park, *Angew Chem Int Edit*, 2017, **56**, 3827-3832.
10. R. K. Yadav, J. O. Baeg, G. H. Oh, N. J. Park, K. J. Kong, J. Kim, D. W. Hwang and S. K. Biswas, *J Am Chem Soc*, 2012, **134**, 11455-11461.
11. J. Liu and M. Antonietti, *Energ Environ Sci*, 2013, **6**, 1486-1493.
12. J. H. Huang, M. Antonietti and J. Liu, *J Mater Chem A*, 2014, **2**, 7686-7693.
13. R. K. Yadav, G. H. Oh, N. J. Park, A. Kumar, K. J. Kong and J. O. Baeg, *J Am Chem Soc*, 2014, **136**, 16728-16731.
14. L. C. Sun, B. Akermark and S. Ott, *Coordination Chemistry Reviews*, 2005, **249**, 1653-1663.
15. A. Yella, H. W. Lee, H. N. Tsao, C. Yi, A. K. Chandiran, M. K. Nazeeruddin, E. W. Diau, C. Y. Yeh, S. M. Zakeeruddin and M. Gratzel, *Science*, 2011, **334**, 629-634.
16. J. H. Kim, S. H. Lee, J. S. Lee, M. Lee and C. B. Park, *Chem Commun*, 2011, **47**, 10227-10229.
17. M. Lee, J. H. Kim, S. H. Lee, S. H. Lee and C. B. Park, *Chemsuschem*, 2011, **4**, 581-586.
18. J. S. Yanzi Wang, Haohai Zhang, Zhiping Zhao，Wenfang Liu, *Catal Sci Technol*, 2018, **8**, 2578.
19. J. Estager, J. D. Holbrey and M. Swadzba-Kwasny, *Chem Soc Rev*, 2014, **43**, 847-886.
20. H. K. Song, S. H. Lee, K. Won, J. H. Park, J. K. Kim, H. Lee, S. J. Moon, D. K. Kim and C. B. Park, *Angew Chem Int Edit*, 2008, **47**, 1749-1752.

21. X. Y. Ji, Z. G. Su, P. Wang, G. H. Ma and S. P. Zhang, *Small*, 2016, **12**, 4753-4762.
22. Z. B. Zhang, J. Muschiol, Y. H. Huang, S. B. Sigurdardottir, N. von Solms, A. E. Daugaard, J. Wei, J. Q. Luo, B. H. Xu, S. J. Zhang and M. Pinelo, *Green Chem*, 2018, **20**, 4339-4348.
23. J. Q. Luo, A. S. Meyer, R. V. Mateiu, D. Kalyani and M. Pinelo, *Acs Appl Mater Inter*, 2014, **6**, 22894-22904.
24. Y. Z. Wang, Y. Z. Chen, C. H. Wang, J. Sun, Z. P. Zhao and W. F. Liu, *Acs Appl Mater Inter*, 2018, **10**, 29003-29009.
25. S. L. Anne Brisach Wittmeyer, Maurice Gross, Alain Giraudeau, *Journal of Electroanalytical Chemistry*, 2005, **576**, 129-137.
26. H. Zhang, J. Wei, J. Dong, G. Liu, L. Shi, P. An, G. Zhao, J. Kong, X. Wang, X. Meng, J. Zhang and J. Ye, *Angewandte Chemie*, 2016, **55**, 14310-14314.
27. Y. B.-h. NIU Jin-fen, YU Xiao-jiao, PENG Chao, LU Lei-lei, *Journal of Functional Materials*, 2013, **44**, 1132-1135.
28. M. Wei, J. M. Wan, Z. W. Hu, Z. Q. Peng and B. Wang, *Applied Surface Science*, 2016, **377**, 149-158.
29. E. K.-M. Affaro Affandy, Henk K. Versteeg, *J Membrane Sci*, 2013, **437**, 150-159.
30. R. Barin, D. Biria, S. Rashid-Nadimi and M. A. Asadollahi, *J Co2 Util*, 2018, **28**, 117-125.
31. J. Q. Luo, A. S. Meyer, R. V. Mateiu and M. Pinelo, *New Biotechnol*, 2015, **32**, 319-327.
32. X. L. Wang, Z. Li, J. F. Shi, H. Wu, Z. Y. Jiang, W. Y. Zhang, X. K. Song and Q. H. Ai, *Acs Catal*, 2014, **4**, 962-972.

Chapter 6 – Conclusions and Future Perspectives

Ionic liquids (ILs) are melting salts with unique properties, such as negligible vapor pressure and high thermal stability, which have been applied in many different scientific fields and have become one of the most rapidly developing areas in green chemistry. In this thesis, ILs are shown as advantageous substitutes of conventional buffers normally-used in enzymatic reactions, which improved the efficiency of the studied enzymatic reaction system and compensate the deficiencies of conventional buffers such system.

At the beginning of this study, an important observation was noticed: degradation of NADH occurs during the standard conditions at which this enzymatic reaction has been performed. Such degradation led to an overestimation of CO_2 conversion when measured by NADH absorbance (method N) that has been the standard method to follow this reaction by a number of authors. Obviously, NADH degradation also results in reducing conversion of CO_2. After investigating degradation mechanism of NADH using different analytical techniques, acidity was the main reason for degradation. By introducing IL ($BmimBF_4$) in the system, NADH was found to be "protected" because CO_2 was captured by the IL for preventing disassociation of the proton. Furthermore, the occurrence of IL also contributes to enhancing the concentration of substrate CO_2, which also benefitted the conversion of CO_2. Indeed, the concentration of CO_2 in ILs increased around 15-fold compared to conventional buffer. By incorporating the IL, there was more than twice as much CO_2 conversion compared to the conversion reached by the enzymatic reaction in phosphate buffer (traditional buffer).

Furthermore, the use of the biocompatible IL [CH][Glu] was found to change the conformation of formate dehydrogenase, which was demonstrated using molecular simulation dynamics. While CO_2 easily diffuses out of the active site in the other ILs tested, and especially in water, the conformation of FDH in the presence of [CH][Glu] was such that CO_2 stays for a longer time in the vicinity of the active site of the enzyme. Such longer CO_2 retention times resulted in a higher conversion of CO_2. By using this IL [CH][Glu], the yield of the product

methanol was increased three-fold compared to the yield in Tris-HCl buffer.

As regarding the NADH regeneration part, the results showed that an IL photosensitizer with lower reduction potential can efficiently activate electron transfer from photosensitizer to electron mediator under visible light, thus ensuring that NADH regeneration can be successfully achieved. Furthermore, the aggregation extent of ionic photosensitizers was lower than molecule photosensitizer and therefore electrons were enabled to efficiently transfer from the photosensitizer to in aqueous solution. Efficient photosensitizers show promise as tools for developing future artificial photosynthetic systems.

In this thesis, ILs were used as versatile aid that worked efficiently as 1) CO_2 adsorbents, 2) co-solvents for more efficient enzyme reactions, 3) photosensitizers. ILs were shown to be therefore promising alternatives (or co-solvents) to conventional buffers.

In future work, it will be important to pay more attention to the separation of products from ILs, so that ILs can be recycled IL and cost of using them can be decreased. Likewise, the catalytic efficiency of enzymes involved in CO_2 conversion should be improved to decrease costs of large scale use of enzymes. Therefore the research developed in the thesis pretends to be the proof of concept needed to develop the presented systems further that offers the possibility for potential industrial application of these solutions in the future.

References

1. T. Sakakura, J. C. Choi and H. Yasuda, *Chemical reviews*, 2007, **107**, 2365-2387.
2. Q. Ma, *Greenhouse Gases: Refining the Role of Carbon Dioxide*, 1998.
3. R. M. A. Corinne Le Quéré, Josep G. Canadell, Stephen Sitch, Jan Ivar Korsbakken, *Earth System Scientific Data*, 2016, **8**, 605-649.
4. G. A. Olah, *Angew Chem Int Edit*, 2005, **44**, 2636-2639.
5. B. Smit, *Faraday discussions*, 2016, **192**, 9-25.
6. P. Markewitz, W. Kuckshinrichs, W. Leitner, J. Linssen, P. Zapp, R. Bongartz, A. Schreiber and T. E. Muller, *Energ Environ Sci*, 2012, **5**, 7281-7305.
7. W. H. Wang, Y. Himeda, J. T. Muckerman, G. F. Manbeck and E. Fujita, *Chemical reviews*, 2015, **115**, 12936-12973.
8. L. J. Liu, H. L. Zhao, J. M. Andino and Y. Li, *Acs Catal*, 2012, **2**, 1817-1828.
9. J. Shi, Y. Jiang, Z. Jiang, X. Wang, X. Wang, S. Zhang, P. Han and C. Yang, *Chem Soc Rev*, 2015, **44**, 5981-6000.
10. Y. Yan, E. L. Zeitler, J. Gu, Y. Hu and A. B. Bocarsly, *J Am Chem Soc*, 2013, **135**, 14020-14023.
11. G. Fuchs, *Annu Rev Microbiol*, 2011, **65**, 631.
12. X. L. Wang, Z. Li, J. F. Shi, H. Wu, Z. Y. Jiang, W. Y. Zhang, X. K. Song and Q. H. Ai, *Acs Catal*, 2014, **4**, 962-972.
13. R. Obert and B. C. Dave, *J Am Chem Soc*, 1999, **121**, 12192-12193.
14. W. B. Hou, W. H. Hung, P. Pavaskar, A. Goeppert, M. Aykol and S. B. Cronin, *Acs Catal*, 2011, **1**, 929-936.
15. A. Gimat, V. Kasneryk, A. L. Dupont, S. Paris, F. Averseng, J. Fournier, P. Massiani and V. Rouchon, *New J Chem*, 2016, **40**, 9098-9110.
16. R. Castillo, M. Oliva, S. Marti and V. Moliner, *J Phys Chem B*, 2008, **112**, 10012-10022.
17. J. L. L. Carter, M. Bekhouche, A. Noiriel, L. J. Blum and B. Doumeche, *Chembiochem*, 2014, **15**, 2710-2718.
18. M. Beller and U. T. Bornscheuer, *Angew Chem Int Edit*, 2014, **53**, 4527-4528.
19. Y. Amao, N. Shuto, K. Furuno, A. Obata, Y. Fuchino, K. Uemura, T. Kajino, T. Sekito, S. Iwai, Y. Miyamoto and M. Matsuda, *Faraday discussions*, 2012, **155**, 289-296; discussion 297-308.
20. R. K. Yadav, J. O. Baeg, G. H. Oh, N. J. Park, K. J. Kong, J. Kim, D. W. Hwang and S. K. Biswas, *J Am Chem Soc*, 2012, **134**, 11455-11461.

21. T. Reda, C. M. Plugge, N. J. Abram and J. Hirst, *Proceedings of the National Academy of Sciences of the United States of America*, 2008, **105**, 10654-10658.
22. Y. Lu, Z. Y. Jiang, S. W. Xu and H. Wu, *Catal Today*, 2006, **115**, 263-268.
23. S. Kuwabata, R. Tsuda and H. Yoneyama, *J Am Chem Soc*, 1994, **116**, 5437-5443.
24. Z. B. Zhang, J. Muschiol, Y. H. Huang, S. B. Sigurdardottir, N. von Solms, A. E. Daugaard, J. Wei, J. Q. Luo, B. H. Xu, S. J. Zhang and M. Pinelo, *Green Chem*, 2018, **20**, 4339-4348.
25. J. Q. Luo, A. S. Meyer, R. V. Mateiu and M. Pinelo, *New Biotechnol*, 2015, **32**, 319-327.
26. U. M. Ulrich RUSCHING, Peter WILLNOW, Thomas HÖPNER, *European Journal of Biochemistry*, 1976, **70**, 325-330.
27. Z. B. Zhang, Q. Zhou, X. M. Lu, C. Z. Qiao and S. J. Zhang, *J Chem Eng Data*, 2014, **59**, 2377-2388.
28. L. A. Blanchard, Z. Y. Gu and J. F. Brennecke, *J Phys Chem B*, 2001, **105**, 2437-2444.
29. X. P. Zhang, X. C. Zhang, H. F. Dong, Z. J. Zhao, S. J. Zhang and Y. Huang, *Energ Environ Sci*, 2012, **5**, 6668-6681.
30. E. D. Bates, R. D. Mayton, I. Ntai and J. H. Davis, *J Am Chem Soc*, 2002, **124**, 926-927.
31. M. D. Fujita K, Forsyth M., *Chem Commun*, 2005, **38**, 4804-4806.
32. F. M. Fujita K, MacFarlane DR, Reid RW, Elliott GD., *Biotechnol Bioeng*, 2006, **94**, 1209-1213.
33. F. Hollmann, I. Arends and D. Holtmann, *Green Chem*, 2011, **13**, 2285-2314.
34. A. Weckbecker, H. Groger and W. Hummel, in *Biosystems Engineering I: Creating Superior Biocatalysts*, eds. C. Wittmann and W. R. Krull, 2010, vol. 120, pp. 195-242.
35. G. W. Rafter and S. P. Colowick, *Method Enzymol*, 1957, **3**, 887-890.
36. F. Hollmann, I. W. C. E. Arends and D. Holtmann, *Green Chem*, 2011, **13**, 2285-2314.
37. J. H. Kim, S. H. Lee, J. S. Lee, M. Lee and C. B. Park, *Chem Commun*, 2011, **47**, 10227-10229.
38. S. H. Lee, J. H. Kim and C. B. Park, *Chem-Eur J*, 2013, **19**, 4392-4406.
39. P. Jochems, Y. Satyawali, L. Diels and W. Dejonghe, *Green Chem*, 2011, **13**, 1609-1623.
40. J. Q. Luo, A. S. Meyer, G. Jonsson and M. Pinelo, *Biochem Eng J*, 2014, **83**, 79-89.

Appendix

Paper 1

Electronic supporting information

Ionic Liquids as Bifunctional Cosolvent Enhanced CO_2 Conversion Catalysed by NADH-dependent Formate Dehydrogenase

Zhibo Zhang[1, 2], Bao-hua Xu [2], Jianquan Luo [3], Nicolas von Solms [1], Hongyan He [2], Yaqin Zhang [2], Manuel Pinelo [1 *] and Suojiang Zhang[2 *]

[1] Department of Chemical and Biochemical Engineering, Building 229, Technical University of Denmark, DK-2800 Kgs. Lyngby, Denmark.
[2] Beijing Key Laboratory of Ionic Liquids Clean Process, Key Laboratory of Green Process and Engineering, State Key Laboratory of Multiphase Complex Systems, Institute of Process Engineering, Chinese Academy of Sciences, Beijing 100190, P. R. China.
[3] State Key Laboratory of Biochemical Engineering, Institute of Process Engineering, Chinese Academy of Sciences, Beijing 100190, PR China
*Correspondence: mp@kt.dtu.dk; Tel: +45-52695821; sjzhang@ipe.ac.cn; Tel: +86-010-82627080.

Supporting Information

1 General information 1
2 Analytical methods 2
2.1 N Methods for standard calibration curve 2
2.2 C Method for standard calibration curve 2
3 Results for degradation of NADH research. 3
3.1 Kinectic degradation of NADH. 3
3.2 Stability of NADH in ILs 4
3. 3 DFT calculation. 5
4 Chemicals Characterization 15
4.1 NMR of 1-butyl-3-methylimidazolium tetrafluoroborate (BmimBF$_4$) 16
4.2 NMR of Nicotinamide adenine dinucleotide (NADH) 16
4.3 NMR of nicotinamide adenine dinucleotide (NAD$^+$) 16
4.4 NMR of Mixture of NADH and BmimBF$_4$. 17
4.5 NMR for degradation of NADH. 17

1 General information

Enzyme reagent were all purchased from sigma-aldrich. Reagent (+98%) were commercially available unless otherwise stated. UV-Visible spectra were acquired with a Shimadzu UV-2550 UV–Visible spectrophotometer. NMR spectra were recorded on a Bruker ASCEND spectrometer (^{1}H, 600 MHz). ^{1}H NMR chemical shift δ is given relative to TMS and referenced to the solvent signal. The enzymatic reaction was conducted in a stainless-steel reactor (25 ml) equipped with two valves and a pressure gage. In such a reactor,

a buffer solution of FDH (3 μL) and NADH (1 mM) was bubbled with CO_2 for 5 min to remove the residual air, of which the pressure was adjusted to 1 bar afterwards. It was positioned in water bath at 37 °C for 3h. A sample was then taken out from reactor and prepared accordingly for analysis.

2 Analytical methods

2.1 N Methods for standard calibration curve

0.05, 0.1, 0.2, 0.3, 0.4, 0.5 mM NADH solution were prepared with 100mM phosphate buffer, and measured at 340nm by UV-vis spectrometer. Standard calibration curve is presented in Figure S1.

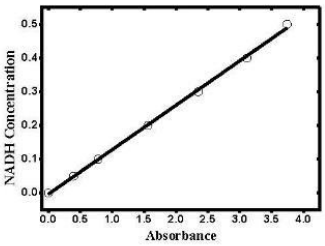

Figure S1. Standard calibration curve for NADH method.
Standard equation: $y = -0.00329+0.13173x$; $R^2=0.9988$

2.2 C Method for standard calibration curve

In case of formate in buffer, samples (0, 0.05, 0.1, 0.2, 0.3, 0.4, 0.5 mM formate solution) were prepared with 100mM phosphate buffer. Similarly, In case of formate in ILs, samples (0, 0.05, 0.1, 0.2, 0.3, 0.4, 0.5 mM formate solution) were prepared with accordingly contained-IL phosphate buffer. In a 10mL vial, 3.5 mL of 100% acetic anhydride, 50 μL of 30% (w/v) sodium acetate, and 1 mL of 2-propanol solution containing 0.5% (w/v) citric acid and 10% (w/v) acetamide were added. Assasy solution was added 0.5 mL of sample with 90min of incubation time at 25 °C. Using a UV–visible spectrophotometer, the absorbance was determined at 515 nm. The formate standard calibration curve is presented in Figure S2, S3, S4.

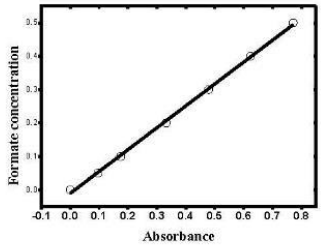

Figure S2. Standard calibration of formate for colorimetric method in buffer
Standard equation: $y=-0.01046+0.65532x$; $R^2=0.9987$

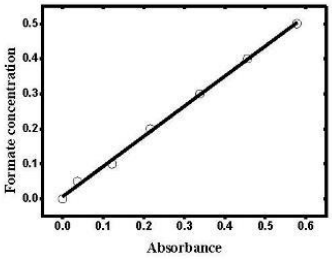

Figure S3. Standard calibration curve of formate for colorimetric method in $BmimBF_4$.
Standard equation: $y=-0.00702+0.85863x$; $R^2=0.9978$

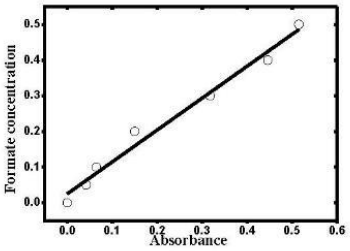

Figure S4. Standard calibration curve of formate for colorimetric method in BmimDCA.
Standard equation: $y=-0.02502+0.89511x$; $R^2=0.9794$

3 Results for degradation of NADH research.

3.1 Kinectic degradation of NADH.

The aqueous reaction of NADH with $BmimBF_4$ (5.0 equiv.) was conducted within a temperature range from 10 to 80 °C and Temperature-course plot (time interval: 10 min), which was monitored by an in-situ UV-vis spectrum.

To obtain the relation between NADH degradation kinetic rate (k) and temperature (T), data for NADH degradation is correlated by Arrhenius equation. According to kinetic law, the degradation of NADH follows the expressions:

r (rate) = dx/dt = k c(NADH) c($BmimBF_4$) (1)

Since degradation of NADH follows first-order kinetic.[1] Therefore,

r (rate) = dx/dt = k c(NADH) (2);

$$k = \frac{1}{t} ln \frac{1}{1-y} \quad (3)$$

According to Arrhenius equation:

$$lnk = lnA - \frac{Ea}{RT} \quad (4)$$

r, reaction rate; dx, changing in concentration; t, min; k, rate constant; c, subtract concentration; A, pre-exponential factor; Ea, activation energy; R, constant; T, temperature; y, conversion ratio.

Data for degradation of NADH in $BmimBF_4$ is correlated by Arrhenius equation, as follows:

$y = 18.0 - 7157.1x$, $R^2 = 0.989$ (5)

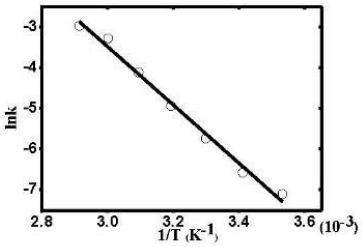

Figure S5. Arrhenius plots for degradation of NADH in $BmimBF_4$ as temperature increases.
Arrhenius equation: $y = 18.0 - 7157.1x$, $R^2 = 0.989$

3.2 Stability of NADH in ILs

pH solutions (from 7.0 to 4.5) were prepared by progressively adding phosphoric acid in phosphate solution (pH=7), which is monitored by pH meter in the whole process (Figure S6). A buffer solution (2 mL) of $BmimBF_4$ (V_{IL}/V_{buffer} = 20%) and NADH (2 μmol) was prepared, which was incubation at 37 °C for 3h, an apparent decrease of the absorption intensity at 340 nm accompanied with an increase of that at 260 nm was observed (Figure S7). The aqueous reaction of NADH with ILs (5.0 equiv.) was incubation at 37 °C for 3h, which was monitored by an in-situ UV-vis spectrum (Figure S8).

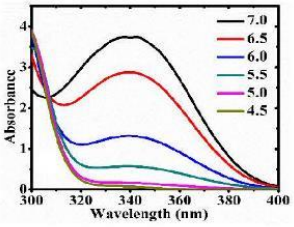

Figure S6. NADH degrades in phosphate buffer whose pH in range from 7.0 to 4.5.

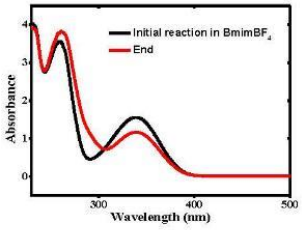

Figure S7. NADH degrades in contained-$BmimBF_4$ reaction.

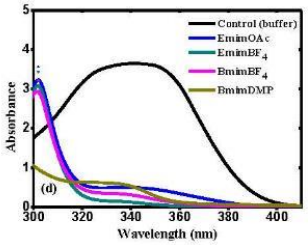

Figure S8. NADH degrades in ILs.

3.3 DFT calculation.

All the DFT calculations throughout this work were carried out with the Gaussian09 software package.[2] The structures in pH calculations were computed with a polarized continuum model (PCM)[3,4] in water using the B3LYP method in conjunction with the 6-311+g(d,p) basis set,[5,6] that were ensured by the absence of imaginary vibrational frequency.

3.3.1 Mechanism for NADH degradation.

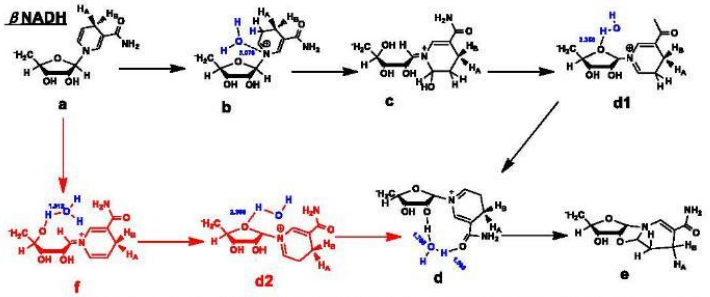

Figure S9. Two possible pathway (red and black) for NADH degradation mechanism proposed by the Norman and co-worker.[7]

Table S1 Structure for the NADH and its derivatives

	H	-1.54329	-0.87756	-1.61359
	H	-0.79383	0.468388	3.06538
	H	-3.04744	0.975792	1.828549
	N	-0.1947	-0.79955	0.014145
	C	-2.47443	0.064574	1.630025
	C	-3.87299	0.020432	-0.52711
	O	-4.48897	1.039046	-0.23225
	N	-4.27829	-0.84724	-1.4995
	H	-3.93582	-1.79604	-1.52931
	H	-5.17627	-0.66385	-1.92919
	H	-2.95105	-0.72563	2.228756
	H	-0.50467	1.416624	1.253909
	O	-0.13198	2.320283	0.528372
	H	0.429495	1.872383	-0.16954
	H	-0.8519	2.823444	0.111275
	O	3.202465	0.015857	1.135174
	H	3.510908	-0.70586	1.702522
	O	2.084541	-2.34216	0.646897
	H	1.902313	-3.25629	0.394611
	H	4.286006	-0.74351	-0.47063
	H	2.546351	-2.10912	-1.36096
b				
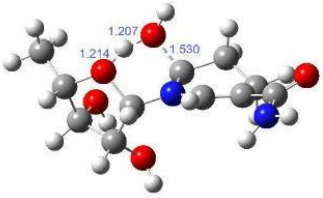	C	-1.15013	0.074113	1.010679
	O	-2.22593	0.889708	0.707569
	C	-3.39777	0.102873	0.269319
	C	-2.80836	-1.24756	-0.13046
	C	-1.66364	-1.38604	0.894197
	H	-0.73585	0.325794	1.990714
	H	-4.02551	-0.0365	1.158035
	C	-4.16054	0.874818	-0.78695
	H	-5.08807	0.346815	-1.0286
	H	-4.42379	1.86529	-0.40674
	H	-3.58098	0.977272	-1.7064
	C	-0.15152	1.110706	-0.98061
	C	1.298414	-0.10736	0.455021
	C	1.004505	1.502821	-1.83128
	H	-1.15508	1.481052	-1.15833
	C	2.330439	-0.06667	-0.39765
	H	1.351262	-0.45951	1.475459
	H	0.657083	1.689521	-2.85135
	H	3.087678	0.945724	-2.11207
	N	0.006181	0.364181	0.062093
	C	2.151551	0.483578	-1.79067
	C	3.72196	-0.47126	0.019972
	O	4.682188	0.165937	-0.391
	N	3.822494	-1.51627	0.89152

	H	3.076325	-2.18766	0.993483
	H	4.757003	-1.81521	1.139929
	H	1.955989	-0.34916	-2.48088
	H	1.333281	2.482236	-1.44144
	O	0.477842	2.467189	2.258978
	H	-0.17283	3.125581	2.538566
	H	1.309867	2.748282	2.663323
	O	-2.29174	-1.17082	-1.44896
	H	-1.79224	-1.98043	-1.62985
	O	-0.64057	-2.2842	0.50422
	H	-0.78947	-3.14896	0.909325
	H	-3.55073	-2.05074	-0.03709
	H	-2.07851	-1.65748	1.872772
TS-bc				
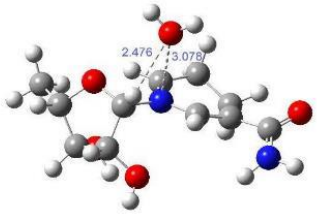	C	0.854297	-0.98083	-0.38796
	O	1.787007	-0.21629	-1.28926
	C	3.192518	-0.56202	-0.93495
	C	3.129582	-0.71422	0.581694
	C	1.773398	-1.42371	0.815753
	H	0.526766	-1.84959	-0.96167
	H	3.367847	-1.53896	-1.39856
	C	4.131308	0.481831	-1.50038
	H	5.161809	0.181433	-1.28828
	H	4.018009	0.551085	-2.5853
	H	3.965803	1.458964	-1.04257
	C	-0.04925	1.173969	0.359078
	C	-1.57809	-0.61054	-0.45013
	C	-1.32428	1.984806	0.568768
	H	0.625886	1.174781	1.212288
	C	-2.66828	-0.05336	0.10152
	H	-1.61391	-1.40904	-1.18482
	H	-1.11182	2.804765	1.259075
	H	-3.40395	1.692562	1.086198
	N	-0.27603	-0.16393	-0.11453
	C	-2.48373	1.105462	1.052417
	C	-4.06461	-0.40579	-0.31838
	O	-4.94442	0.447232	-0.30699
	N	-4.28313	-1.68675	-0.75605
	H	-3.69991	-2.44753	-0.44167
	H	-5.24082	-1.91637	-0.98905
	H	-2.29295	0.736395	2.069852
	H	-1.62339	2.431695	-0.38906
	O	0.819529	1.873578	-0.68819
	H	1.455727	0.937362	-1.1076
	H	0.260618	2.275893	-1.37671
	O	3.119538	0.577226	1.154624

	H	2.993899	0.488264	2.11129
	O	1.261389	-1.05293	2.077699
	H	0.822888	-1.79785	2.50786
	H	3.968768	-1.31472	0.954177
	H	1.911259	-2.50856	0.750911
c				
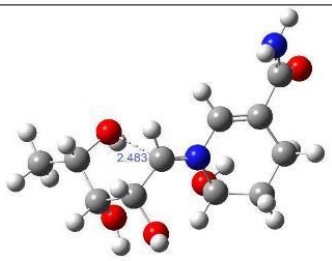	C	0.76704	-0.14284	1.123088
	O	1.872003	-1.78319	-0.37736
	C	3.183888	-1.39853	0.068743
	C	3.184652	0.119487	0.284299
	C	2.096009	0.553802	1.324202
	H	0.652837	-1.0817	1.657325
	H	3.304072	-1.89116	1.04128
	C	4.277391	-1.87532	-0.88094
	H	5.267372	-1.63733	-0.47876
	H	4.209561	-2.95861	-1.00581
	H	4.183099	-1.39575	-1.85918
	C	-0.348	1.456844	-0.4665
	C	-1.49163	-0.52117	0.562193
	C	-1.64759	2.211727	-0.21703
	H	0.525349	2.058497	-0.24238
	C	-2.67905	-0.06285	0.133949
	H	-1.34258	-1.53315	0.923082
	H	-1.62403	2.599025	0.807592
	H	-3.16009	1.221966	-1.47993
	N	-0.3036	0.274381	0.512567
	C	-2.87987	1.320568	-0.42273
	C	-3.85944	-1.00132	0.019548
	O	-4.52129	-0.98805	-1.00891
	N	-4.08739	-1.84627	1.062822
	H	-3.70087	-1.67678	1.979232
	H	-4.89856	-2.44875	1.00002
	H	-3.75835	1.778298	0.045856
	H	-1.67347	3.076516	-0.88624
	O	-0.19202	0.945126	-1.7516
	H	1.746016	-1.43879	-1.27678
	H	-1.04383	0.700905	-2.1429
	O	2.922981	0.726637	-0.95997
	H	3.133083	1.669579	-0.92014
	O	1.999853	1.972643	1.280427
	H	2.050322	2.344505	2.170867
	H	4.149628	0.446577	0.695057
	H	2.444679	0.221601	2.310448
TS-cd				
	C	-0.79296	-0.76485	-0.06971
	O	-1.51039	-0.27069	1.155577

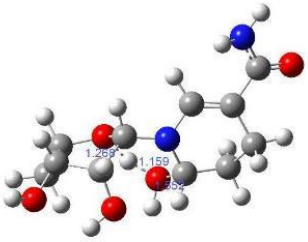

C	-2.92197	-0.71816	1.113676
C	-3.13576	-1.2064	-0.3572
C	-1.89264	-0.69489	-1.1301
H	-0.53836	-1.81205	0.11116
H	-2.96405	-1.56541	1.803494
C	-3.8289	0.397123	1.595824
H	-4.8581	0.033998	1.644048
H	-3.53369	0.711376	2.600982
H	-3.81746	1.255268	0.918992
C	0.368133	1.403784	-0.34636
C	1.64828	-0.67563	0.079173
C	1.703272	2.093129	-0.10402
H	-0.13167	1.694578	-1.26813
C	2.833427	-0.10958	-0.1925
H	1.547213	-1.65891	0.525569
H	1.647771	3.110339	-0.50175
H	3.815391	1.766003	-0.42638
N	0.414977	-0.02586	-0.20297
C	2.867654	1.305073	-0.71418
C	4.137171	-0.75783	0.168583
O	5.097133	-0.07209	0.498704
N	4.176091	-2.12975	0.159178
H	3.563	-2.65538	-0.4459
H	5.078816	-2.54357	0.354852
H	2.825342	1.31201	-1.81253
H	1.853411	2.163857	0.978154
O	-0.60304	1.896318	0.759861
H	-1.20177	0.957121	1.078863
H	-1.18949	2.585343	0.403116
O	-4.30993	-0.6548	-0.93053
H	-4.85665	-1.34269	-1.33131
O	-2.10605	0.647906	-1.5281
H	-3.02029	0.702483	-1.85763
H	-3.17001	-2.30023	-0.38175
H	-1.64298	-1.32858	-1.9906

d1

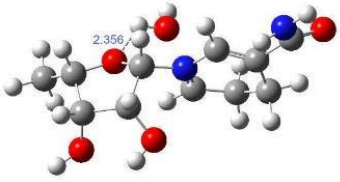

C	0.92133	-0.38466	-0.77534
O	1.908286	0.612259	-0.80902
C	3.175028	-0.07937	-0.99585
C	3.079167	-1.30833	-0.06589
C	1.534993	-1.59243	0.025638
H	0.637102	-0.689	-1.79114
H	3.201051	-0.44001	-2.03607
C	4.316979	0.883942	-0.74879
H	5.273129	0.379319	-0.91976
H	4.258131	1.725323	-1.44395

S10

	H	4.298255	1.258728	0.27645
	C	-0.2091	0.93468	0.894707
	C	-1.56244	-0.28933	-0.64348
	C	-1.43087	1.44088	1.57068
	H	0.784897	1.240034	1.195388
	C	-2.675	-0.15467	0.090981
	H	-1.53029	-0.68589	-1.65013
	H	-1.19395	1.684184	2.609874
	H	-3.55668	0.99423	1.649259
	N	-0.29423	0.150528	-0.13732
	C	-2.61613	0.47126	1.461546
	C	-4.03656	-0.51159	-0.45701
	O	-4.98839	0.212925	-0.20418
	N	-4.10993	-1.61178	-1.25971
	H	-3.41078	-2.33837	-1.22361
	H	-5.02957	-1.86926	-1.59552
	H	-2.53868	-0.3275	2.212107
	H	-1.64999	2.400372	1.074191
	O	0.417131	3.201945	-0.51794
	H	1.190169	2.849161	-0.98086
	H	0.385444	4.147428	-0.7144
	O	3.537621	-1.03244	1.254103
	H	4.385545	-1.46221	1.422574
	O	1.075499	-1.60721	1.349881
	H	1.859362	-1.50256	1.923285
	H	3.613593	-2.16398	-0.48739
	H	1.26688	-2.53334	-0.46707
d				
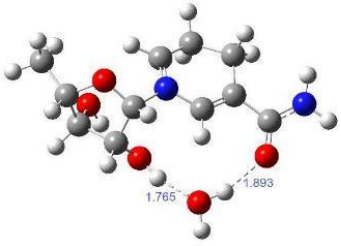	C	-1.19445	0.314358	-1.08075
	O	-2.32466	-0.43667	-1.33071
	C	-3.48345	0.087582	-0.57743
	C	-2.85341	0.834325	0.591566
	C	-1.57799	1.4313	-0.03869
	H	-0.76281	0.706924	-2.00782
	H	-3.97847	0.813812	-1.2343
	C	-4.4286	-1.05154	-0.25926
	H	-5.33402	-0.65442	0.209677
	H	-4.71931	-1.56402	-1.1799
	H	-3.97693	-1.76719	0.430672
	C	-0.35524	-1.71553	0.039734
	C	1.204121	-0.01299	-0.50926
	C	0.708438	-2.48941	0.736374
	H	-1.39187	-2.03612	0.02755
	C	2.277779	-0.70928	-0.11592
	H	1.260137	1.007948	-0.85692
	H	0.581943	-2.23308	1.802617

	H	2.398072	-2.79034	-0.60751
	N	-0.10059	-0.57483	-0.51067
	C	2.141165	-2.16855	0.262379
	C	3.58451	0.042206	-0.12278
	O	3.607736	1.276399	-0.13898
	N	4.715907	-0.69803	-0.09395
	H	4.726405	-1.70371	-0.16581
	H	5.601682	-0.20966	-0.11733
	H	2.840673	-2.4362	1.059145
	H	0.490062	-3.55865	0.665325
	O	1.479339	3.141418	0.040481
	H	1.680693	4.083231	0.107969
	H	2.328784	2.65507	0.078246
	O	-2.50231	-0.08788	1.614377
	H	-1.95795	0.392331	2.257372
	O	-0.62656	1.673402	0.9585
	H	0.045183	2.341703	0.688204
	H	-3.51934	1.616593	0.9754
	H	-1.82575	2.337696	-0.60552
TS-de				
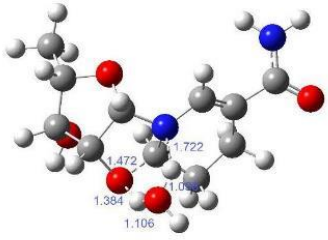	C	-1.21123	0.33302	-1.16138
	O	-1.48652	-1.0217	-1.06041
	C	-2.8912	-1.1704	-0.66519
	C	-3.12508	-0.02909	0.340325
	C	-2.17305	1.096337	-0.1931
	H	-1.20594	0.691171	-2.19712
	H	-3.50112	-0.97474	-1.5587
	C	-3.12277	-2.58307	-0.17421
	H	-4.17742	-2.71382	0.085257
	H	-2.87414	-3.29611	-0.96418
	H	-2.52195	-2.79444	0.711605
	C	-0.19573	0.872918	0.914876
	C	1.257358	-0.29696	-0.7279
	C	1.008432	1.474688	1.596088
	H	-0.4512	-0.11241	1.318615
	C	2.201194	-0.34474	0.218819
	H	1.26452	-0.8433	-1.66216
	H	1.265135	2.42638	1.118626
	H	2.130275	-0.24791	2.336166
	N	0.139154	0.64079	-0.55368
	C	2.174567	0.46173	1.499445
	C	3.452557	-1.17129	-0.00352
	O	4.54145	-0.69146	0.277583
	N	3.281011	-2.4036	-0.55582
	H	2.382501	-2.86256	-0.56921
	H	4.106468	-2.97624	-0.67857

	H	3.140179	0.966823	1.596724
	H	0.771958	1.685311	2.64213
	O	0.889728	3.045717	-1.81995
	H	1.68226	3.154416	-2.364
	H	0.424709	1.563945	-0.95535
	O	-2.76451	-0.45971	1.637515
	H	-3.04753	0.197365	2.287764
	O	-1.33424	1.686081	0.812664
	H	0.540503	3.934378	-1.66602
	H	-4.16942	0.301674	0.313953
	H	-2.71847	1.909418	-0.67379
e				
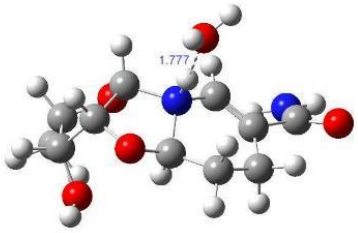	C	-1.0907	-0.10757	-1.20735
	O	-1.36599	-1.39064	-0.70657
	C	-2.78553	-1.45767	-0.40177
	C	-3.0935	-0.09215	0.249723
	C	-2.1368	0.852264	-0.54339
	H	-1.10041	-0.09983	-2.30459
	H	-3.33613	-1.51153	-1.35388
	C	-3.0688	-2.69009	0.431191
	H	-4.13963	-2.75653	0.645323
	H	-2.7745	-3.58471	-0.1229
	H	-2.52715	-2.65565	1.377647
	C	-0.15005	0.926103	0.644721
	C	1.387749	-0.33116	-0.77797
	C	1.008243	1.662919	1.274877
	H	-0.49908	0.112004	1.284923
	C	2.333607	-0.22338	0.169159
	H	1.503051	-0.92134	-1.68024
	H	1.30843	2.52498	0.667766
	H	2.063745	0.037317	2.276902
	N	0.182436	0.435892	-0.70766
	C	2.185923	0.666521	1.385981
	C	3.674797	-0.89094	0.008619
	O	4.690215	-0.32229	0.391953
	N	3.689066	-2.10708	-0.6143
	H	2.865476	-2.68912	-0.64739
	H	4.5866	-2.56912	-0.68386
	H	3.124942	1.208211	1.529904
	H	0.723682	2.03778	2.261441
	O	-0.23516	2.87985	-1.4866
	H	0.349673	3.656067	-1.46155
	H	0.261851	1.968098	-1.48861
	O	-2.7823	-0.13576	1.62765
	H	-3.23613	0.578022	2.094419
	O	-1.33674	1.735418	0.322041

	H	-0.82005	2.654091	-0.57528
	H	-4.13897	0.192183	0.090387
	H	-2.66587	1.49571	-1.24725
f				
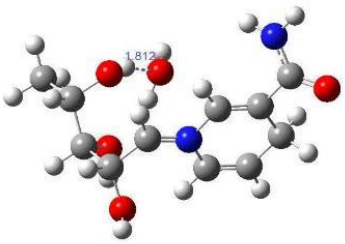	C	-0.60436	0.461962	-1.22202
	O	-1.75051	-1.68448	-0.48823
	C	-3.04886	-1.10755	-0.63257
	C	-2.99726	0.39635	-0.32481
	C	-1.9514	1.146041	-1.21296
	H	-0.47224	-0.30191	-1.97735
	H	-3.28867	-1.20336	-1.69962
	C	-4.11654	-1.84627	0.173037
	H	-5.11038	-1.43536	-0.03149
	H	-4.11837	-2.90195	-0.10859
	H	-3.93112	-1.76857	1.247409
	C	0.510928	1.648575	0.585745
	C	1.619918	-0.10791	-0.71529
	C	1.623935	1.807481	1.30825
	H	-0.39107	2.220638	0.720997
	C	2.738391	0.018069	0.009064
	H	1.5209	-0.79542	-1.54564
	H	1.606723	2.557867	2.09277
	H	3.160659	0.51915	2.047514
	N	0.449056	0.687993	-0.47732
	C	2.876342	1.022807	1.111408
	C	3.985468	-0.75839	-0.34746
	O	5.069896	-0.19719	-0.28364
	N	3.814198	-2.04369	-0.76698
	H	2.975581	-2.56387	-0.55539
	H	4.652542	-2.57351	-0.97004
	H	3.728147	1.680599	0.886668
	H	-1.61126	-0.69766	2.308439
	O	-1.03689	-1.46866	2.173362
	H	-1.53749	-1.8012	0.464381
	H	-1.14392	-2.0485	2.938327
	O	-2.68741	0.602846	1.050154
	H	-2.93989	1.504016	1.29472
	O	-1.93096	2.493897	-0.76278
	H	-1.78869	3.10114	-1.50161
	H	-3.96861	0.850357	-0.56037
	H	-2.31801	1.089136	-2.24625
d2				
	C	1.061894	-0.24656	-1.08996
	O	2.192444	0.539155	-0.91869
	C	3.319313	-0.25016	-0.36899
	C	2.641738	-1.46031	0.267083

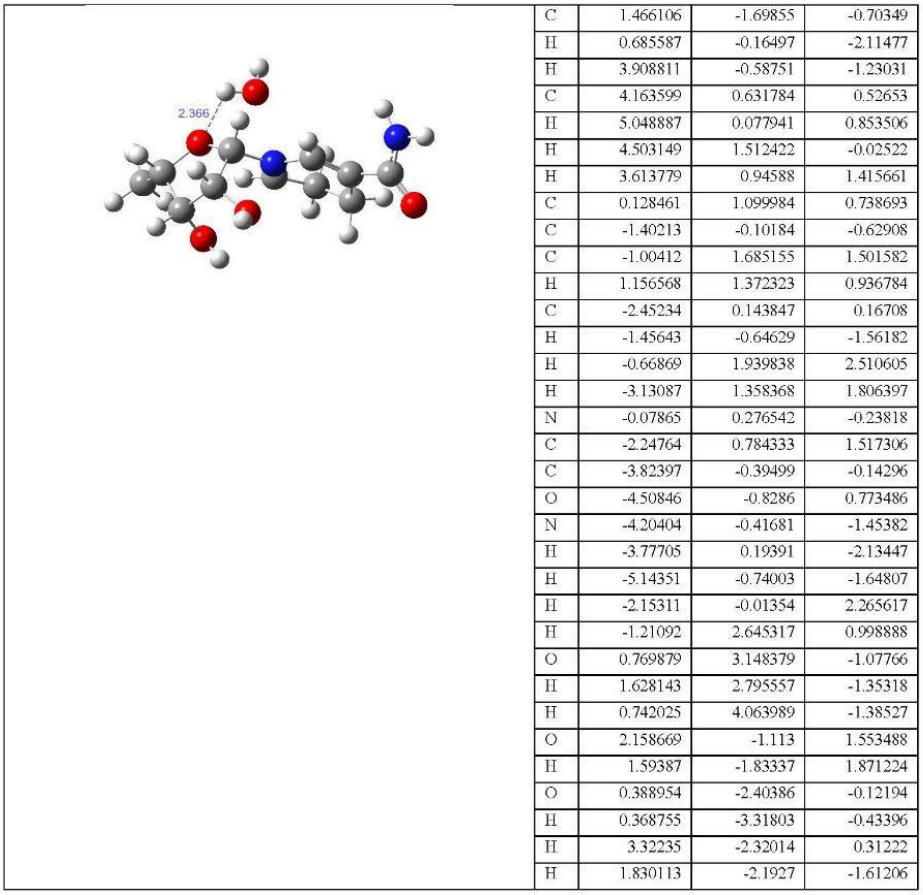

C	1.466106	-1.69855	-0.70349
H	0.685587	-0.16497	-2.11477
H	3.908811	-0.58751	-1.23031
C	4.163599	0.631784	0.52653
H	5.048887	0.077941	0.853506
H	4.503149	1.512422	-0.02522
H	3.613779	0.94588	1.415661
C	0.128461	1.099984	0.738693
C	-1.40213	-0.10184	-0.62908
C	-1.00412	1.685155	1.501582
H	1.156568	1.372323	0.936784
C	-2.45234	0.143847	0.16708
H	-1.45643	-0.64629	-1.56182
H	-0.66869	1.939838	2.510605
H	-3.13087	1.358368	1.806397
N	-0.07865	0.276542	-0.23818
C	-2.24764	0.784333	1.517306
C	-3.82397	-0.39499	-0.14296
O	-4.50846	-0.8286	0.773486
N	-4.20404	-0.41681	-1.45382
H	-3.77705	0.19391	-2.13447
H	-5.14351	-0.74003	-1.64807
H	-2.15311	-0.01354	2.265617
H	-1.21092	2.645317	0.998888
O	0.769879	3.148379	-1.07766
H	1.628143	2.795557	-1.35318
H	0.742025	4.063989	-1.38527
O	2.158669	-1.113	1.553488
H	1.59387	-1.83337	1.871224
O	0.388954	-2.40386	-0.12194
H	0.368755	-3.31803	-0.43396
H	3.32235	-2.32014	0.31222
H	1.830113	-2.1927	-1.61206

4 Chemicals Characterization

Table S2. Summary of chemicals NMR data

Compound	NMR results ^{1}H NMR (600 MHz, D_2O, 298K)
$BmimBF_4$	δ = 8.70 (s, 1H), 7.47 (s, 1H), 7.42 (s, 1H), 4.20 (t, *J* = 7.1 Hz, 2H), 3.89 (s, 3H), 2.03 – 1.58 (m, 2H), 1.32 (q, *J* = 7.5 Hz, 2H), 0.93 (t, *J* = 7.4 Hz, 3H).
NADH	δ = 8.49 (s, 1H), 8.25 (s, 1H), 6.95 (s, 1H), 6.14 (d, J = 5.7 Hz, 1H), 6.00 (d, J = 8.4 Hz, 1H), 4.72 (t, J = 5.2 Hz, 1H), 4.52 (s, 1H), 4.39 (s, 1H), 4.30 – 4.17 (m, 2H), 4.09 (d, J = 7.0 Hz, 2H), 3.65 (s, 1H), 2.81 (d, J = 18.1 Hz, 1H), 2.69 (d, J = 15.8 Hz, 1H), 1.18 (s, 1H)
NAD^+	δ = 9.43 (s, 1H), 9.27 (d, J = 6.2 Hz, 1H), 8.94 (d, J = 7.6 Hz, 1H), 8.60 (s, 1H), 8.39 (s, 1H), 8.29 (t, J = 7.0 Hz, 1H), 6.17 (d, J = 5.5 Hz, 1H), 6.15 (d, J = 5.6 Hz, 1H), 4.60 (s, 1H), 4.57 (t, J = 5.3 Hz, 1H), 4.53 (t, J = 4.2

	Hz, 1H), 4.48 (s, 1H), 4.40 (s, 2H), 4.26 (d, J = 12.2 Hz, 2H), 4.22 (d, J = 11.2 Hz, 1H), 2.23 (s, 1H)
NADH+BmimBF4	δ = 9.43 (s, 1H), 9.27 (d, J = 6.2 Hz, 1H), 8.94 (d, J = 7.6 Hz, 1H), 8.60 (s, 1H), 8.39 (s, 1H), 8.29 (t, J = 7.0 Hz, 1H), 6.17 (d, J = 5.5 Hz, 1H), 6.15 (d, J = 5.6 Hz, 1H), 4.60 (s, 1H), 4.57 (t, J = 5.3 Hz, 1H), 4.53 (t, J = 4.2 Hz, 1H), 4.48 (s, 1H), 4.40 (s, 2H), 4.26 (d, J = 12.2 Hz, 2H), 4.22 (d, J = 11.2 Hz, 1H), 2.23 (s, 1H)

4.1 NMR of 1-butyl-3-methylimidazolium tetrafluoroborate (BmimBF4)

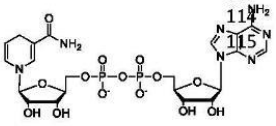

^{1}H NMR (600 MHz, D_2O, 298K): δ = 8.70 (s, 1H), 7.47 (s, 1H), 7.42 (s, 1H), 4.20 (t, *J* = 7.1 Hz, 2H), 3.89 (s, 3H), 2.03 – 1.58 (m, 2H), 1.32 (q, *J* = 7.5 Hz, 2H), 0.93 (t, *J* = 7.4 Hz, 3H).

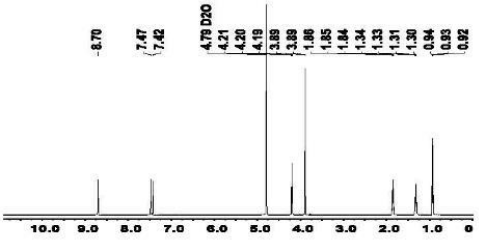

4.2 NMR of Nicotinamide adenine dinucleotide (NADH)

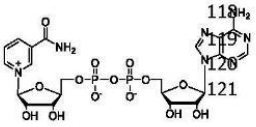

NADH ^{1}H NMR (600 MHz, D_2O, 298K): δ = 8.49 (s, 1H), 8.25 (s, 1H), 6.95 (s, 1H), 6.14 (d, J = 5.7 Hz, 1H), 6.00 (d, J = 8.4 Hz, 1H), 4.72 (t, J = 5.2 Hz, 1H), 4.52 (s, 1H), 4.39 (s, 1H), 4.30 – 4.17 (m, 2H), 4.09 (d, J = 7.0 Hz, 2H), 3.65 (s, 1H), 2.81 (d, J = 18.1 Hz, 1H), 2.69 (d, J = 15.8 Hz, 1H), 1.18 (s, 1H).

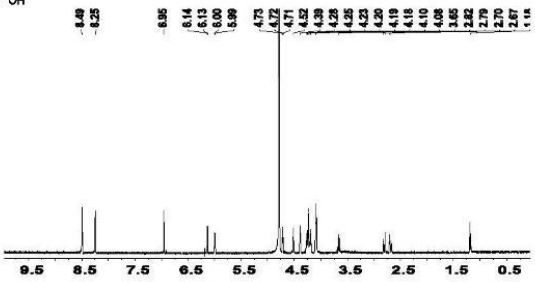

4.3 NMR of nicotinamide adenine dinucleotide (NAD$^+$)

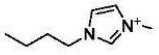

NAD$^+$ ^{1}H NMR (600 MHz, D_2O, 298K): δ = 9.43 (s, 1H), 9.27 (d, J = 6.2 Hz, 1H), 8.94 (d, J = 7.6 Hz, 1H), 8.60 (s, 1H), 8.39 (s, 1H), 8.29 (t, J = 7.0 Hz, 1H), 6.17 (d, J = 5.5 Hz, 1H), 6.15 (d, J = 5.6 Hz, 1H), 4.60 (s, 1H), 4.57 (t, J = 5.3 Hz, 1H), 4.53 (t, J = 4.2 Hz, 1H), 4.48 (s, 1H), 4.40 (s, 2H), 4.26 (d, J = 12.2 Hz, 2H), 4.22 (d, J = 11.2 Hz, 1H), 2.23 (s, 1H).

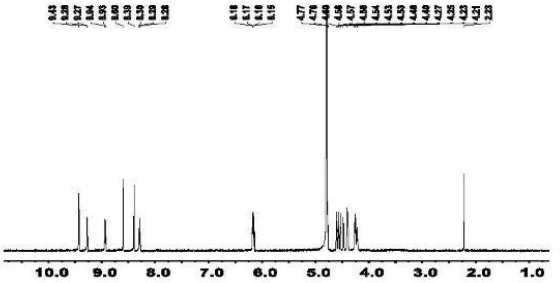

4.4 NMR of Mixture of NADH and $BmimBF_4$.

NADH + $BmimBF_4$ ^{1}H NMR (600 MHz, D_2O, 298K): δ = 1H NMR (600 MHz, Deuterium Oxide) δ 8.67 (s, 1H), 8.50 (s, 3H), 8.25 (s, 4H), 7.43 (s, 3H), 6.13 (d, J = 6.1 Hz, 3H), 5.29 (s, 1H), 5.18 (s, 2H), 4.78 – 4.73 (m, 8H), 4.54 – 4.50 (m, 4H), 4.38 (s, 2H), 4.22 – 4.13 (m, 7H), 4.06 (d, J = 15.1 Hz, 1H), 4.02 – 3.96 (m, 2H), 3.85 (s, 7H), 1.81 (s, 1H), 1.28 (d, J = 8.5 Hz, 2H), 0.89 (s, 4H).

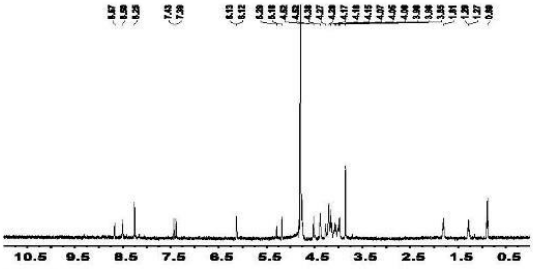

4.5 NMR for degradation of NADH.

A mixture of NADH (1.4 mg) and $BmimBF_4$ (0.452 mg) (molar ratio = 1:1) was incubated for 3h at 60°C. Then samples are separately identified by NMR (Figure S8). NADH (1.4mg) was dissvoled in deuteroxide (0.5 mL), and then solution (0.25mM NADH) is gradually added by deuterosulfuric acid to adjust pH (3, 1), which is monitored by pH meter. After that, the samples are incubated for three hours at 37 °C and measured.

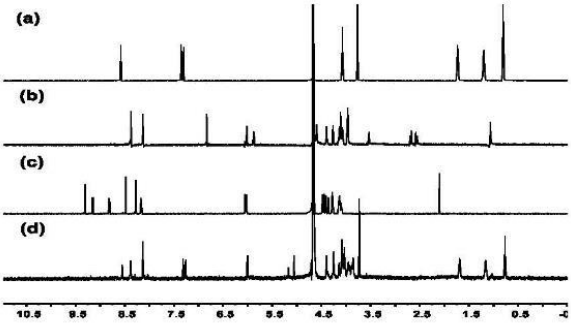

Figure S10. ^{1}H NMR (600 MHz, D_2O, 298K) (δ: ppm). (a) $BmimBF_4$; (b) NADH; (c), NAD^+; (d) a mixture of NADH and $BmimBF_4$ (molar ratio = 1:1); D_2O was used as the solvent.

Abbreviation:

DBULat: 1,8-Diazabicyclo[5.4.0]undec-7-ene lactate
$BmimBF_4$: 1-butyl-3-methylimidazolium tetrafluoroborate
BmimDCA: 1-butyl-3-methylimidazolium dicyanamide
BmimDMP: 1-butyl-3-methylimidazolium dimethylphosphate
$EmimBF_4$: 1-ethyl-3-methylimidazolium tetrafluoroborate
EmimOAc: 1-ethyl-3-methylimidazolium acetate
NADH: reduced nicotinamide adenine dinucleotide
NAD^+: nicotinamide adenine dinucleotide

(1) Wu, J. T.; Wu, L. H.; Knight, J. A. *Clin Chem* **1986**, *32*, 314.
(2) Frisch, M. J. T., G. W.; Schlegel, H. B.; Scuseria, G. E.; Robb, M. A.; Cheeseman, J. R.; Scalmani, G.; Barone, V.; Mennucci, B.; Petersson, G. A.; Nakatsuji, H.; Caricato, M.; Li, X.; Hratchian, H. P.; Izmaylov, A. F.; Bloino, J.; Zheng, G.; Sonnenberg, J. L.; Hada, M.; Ehara, M.; Toyota, K.; Fukuda, R.; Hasegawa, J.; Ishida, M.; Nakajima, T.; Honda, Y.; Kitao, O.; Nakai, H.; Vreven, T.; Montgomery Jr, J. A.; Peralta, J. E.; Bearpark, M. J.; Heyd, J.; Brothers, E. N.; Kudin, K. N.; Staroverov, V. N.; Kobayashi, R.; Normand, J.; Raghavachari, K.; Rendell, A. P.; Burant, J. C.; Iyengar, S. S.; Tomasi, J.; Cossi, M.; Rega, N.; Millam, N. J.; Klene, M.; Knox, J. E.; Cross, J. B.; Bakken, V.; Adamo, C.; Jaramillo, J.; Gomperts, R.; Stratmann, R. E.; Yazyev, O.; Austin, A. J.; Cammi, R.; Pomelli, C.; Ochterski, J. W.; Martin, R. L.; Morokuma, K.; Zakrzewski, V. G.; Voth, G. A.; Salvador, P.; Dannenberg, J. J.; Dapprich, S.; Daniels, A. D.; Foresman, J. B.; Ortiz, J. V.; Cioslowski, J.; Fox, D. J. *Gaussian 09, Revision D. 01, Gaussian, Inc., Wallingford CT*, 2013.
(3) Scalmani, G.; Frisch, M. J. *J Chem Phys* **2010**, *132*.
(4) Tomasi, J.; Mennucci, B.; Cammi, R. *Chemical Reviews* **2005**, *105*, 2999.
(5) Zhang, Y. Q.; He, H. Y.; Dong, K.; Fan, M. H.; Zhang, S. J. *Rsc Adv* **2017**, *7*, 12670.
(6) Damas, G. B.; Dias, A. B. A.; Costa, L. T. *J Phys Chem B* **2014**, *118*, 9046.
(7) O.Kaplan, N. J. O. a. N. *Biochemistry-Us* **1974**, *13*, 4675.

Electronic supporting information

Efficient Ionic Liquid–based platform for Multi-Enzymatic Conversion of Carbon Dioxide to Methanol

Zhibo Zhang,[a, b] Jan Muschiol,[a] Yuhong Huang,[a] Sigyn Björk Sigurdardóttir,[a] Nicolas von Solms,[a] Anders E. Daugaard,[a] Jiang Wei,[a] Jianquan Luo,[c] Bao-Hua Xu,[b] Suojiang Zhang[b,c] and Manuel Pinelo[a]*

[a] *Department of Chemical and Biochemical Engineering, Building 229, Technical University of Denmark, DK-2800 Kgs. Lyngby, Denmark.*
[b] *Beijing Key Laboratory of Ionic Liquids Clean Process, Key Laboratory of Green Process and Engineering, State Key Laboratory of Multiphase Complex Systems, Institute of Process Engineering, Chinese Academy of Sciences, Beijing 100190, P. R. China.*
[c] *State Key Laboratory of Biochemical Engineering, Institute of Process Engineering, Chinese Academy of Sciences, Beijing 100190, PR China*
E-mail: mp@kt.dtu.dk; sjzhang@ipe.ac.cn

Table of contents

1. **Structure of the cation and anions of [CH][AA] ILs.**
2. **^{1}H NMR spectra for amino acid ionic liquids.**
3. **Figures and Tables for results part.**

Synthesis of [Ch][AA] ILs. ILs were prepared and purified according to the literature.[1] [Ch][OH] aqueous solution (about 4 M) was added dropwise under cooling to an amino acid aqueous solution or suspension to obtain a slight excess (about 10 mol%) of amino acid. Taking synthesis of [CH][Glu] as an example. 17.9 g of choline hydroxide (46 wt%) was diluted to 4 M with adding to 17 ml deionized water. Then prepared 4 M [Ch][OH] aqueous solution was added dropwise undercooling to 11g of L-glutamic acid dissolved in 200 ml deionized water (about 0.4 M). The mixture was stirred at about 3 °C overnight in the dark. Water was then removed under reduced pressure at 50 °C using a rotavapor. Acetonitrile/methanol (9 : 1, v/v) was then added under vigorous stirring to precipitate the excess of amino acid. The mixture was left stirring overnight and the excess of amino acid was then filtered off. The filtrate was evaporated to remove solvents at 50 °C. The product was dried under vacuum for 72 h at 60 °C. The other synthesis of ILs was conducted with same procedure. All the peaks and corresponding chemical shifts obtained confirmed the structure of ILs. From NMR spectra and elemental analysis, the purity of ILs was more than 98 %.

[CH][Glu]: ^{1}H NMR (600 MHz, D_2O, 25°C): δ = 2.04 – 2.23 (m, 2H, CH_2), 2.40 (apparent q, 2H, CH_2), 3.25 (s, 9H, CH_3, CH_3, CH_3), 3.58 (apparent t, 2H, CH_2), 3.8 (q, J = 4.8, 7.2 Hz, 1H, CH-N), 4.11 (m, 2H, CH_2); ^{13}C NMR (600 MHz, D_2O, 25°C) δ = 181.2, 174.5, 67.4, 55.6, 54.7, 53.8, 33.5, 26.9 ppm. Elemental analysis (%) calcd for: C 47.99, H 8.86, N 11.19; found C 47.96, H 8.62, N 11.46.

[CH][Gly]: ^{1}H NMR (600 MHz, D_2O, 25°C): δ = 3.21 (s, 2H, CH_2-N), 3.24 (s, 9H, CH_3, CH_3, CH_3), 3.54 –3.58 (m, 2H, CH_2), 4.10 (m, 2H, CH_2); ^{13}C NMR (600 MHz, D_2O, 25°C) δ =180.5, 67.4, 55.6, 53.8, 33.5, 44.3 ppm. Elemental analysis (%) calcd for: C 47.17, H 10.18, N 15.72; found: C 47.05, H 10.50, N 15.81.

[CH][His]: ^{1}H NMR (600 MHz, D_2O, 25°C): δ = 2.86 (m, 1H, CH_2), 2.97 (m, 1H, CH_2), 3.23 (s, 9H, CH_3, CH_3, CH_3), 3.54 (apparent q, 3H, CH_2, CH-N), 4.07– 4.13 (m, 2H, CH_2), 6.96 (s, 1H, =CH), 7.71 (s, 1H, =CH); ^{13}C NMR (600 MHz, D_2O, 25°C) δ =181.7, 135.8, 67.4, 56.0, 55.6, 53.8, 31.7 ppm. Elemental analysis (%) calcd for: C 51.15, H 8.58, N 21.69; found: C 51.02, H 8.67, N 21.75.

[CH][Pro]: ^{1}H NMR (600 MHz, D_2O, 25°C): δ = 1.75 – 1.89 (m, 3H, CH_2, CH_2), 2.13 – 2.24 (m, 1H, CH_2), 2.84 – 2.93 (m, 1H, CH_2-N), 3.11 – 3.18 (m, 1H, CH_2-N), 3.24 (s, 9H, CH_3, CH_3, CH_3), 3.56 – 3.73 (m, 3H, CH-N, CH_2), 4.07 – 4.13 (m, 2H, CH_2);

^{13}C NMR (600 MHz, D_2O, 25°C) δ =180.6, 67.4, 61.4, 55.6, 53.8, 46.0, 30.3, 24.8 ppm; Elemental analysis (%) calcd for: C 55.02, H 10.16, N 12.83; found: C 53.97, H 9.71, N 12.28.

1. Structure of the cation and anions of [CH][AA] ILs.

Cation

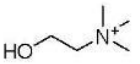

(Choline / CH)

Anions

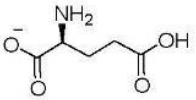

Glutamate / Glu

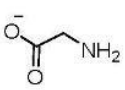

Glycine / Gly

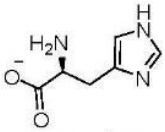

Histidine / His

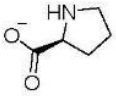

Proline / Pro

2. ^{1}H NMR spectra for amino acid ionic liquids.

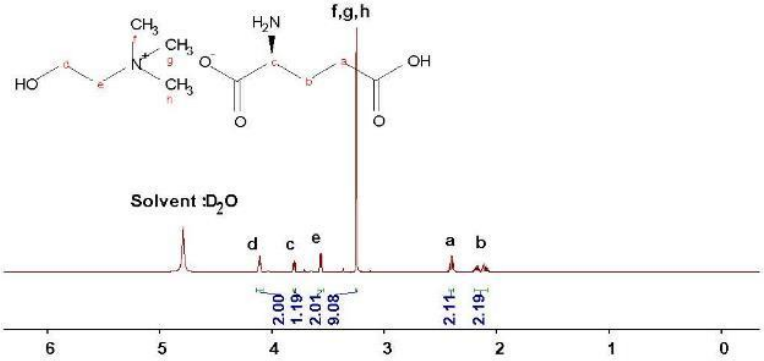

[CH][Glu]: ^{1}H NMR (600 MHz, D_2O) δ: 2.04 – 2.23 (m, 2H, CH_2), 2.40 (apparent q, 2H, CH_2), 3.25 (s, 9H, CH_3, CH_3, CH_3), 3.58(apparent t, 2H, CH_2), 3.8 (q, J = 4.8, 7.2 Hz, 1H, CH-N), 4.11 (m, 2H, CH_2).

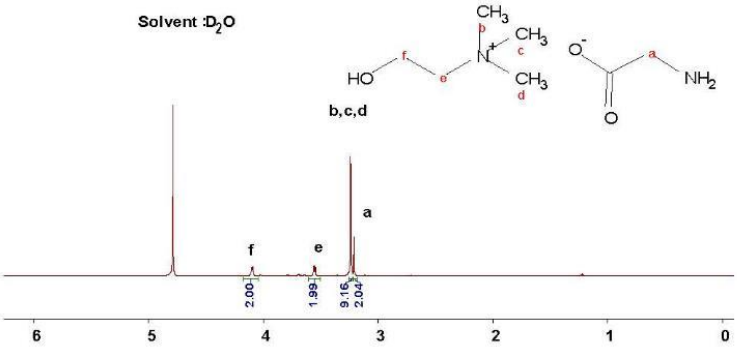

[CH][Gly]: ^{1}H NMR (600 MHz, D_2O) δ: 3.21 (s, 2H, CH_2-N), 3.24 (s, 9H, CH_3, CH_3, CH_3), 3.54 –3.58 (m, 2H, CH_2), 4.10 (m, 2H, CH_2).

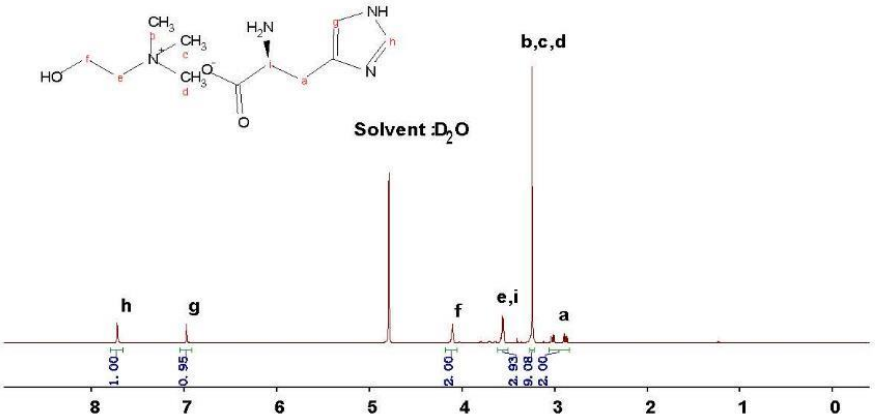

[CH][His]: ^{1}H NMR (600 MHz, D_2O) δ: 2.86(m, 1H, CH_2), 2.97 (m, 1H, CH_2), 3.23 (s, 9H, CH_3, CH_3, CH_3), 3.54 (apparent q, 3H, CH_2, CH-N), 4.07– 4.13 (m, 2H, CH_2), 6.96 (s, 1H, =CH), 7.71 (s, 1H, =CH).

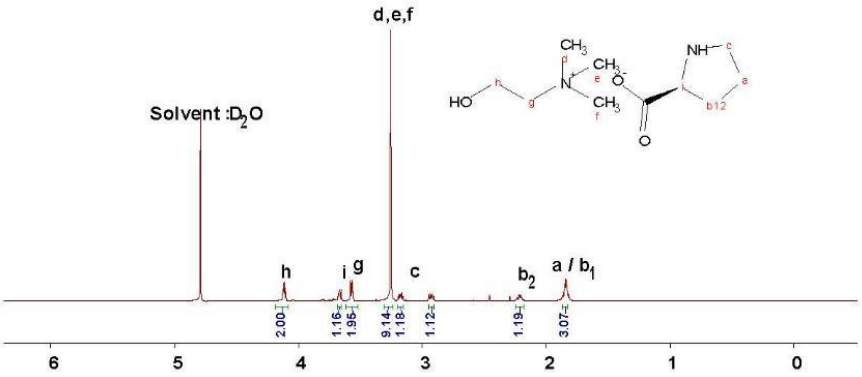

[CH][Pro]: ^{1}H NMR (600 MHz, D_2O) δ: 1.75 – 1.89 (m, 3H, CH_2, CH_2), 2.13 – 2.24 (m, 1H, CH_2),2.84 – 2.93 (m, 1H, CH_2-N), 3.11 – 3.18 (m, 1H, CH_2-N), 3.24 (s, 9H, CH_3, CH_3, CH_3), 3.56 – 3.73 (m, 3H, CH-N, CH_2), 4.07 – 4.13 (m, 2H, CH_2).

3. ^{13}C NMR spectra for amino acid ionic liquids.

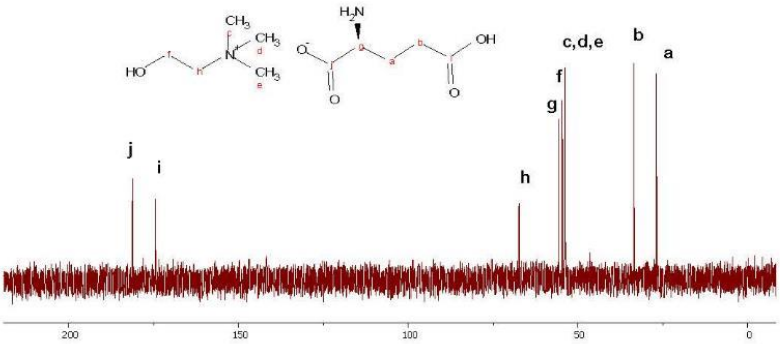

[CH][Glu]: ^{13}C NMR (600 MHz, D_2O, 25°C) δ=181.2, 174.5, 67.4, 55.6, 54.7, 53.8, 33.5, 26.9 ppm.

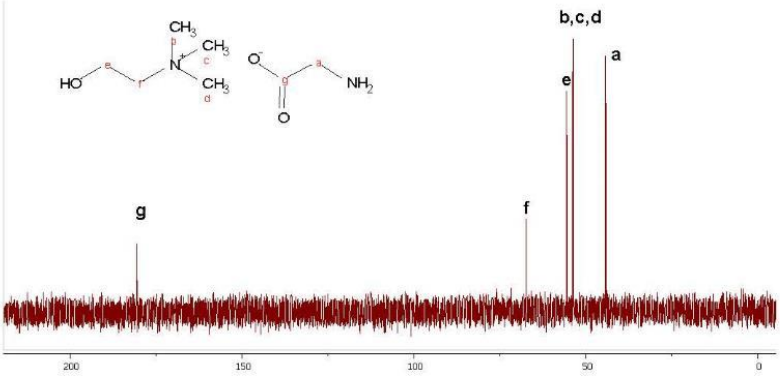

[CH][Gly]: ^{13}C NMR (600 MHz, D_2O, 25°C) δ=180.5, 67.4, 55.6, 53.8, 33.5, 44.3 ppm.

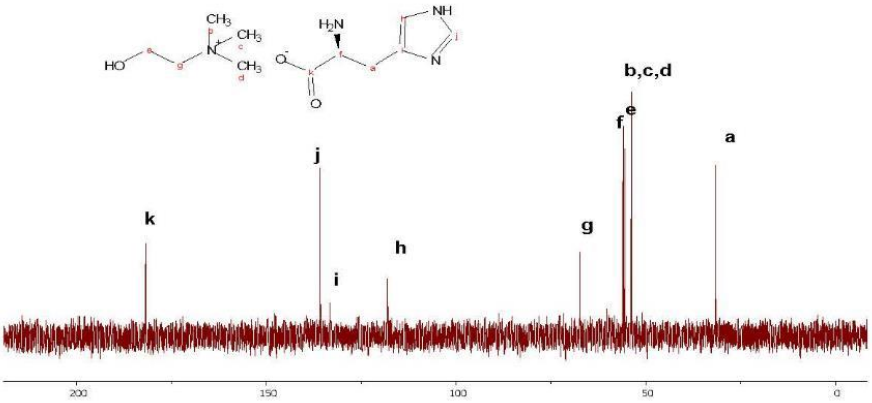

[CH][His]: ^{13}C NMR (600 MHz, D_2O, 25°C) δ=181.7, 135.8, 67.4, 56.0, 55.6, 53.8, 31.7 ppm.

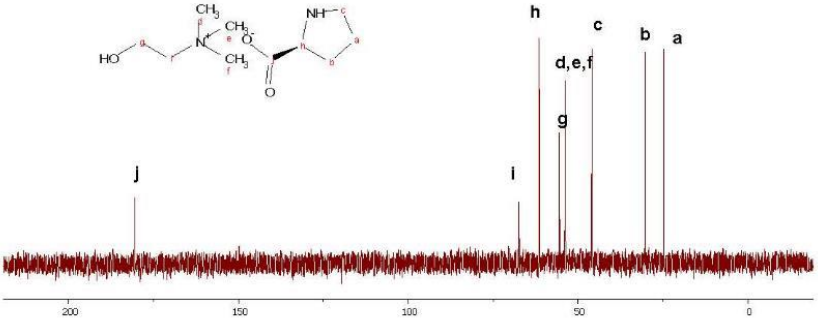

[CH][Pro]: ^{13}C NMR (600 MHz, D_2O, 25°C) δ=180.6, 67.4, 61.4, 55.6, 53.8, 46.0, 30.3, 24.8 ppm.

4. Figures and Tables for results part.

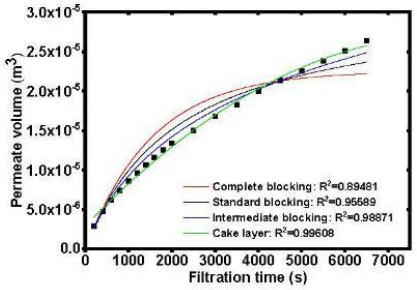

Figure S1. Evaluation of the predominant membrane fouling mechanisms at a constant pressure of 2 bar during immobilization.

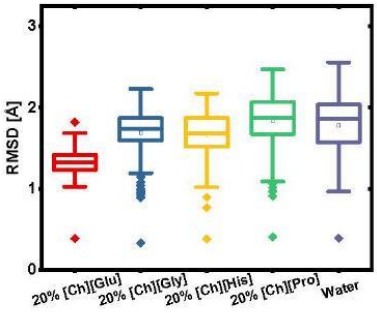

Figure S2: Statistical evaluation of the RMSD values for the Cα backbone over an MD simulation time of 18.1 ns.

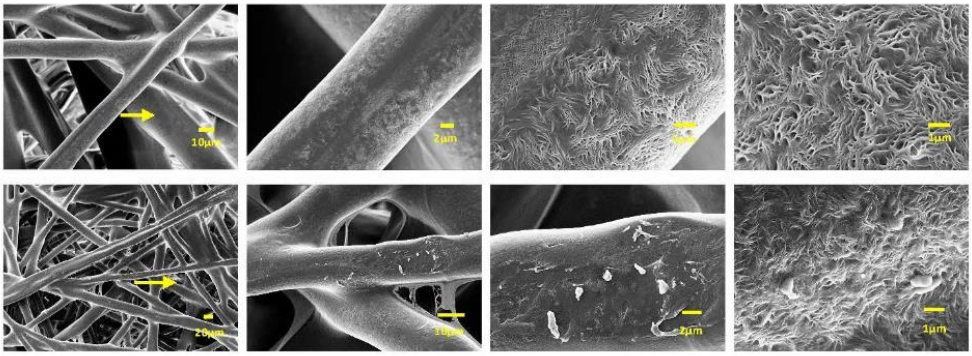

Figure S3. SEM images of Support layer (nonwoven polypropylene) before enzymes immobilization in the first line, and view of support layer after enzymes immobilization in the second line.

Table S1. Summary of membrane fouling models and mechanism under constant pressure filtration.

Models	Equations	Schematic description
Complete blocking	$V = \frac{V_0}{k_b}[1 - exp(-k_b t)]$	
Standard blocking	$V = (V_0 t)(1 + \frac{V_0 k_s}{A_0} t)^{-1}$	
Intermediate blocking	$V = \frac{1}{k_i} ln[1 + k_i V_0 t)]$	
Cake layer	$V = \frac{1}{V_0 k_c}(\sqrt{1 + (2k_c V_0^2 t)} - 1)$	

Nomenclature

V	filtrate volume, m^3	k_b	complete blocking constant, s^{-1}
t	filtration time, s	k_s	standard blocking constant, m^{-1}
V_0	initial volumetric flowrate, m^3/s	k_i	intermediate blocking constant,m^3
A_0	initial membrane frontal area, m^2	k_c	cake filtration blocking constant, $s\ m^{-6}$

Table S2. Thermodynamic parameters determined.

Enzyme	Ligand	Solvent	ΔG (KJ/mol)
FDH	CO_2	Water	-17.12
	CO_2	20%[CH][Glu]+water	-18.75

Table S3. Densities used for the molecular dynamics simulations

Solvent	ρ [g/cm³]	Weighted ρ [g/ cm³]
H_2O	0,997	0,7976
[Ch][Glu]	1,168	0,2336
[Ch][Gly]	1,156	0,2312
[Ch][His]	1,204	0,2408
[Ch][Pro]	1,138	0,2276

Table S4. Detailed analysis of distances between residues and amino acid residues involved in formation of the transition state. All numbers are given in Å.

Analyzed distances	Solvent system					
	20% [Ch][Glu]	20% [Ch][Gly]	20% [Ch][His]	20% [Ch][Pro]	H_2O	TS[a]
C4(NAD)-C(CO2)	3,596 ± 0,181	3,725 ± 0,251	4,069 ± 0,369	4,624 ± 0,505	17,990 ± 23,227	2,662 ± 0,064
Ht-C4(NAD)	1,085 ± 0,029	1,086 ± 0,029	1,089 ± 0,029	1,092 ± 0,028	1,088 ± 0,027	1,415 ± 0,032
Ht-C(CO2)	2,821 ± 0,182	3,034 ± 0,336	3,221 ± 0,412	3,880 ± 0,571	17,273 ± 23,271	1,304 ± 0,031
O8(NAD)-C7(NAD)	1,221 ± 0,022	1,224 ± 0,023	1,223 ± 0,021	1,220 ± 0,023	1,224 ± 0,023	1,266 ± 0,018
C7(NAD)-C3(NAD)	1,414 ± 0,024	1,421 ± 0,023	1,419 ± 0,025	1,419 ± 0,023	1,419 ± 0,023	1,491 ± 0,026
O2(CO2)-HD21(N119)	2,442 ± 0,386	4,271 ± 1,384	5,936 ± 1,910	7,029 ± 2,071	18,144 ± 22,442	1,978 ± 0,151

O2(CO2)-H(V93)	2,440 ± 0,305	4,440 ± 1,388	5,364 ± 1,618	6,509 ± 1,802	17,635 ± 21,940	2,034 ± 0,158
O1(CO2)-HH22(R258)	2,916 ± 0,459	3,326 ± 0,972	3,914 ± 1,007	4,439 ± 1,073	16,764 ± 21,351	2,461 ± 0,293
O1(CO2)-HH12(R258)	2,913 ± 0,489	3,070 ± 0,882	3,593 ± 0,917	3,732 ± 0,936	17,100 ± 21,522	2,048 ± 0,179
O2(CO2)-HH22(R258)	4,286 ± 0,337	3,786 ± 0,989	3,805 ± 0,925	4,259 ± 1,059	16,225 ± 21,709	3,770 ± 0,207
O2(CO2)-HH12(R258)	4,824 ± 0,337	3,739 ± 0,976	3,636 ± 0,945	3,688 ± 0,929	16,346 ± 21,960	4,270 ± 0,189
O1(CO2)-HE2(H311)	3,009 ± 0,717	3,892 ± 0,806	4,638 ± 1,362	6,069 ± 1,854	18,338 ± 22,006	2,381 ± 0,250
O8(NAD)-HE2(H311)	2,767 ± 0,461	2,802 ± 0,397	6,581 ± 2,042	8,654 ± 2,067	3,484 ± 0,913	2,165 ± 0,212
H92(NAD)-O(T256)	2,983 ± 0,549	2,084 ± 0,178	2,141 ± 0,218	2,139 ± 0,261	2,460 ± 0,666	1,898 ± 0,146
H91(NAD)-OD1(D282)	2,515 ± 0,492	2,714 ± 0,364	3,131 ± 0,681	3,397 ± 0,456	3,411 ± 0,835	2,361 ± 0,231
H91(NAD)-OD2(D282)	2,952 ± 0,488	2,670 ± 0,455	4,907 ± 0,956	5,186 ± 0,784	3,816 ± 1,253	2,412 ± 0,295
H91(NAD)-OG(S313)	2,824 ± 0,355	2,696 ± 0,314	3,077 ± 0,757	2,960 ± 0,618	3,159 ± 0,756	2,721 ± 0,217
HG(S313)-OD2(D282)	2,805 ± 0,164	2,692 ± 0,133	3,930 ± 0,600	4,211 ± 0,464	3,163 ± 0,778	1,751 ± 0,155
ND1(H311)-HE21(Q287)	4,627 ± 0,358	3,327 ± 0,734	3,829 ± 0,527	5,922 ± 0,593	3,516 ± 0,735	3,442 ± 0,159
ND1(H311)-HE22(Q287)	5,775 ± 0,300	3,763 ± 0,934	4,657 ± 0,626	6,561 ± 0,961	4,067 ± 1,000	1,862 ± 0,120

[a] as reported by Castillo, et al. (J. Phys. Chem. B 2008, 112, 10012–10022)

[1] S. De Santis, G. Masci, F. Casciotta, R. Caminiti, E. Scarpellini, M. Campetella, L. Gontrani, *Phys Chem Chem Phys* **2015**, *17*, 20687-20698.

Process and Systems Engineering Centre (PROSYS)
Department of Chemical and Biochemical Engineering
Technical University of Denmark
Søltofts Plads, Building 229
DK - 2800 Kgs. Lyngby
Denmark

Phone: +45 45 25 28 00
Web: www.kt.dtu.dk/forskning/prosys